ARISTOTLE UNIVERSITY OF THESSALONIKI
Interinstitutional Program of Postgraduate Studies in
PALAEONTOLOGY – GEOBIOLOGY

CHRISTINA KALAITZI
Geologist

RUSCINIAN LAGOMORPHA FROM MEGALO EMVOLON, THESSALONIKI

MASTER THESIS

DIRECTION: Macropalaeontology
Directed by: Aristotle University of Thessaloniki

THESSALONIKI
2024

Interinstitutional
Program of
Postgraduate
Studies in
PALAEONTOLOGY – GEOBIOLOGY

supported by:

Τμήμα Γεωλογίας ΑΠΘ
School of Geology AUTh

Τμήμα Βιολογίας ΑΠΘ
School of Biology AUTh

National and Kapodistrian University of Athens
Faculty of Geology and Geoenvironment

Τμήμα Γεωλογίας & Γεωπεριβάλλοντος ΕΚΠΑ
Faculty of Geology & Geoenvironment NKUA

Department of GEOLOGY

Τμήμα Γεωλογίας Παν/μίου Πατρών
Department of Geology, Patras Univ.

UNIVERSITY OF THE AEGEAN

Τμήμα Γεωγραφίας Παν/μίου Αιγαίου
Department of Geography, Aegean Univ.

CHRISTINA KALAITZI
ΧΡΙΣΤΙΝΑ ΚΑΛΑΪΤΖΗ
Πτυχιούχος Γεωλόγος

RUSCINIAN LAGOMORPHA FROM MEGALO EMVOLON, THESSALONIKI

ΡΟΥΣΙΝΙΑ LAGOMORPHA ΑΠΟ ΤΟ ΜΕΓΑΛΟ ΕΜΒΟΛΟ, ΘΕΣΣΑΛΟΝΙΚΗ

Υποβλήθηκε στο ΔΠΜΣ Παλαιοντολογία-Γεωβιολογία

Ημερομηνία Προφορικής Εξέτασης: 07/03/2024
Oral Examination Date: 07/03/2024

Three-member Examining Board

Professor Dimitrios S. Kostopoulos, Supervisor
Laboratory and Teaching Staff Dr Ioanna Sylvestrou, Member
Laboratory and Teaching Staff Dr Georgios Lazaridis, Member

Τριμελής Εξεταστική Επιτροπή

Καθηγητής Δημήτρης Σ. Κωστόπουλος, Επιβλέπων
ΕΔΙΠ Δρ. Ιωάννα Συλβέστρου, Μέλος Τριμελούς Εξεταστικής Επιτροπής
ΕΔΙΠ Δρ. Γεώργιος Λαζαρίδης, Μέλος Τριμελούς Εξεταστικής Επιτροπής

Citation:
Kalaitzi C., 2024. – Ruscinian Lagomorpha from Megalo Emvolon, Thessaloniki. Master Thesis, Interinstitutional Program of Postgraduate Studies in Palaeontology-Geobiology. School of Geology, Aristotle University of Thessaloniki, 119 pp.

CONTENTS

1 Introduction
1.1 Purpose and scope of the study ……12
1.2 The order of Lagomorpha ……12
1.2.1 Evolutionary history and phylogenetic relationships of the Lagomorpha ……13
1.2.2 The extant leporids (hares and rabbits) ……14
1.2.2.1 Morphology and physical characteristics of leporids ……...14
1.2.2.2 Geographical range and habitat ……15
1.3 Leporids in the fossil record ……16
1.4 Presence of Lagomorpha in Greece ……..17
2 Materials and methods
2.1 Geological and palaeontological setting ……18
2.2 Studied material ……22
2.2.1 Cranial material ……...22
2.2.2 Dental material ……23
2.2.3 Postcranial material ……27
2.2.4 3D scanning ……30
2.2.5 Estimated body mass (BM) ……30
3 Systematic Paleontology
3.1 Descriptions ……...32
3.1.1 Cranium ……..32
Dorsal view of the skull ……32
Lateral view of the skull ……...32
Ventral view of the skull ……..32
Occipital view of the skull ……32
3.1.2 The skull bones ……33
Nasals ……...33
Premaxilla ……34
Maxilla ……34
Palatine ……35
Zygomatic and squamosal ……35
Frontal ……..36
Parietal ……36
Basisphenoid, Pterygoid, Presphenoid, Alisphenoid ……...37
Ectotymbanic ……...38
Occipital complex (Basiooccipital, Exoccipital, Supraoccipital) ……38
3.1.2. Mandibles ……...38
3.1.3 Upper dentition ……...40
I1 and I2 ……...40
P2 ……40
Upper molariforms ……...42
3.1.4 Lower dentition ……...43
i1 ……..43
p3 ……43
Lower molariforms ……..45
3.1.5 Postcranial material ……....45
Atlas, axis, and vertebrae ……....45
Scapula ……....46

Humerus ……...47
Ulna and Radius ……...48
Os coxae ……...50
Femur ……...51
Tibiofibula ……...53
Astragalus ……55
Calcaneus ……...57
Navicular ……...58
Cuboid ……59
4 Comparisons
4.1 Cranium ……61
4.1.1 Comparison with extant leporid crania ……61
4.1.2 Comparison with fossil leporid crania ……63
4.2 Dentition ……65
4.3 Dental variation within *T. dumitrescuae* ……71
4.4 Comparison with previous records from Megalo Emvolon ……73
4.5 Postcranial comparisons ……74
Scapula ……74
Humerus ……...74
Ulna and radius ……74
Pelvis ……...75
Femur ……...76
Tibiofibula ……...78
Astragalus ……80
Calcaneus ……82
Navicular ……...83
Cuboid ……85
4.6 Body size estimation ……..86
5 Discussion
5.1 Taxonomical and anatomical remarks ……88
5.2 Palaeoecological remarks ……...91
6 Conclusions ……..97
References ...……99
Appendix I ……105
Appendix II ……...110

ABSTRACT

The research presented in this thesis focuses on the collection of leporids found in Megalo Emvolon-4 (MVL), near Thessaloniki, Greece. The locality has provided a rich collection of remains, including cranial and postcranial bones, along with isolated teeth, all identified as *Trischizolagus dumitrescuae*.

The dental features, particularly the morphology of the p3, exhibit distinctive characteristics aligned with the diagnostic features of the genus *Trischizolagus*. These features include the rhombic outline of p3 with a broad lingual anteroconid, a well-developed anteroflexid, simple and uncrenulated enamel, and a consistent pattern in the lower and upper cheek teeth. Additionally, the presence of the "*Alilepus*" p3 pattern indicates significant similarities with that observed in typical *T. dumitrescuae* from Romania. Metrical comparisons, especially with specimens from Măluşteni (Romania), further support the attribution of MVL material to *T. dumitrescuae*. In addition, the morphological and metrical agreement with dental remains from Megalo Emvolon-1 (MEV) strengthens this association. Hence, the first ever description of the cranium of *T. dumitrescuae* is provided from the MVL specimens. Comparative analysis with extant taxa reveals a combination of *Lepus* and *Oryctolagus* features in MVL *T. dumitrescuae*, suggesting an intermediate skull development between a hare and a rabbit. The estimated body mass of MVL *T. dumitrescuae*, around 1.7 to 2 kilograms, aligns with that of a small-sized *L. europaeus* or an average-sized *O. cuniculus*. Ecomorphological considerations based on limb and skull morphology suggest that MVL *T. dumitrescuae* possessed strong cursorial abilities and the potential for high jumping, indicating adaptation for swift movement. Additionally, the fore- and hindlimb features suggest a capability for digging. Lastly, from a palaeoecological perspective, the ecomorphological adaptations of the MVL leporid align with a mixed/open paleohabitat at Megalo Emvolon, reinforcing the notion that hares are suited for open areas. This study not only provides valuable insights into the morphological, metrical, and ecomorphological aspects of *T. dumitrescuae* in the Greek region and Europe but also enhances our understanding of the paleontological context of the Ruscinian fauna at Megalo Emvolon.

ΠΕΡΙΛΗΨΗ

Στην παρούσα μεταπτυχιακή διπλωματική εργασία μελετάται η συλλογή απολιθωμένων λαγόμορφων (Leporidae, Mammalia) του Κάτω Πλειοκαίνου (Ρουσίνιο) που ανακαλύφθηκαν στη θέση Μεγάλο Έμβολο-4 (MVL), κοντά στη Θεσσαλονίκη. Η συλλογή προσφέρει ένα πλούσιο και καλοδιατηρημένο πλήθος απολιθωμάτων, περιλαμβάνοντας κρανία, οστά του μετακρανιακού σκελετού, καθώς και μεμονωμένα δόντια. Τα οδοντικά χαρακτηριστικά και ιδιαίτερα η μορφολογία του τρίτου προγομφίου της κάτω γνάθου (p3), συμφωνούν με τα διαγνωστικά χαρακτηριστικά του γένους *Trischizolagus*, όπως: το ρομβικό περίγραμμα του p3 με ένα πλατύ γλωσσικό εμπροσθοκωνίδιο, ένα καλά ανεπτυγμένο εμπροσθολεκανίδιο, την απλή και μη ρυτιδωμένη αδαμαντίνη και την απουσία βαθιάς αναδίπλωσης στα δόντια της κάτω γνάθου. Επιπλέον, η παρουσία του μορφότυπου "*Alilepus*" για τον p3 υποδεικνύει σημαντικές ομοιότητες με το τυπικό *T. dumitrescuae* από τη Ρουμανία. Οι μετρικές συγκρίσεις, ειδικά με δείγματα από το Măluşteni (Ρουμανία), υποστηρίζουν περαιτέρω την ταξινόμηση του υλικού της θέσης MVL στο είδος *T. dumitrescuae*. Επιπροσθέτως, η μορφολογική και μετρική συμφωνία με τα οδοντικά υπολείμματα από το Μεγάλο Έμβολο-1 (MEV) ενισχύει περαιτέρω αυτή τη συσχέτιση. Καθώς η μορφολογία του κρανίου του είδος *T. dumitrescuae* δεν ήταν γνωστή έως σήμερα, η πρώτη πλήρης περιγραφή και απεικόνισή του κρανίου του είδους παρουσιάζεται από τα δείγματα της θέσης MVL. Οι συγκρίσεις με σύγχρονα είδη αποκαλύπτουν ότι το κρανίο του *T. dumitrescuae* της MVL φέρει έναν συνδυασμό χαρακτηριστικών από τα γένη *Lepus* και *Oryctolagus*, υποδηλώνοντας μια ενδιάμεση φυλογενετική θέση μεταξύ ενός λαγού και ενός κουνελιού. Η εκτιμώμενη μάζα σώματος του *T. dumitrescuae* της MVL, που υπολογίστηκε στα 1,7 έως 2 κιλά, ευθυγραμμίζεται με αυτή ενός μικρού μεγέθους *L. europaeus* ή ενός μέσου μεγέθους *O. cuniculus*. Από τις οικομορφολογικές αναλύσεις που βασίζονται στη μορφολογία του άκρου και του κρανίου υποδηλώνεται ότι το *T. dumitrescuae* της MVL διέθετε προσαρμογή για γρήγορη κίνηση και ισχυρές δρομικές ικανότητες, καθώς και δυνατότητα για άλματα εις ύψος. Ακόμη, από τα χαρακτηριστικά του εμπρόσθιου και οπίσθιου άκρου υποδηλώνεται η δυνατότητα για σκάψιμο. Τέλος, από παλαιοοικολογική σκοπιά, οι οικομορφολογικές προσαρμογές του λαγόμορφου της MVL βρίσκονται σε συμφωνία με ένα μικτό/ανοιχτό παλαιοβιότοπο όπως αυτός εικάζεται για το Μεγάλο Έμβολο κατά το Κάτω Πλειόκαινο. Η μελέτη αυτή προσφέρει πολύτιμες γνώσεις για τα μορφολογικά, μετρικά και οικολογικά χαρακτηριστικά του είδους *T. dumitrescuae* στην Ελλάδα και την Ευρώπη, αλλά επίσης εμβαθύνει την κατανόησή μας για το παλαιοπεριβαλλοντικό πλαίσιο της Ρουσίνιας πανίδας του Μεγάλου Εμβόλου.

Acknowledgements

I am sincerely grateful to my three supervisors, Professor Dimitrios S. Kostopoulos, Dr. Ioanna Sylvestrou, and Dr. Georgios Lazaridis, for their invaluable guidance and support throughout the process of this thesis. In particular, I am immensely grateful to Professor Kostopoulos for not only entrusting me with the examined material but also for his profound insights and direction. Furthermore, I wish to express my sincere appreciation to the Naturalis Biodiversity Center, and in particular to Dr. Lars von den Hoek Ostende, for graciously providing access to their invaluable collections. This access was pivotal in enabling me to conduct thorough measurements of recent leporid crania, enriching the depth and breadth of my research immeasurably. Additionally, I am grateful to Dr. Georgios Konidaris and Stylianos Koutalis for helping me with the 3D scanning process. Lastly, I want to acknowledge the unwavering support of my friends and family, who stood by me throughout this challenging journey. Your encouragement and understanding have been instrumental in navigating through this demanding, literal rabbit hole.

1. Introduction

1.1. Purpose and scope of the study

Due to their global distribution and their unique characteristics, the order of Lagomorpha and especially the European species of leporids are very well recognizable around the world, making them significant palaeoecological biomarkers. This study examines the rich leporid collection from the new Megalo Emvolon-4 (MVL) site to contribute to the knowledge of the Ruscinian lagomorphs found in Greece and the Balkan Peninsula, as well as to provide further information for the systematics of lagomorphs in general throughout Eurasia during that time. The thesis primarily focuses on leporids, due to the attribution of the studied fossil remains on this family.

Four primary goals can be outlined for this research. First, to identify the newly found material from MVL, which consists of a plethora of cranial, dental, and postcranial fossil remains; second, to examine and present the rich MVL cranial material, which is usually underrepresented in the fossil record because of taphonomic processes. The preserved crania were described in detail, compared with both fossil and extant species and a 3D scan was created to enhance the presentation of the remains. Secondly, dental remains were also thoroughly examined, and compared to both extant and fossil taxa. Lagomorph diagnosis is based primarily on the dentition, specifically the lower third premolar. The new dental material not only allows morphometrical clarification and contribution to the species *T. dumitrescuae* that most likely the studied fossils of MVL belong to, but also provides further information about the lagomorph diversity of the Megalo Emvolon fossil site. The morphometric analysis of the postcranial material comes next, followed by a detailed comparison with fossil and extant species. Finally, palaeoecological inferences and locomotive adaptations of the MVL taxon are investigated based on the facial tilt, maxillary fenestration, estimated body mass, and several postcranial indices providing insights into the region's paleoecology.

Additionally, the study aims to discuss the presence of *Trischizolagus* in Greece. Although research activity on Lagomorpha has been intense in recent years in Europe, the clarification of the *Trischizolagus* genus record remains uncertain in the Mediterranean. This study is intended to provide novel insights into the late Ruscinian *T. dumitrescuae* in Greece and enhance understanding of it. Moreover, as three different lagomorph species are reported in the fossil record of the Megalo Emvolon site this thesis will address the taxonomic issues associated with *T. dumitrescuae* Radulesco and Samson, 1967, *T. maritsae* De Bruijn, Dawson and Mein, 1970, and *Oryctolagus laynensis* López Martínez, 1977.

1.2. The order of Lagomorpha

The order of Lagomorpha Brandt, 1855, consists of two living families: Leporidae Fischer de Waldheim, 1817 (rabbits and hares, Figs. 1A, B) and Ochotonidae Thomas, 1897 (pikas, Fig. 1C). Traditionally, lagomorphs were classified as a suborder of Rodentia. Considering the existence of a second set of nonfunctional upper incisors, which is nonexistent in rodents, lagomorphs were granted their own order in 1912 (Gidley, 1912; Montuire, 2001). In contrast to the second upper pair of incisors, the first set is characterized as “ever-growing”. In extant species, the dental formula is

$\frac{2I\ 0C\ 3P\ 3M}{1i\ 0c\ 2p\ 3m}$ (28 teeth) for leporids and $\frac{2I\ 0C\ 3P\ 2M}{1i\ 0c\ 2p\ 3m}$ (26 teeth) for ochotonids; however, it may change somewhat in fossil taxa (Vasileiadou and Sylvestrou, 2022 and references therein).

With just 12 extant genera, Lagomorpha is one of the least diverse mammalian orders (Hoffmann and Smith, 2005). However, lagomorphs are extremely prolific animals with a remarkably abundant fossil record. They are extremely numerous in European small mammal assemblages, particularly after the Miocene (López-Martinez, 2001), and are of the outmost relevance in paleobiogeographic reconstructions (Angelone, 2008a, Angelone *et al*., 2019).

Figure 1. A) *Oryctolagus cuniculus*, ***B)*** *Lepus europaeus*, and ***C)*** *Ochotona princeps*. Source: Wikipedia.

1.2.1. Evolutionary history and phylogenetic relationships of the Lagomorpha

The Ochotonidae family contains 31 extinct genera and approximately 150 extinct species, aside from the living *Ochotona* Link, 1795 genus (Ge et al., 2013). From the Oligocene of various sites in Asia, *Sinolagomus* Bohlin, 1937 is the family's earliest known representative (Erbajeva et al., 2011; Erbajeva, 2016). The diversity of the family reached its highest point during the Middle Miocene period, and it expanded its range into South Africa in the Early Miocene. During the Late Miocene, a significant extinction event occurred, resulting in the loss of numerous genera. Only 3-4 genera managed to survive the transition from the Miocene to the Pliocene. The sole surviving genus is *Ochotona*, which dates back to the Late Miocene. The genus is currently found in plateau-steppe and talus habitats in Asia and North America (Ge et al., 2013).

According to Ge et al. (2013), there are about 34 genera and 130 species of leporids. The earliest leporids include taxa such as the Eurasian *Lushilagus* Li, 1965 and *Shamolagus* Burke, 1941, as well as the North American *Megalagus* Walker, 1931.

However, since the Middle to Late Eocene, the diversity of leporid genera remained relatively low. The Late Miocene to Pliocene period saw a marked acceleration in the diversification of leporids. During the Pliocene and Pleistocene, it experienced significant growth and spread to Africa and South America. The number of leporid genera experienced a significant decrease during the Holocene (Ge et al., 2013).

Despite ochotonids and leporids sharing an Asian origin, their dispersion territories as well as their body sizes are quite distinct (Ge et al., 2013). The different evolutionary paths of these two families may have been influenced by the ecological vegetation shift brought about by climate change. Throughout the Late Miocene, there was a significant shift known as the "global green revolution" (Chapman and Flux, 1990). This period saw the dominance of C4-type plants over C3 plants in tropical and temperate regions (Zhang et al., 2009). Ge et al. (2013) reports that, there may have been a correlation between the extension of C4 vegetation throughout the Late Miocene and the range reduction and demise of ochotonids. They suggest that worldwide environmental change, notably the rise in C4 vegetation during the Miocene to Pliocene transition, also altered the evolutionary curve of leporids. More specifically, the abundance of ochotonids throughout the Early to middle Miocene was likely tied to the abundance of C3 type of vegetation at the "climatic optimum". Nonetheless, the development of C4 vegetation in the Late Miocene, which was connected to continental aridification, global cooling, and intensification of monsoons, likely caused large-scale range limitation and also extinction of ochotonids but supported diversity and range extension of leporids. Extant pikas have a significant predilection for C3 plants, though leporids diets consisted of more than 16% of C4 plants, among them 31% of which are Poaceae. The adeptness of certain leporids to digest C4 plants is also anticipated to lead to an increase in size and an expansion of their range. Leporids, especially *Lepus* species that can effectively digest C4 plants, are increasing their ranges (Ge et al., 2013).

1.2.2. The extant leporids (hares and rabbits)

Burgin et al. (2018) report that the 12 recognized living lagomorph genera consist of a total of 108 identified species. The Leporidae family comprises 11 genera, among them *Lepus* Linnaeus, 1758 (hares and jackrabbits), *Sylvilagus* Gray, 1867 (cottontail), and *Oryctolagus* Lilljeborg, 1874 (european rabbit) (Naff and Craig, 2012; Graham, 2015). The term "true hare" refers to species of hares and jackrabbits in the genus *Lepus* (Flux and Aneerman, 1990). The rest of the leporid species are known as rabbits. Alternatively, the term "cottontail" is also used to refer to the rabbit species (Chapman and Ceballos, 1990).

1.2.2.1. Morphology and physical characteristics of leporids

Leporids developed a very characteristic skull. Unlike ochotonids, the skull is arched laterally and exhibits a slight constriction between the orbits (Wood-Bailey et al., 2022). Additionally, the skull is strongly fenestrated to a so-called "latticework of bone" to minimize weight. This feature is particularly well-developed in some leporids (Chapman and Flux, 1990; Smith, 2003; Wood-Bailey et al., 2022). The post- and supraorbital processes are very prominent, and the parietal, occipital, and maxillae are fenestrated. The primary incisors are larger in size, while the secondary incisors are smaller and positioned directly behind the primary ones. The primary incisors resemble

those of rodents, except that they are entirely encased in enamel. Canines are absent, and a diastema, a significant gap between the incisors and the cheek teeth, is present. The cheek teeth exhibit a relatively uncomplicated cusp structure, consisting of two transverse ridges on the occlusal surface. The cheek teeth are strongly hypsodont in most species (Smith, 2003).

Generally, lagomorphs are adapted for swift movement when in danger. To escape predators, pikas and rabbits rush to dense cover or burrows, whereas hares are often long-distance runners who can outrun their pursuers (Chapman and Flux, 1990). The leporids, specifically, are known for their exceptional speed and agility. The hind legs are well adapted for cursorial locomotion, which involves running or bounding and are known for their elongated structure. Their ears are large and moveable to permit detection of approaching danger. Hares have longer legs and can reach considerable running speeds. It's worth mentioning that some species can reach up to 80 km/h and can sustain a speed of 50 km/h for extended periods. Hares vary in size, typically measuring between 40 to 75 cm in length and weighing between 1,350 and 6,000 gr. On the other hand, rabbits have shorter legs and are overall smaller. Their body length ranges from 25 to 50 cm, and they typically weigh between 400 and 3,000 gr (Chapman and Flux, 1990; Angerbjörn, 2003). Finally, it has been found that sexual dimorphism is not significant in Lagomorpha as indicated by studies conducted by Weston (1982), Lu (2003), and Smith and Weston (1990), among others.

1.2.2.2. Geographical range and habitat

In contrast to pikas, leporids have a wide global distribution as both native and introduced species. Rabbits and hares inhabit various regions across Africa, Eurasia, and Central, North, and northern South America. They can be found in diverse habitats such as forests, open brush, and savannah environments. The wide geographic distribution of leporids can be attributed primarily to their introduction by humans. Some lagomorph species have been selected for domestication and used for human purposes, while others have been able to establish stable populations in new environments and thrive in the wild. The European rabbit (*Oryctolagus cuniculus (Linnaeus, 1758)*) and hare (*Lepus europaeus* Pallas, 1778) have been introduced in various locations over the past centuries. These locations include Australia, South America, New Zealand, Java, and over 500 oceanic islands over the past few centuries. Additionally, *Sylvilagus floridanus* (J.A. Allen, 1890) can be found in Northern Italy (Chapman and Flux, 1990; Angerbjörn, 2003; Rosin et al., 2009, 2010; Ge et al., 2013)

It is widely recognized that there is a strong relationship between habitat selection and cursorial ability. Hares and rabbits have distinct habitat preferences. Hares are commonly found in open environments, where they have a greater chance of outrunning their predators due to their exceptional speed. Furthermore, the rocks and shrubs present in that particular environment can serve as effective means of camouflage and protection against birds of prey (Flux and Aneerman, 1990). On the other hand, rabbits do not exhibit a strict vegetation community type. Instead, they are typically found in diverse habitats, particularly in closed environments with thick vegetation cover. This allows them to hide and seek shelter among the plants and trees (Chapman and Ceballos, 1990; Angerbjörn, 2003).

1.3. Leporids in the fossil record

Leporids achieved complete dental hypsodonty by flattening the crown shafts. The roots of the teeth are located in a vertical tubercle that extends into the orbit and is separate from the zygoma. Furthermore, the molarization of the upper premolars is evident. The third upper molar is reduced to a single lobe and retained. Both talonids and trigonids have lingual connections, and there is only one noticeable mental foramen of the mandible. The basicranial angle is near 30^{o}. These characteristics are likely derived, while the appearance of a bilobed m3 is considered as a primitive feature. Additional seemingly primitive characteristics, including the uniserial incisor enamel and the extremely reduced or nonexistent premolar foramen, may be secondary acquisitions (López -Martinez, 2008).

According to Boon-Kristkoiz and Kristkoiz (1999), there is no confirmed evidence of leporids in Eurasia prior to the Late Miocene. The "Leporid Datum", an important event during the Turolian period, refers to the relatively rapid spread of leporids across the Old World around 8 million years ago, as described by Flynn et al. (2014). *Alilepus* Dice, 1931 is among the oldest of the Leporinae representatives (Čermák et al., 2015). Its origin can be traced back to North America during the Late Miocene (Voorhies and Timberley, 1997; Flynn et al. 2014), when *Alilepus* entered Eurasia through the Beringia. It is speculated that the widespread occurrence of leporids in Eurasia, the first of which was most likely *Alilepus*, signified the aforementioned "revolution in the ecosystems" (Čermák et al., 2015). Limited fossils of Leporinae are recorded between the timeframe of 16 to 6 million years ago (Voorhies and Timperley, 1997). On the other hand, a significant diversity explosion occurred during the Pliocene combined with a remarkable local heterogeneity, and the appearance of over 16 new taxa. However, several Pliocene leporids went extinct during the Late Pleistocene or the Holocene (López-Martinez, 2008).

Lagomorph diversity is quite significant in the late Ruscinian of SE and central Europe (Čermák, 2009; Čermák and Angelone, 2013). In total, five genera are reported: the ochotonids *Ochotonoma* Sen, 1998, and *Prolagus,* and the leporids *Hypolagus* Dice, 1917, *Pliopentalagus* Gureev & Konkova, 1964, and *Trischizolagus*. Several of them are well described for their paleobiogeographical importance and biochronological significance as MN15b markers (Angelone, 2008a; Čermák and Wagner, 2013). The most prevalent lagomorph, *H. petenyii*, was reported in nearly all central and SE European MN15b faunas (Čermak, 2009 and references therein). *T. dumitrescuae* and *O. csarnotana*, on the other hand, are often found together, with their existence suggesting a somewhat dry and hot environment, as well as the presence of extensive savanna-steppe regions (Popov, 2004). The majority of *T. dumitrescuae* fossils are located in the northern peri-Paratethyan region, associated with early Ruscinian faunas (MN14), although in western regions the record is poor and very restricted to the late Ruscinian (MN 15b) (Čermak et al., 2021). Evidently, in MN15b, a notable number of lagomorph taxa, most of which originated in eastern or southeastern areas, entered central Europe. Such a rapid occurrence of lagomorph species with vastly differing ecological needs shows that the arrival of favorable climatic circumstances was not the sole or key reason for their conspecific spread. However, these paleobiographic dynamics reflect only a small portion of the quite extensive faunal modifications that characterized all of Europe (Čermák et al., 2021).

1.4. Presence of Lagomorpha in Greece

The Greek lagomorph fossil record includes 37 localities, dated from the Early Miocene to the Late Pleistocene (Vasileiadou and Sylvestrou, 2022). In further detail, fifteen localities are attributed to the Miocene, six to the Miocene/Pliocene boundary, six to the Pliocene, and ten to the Pleistocene. The majority (24) are in Northern Greece (Macedonia and Thrace), one in Central Greece, four in Attica, and eight in insular Greece (Chios, Crete, Evia, Karpathos, and Rhodes). The most diverse assemblages of lagomorphs are found at the Pliocene locality of Megalo Emvolon 1, and the latest Pleistocene Loutra Almopias Cave LAC Ia. Both of these localities have reported three lagomorph species (Vasileiadou and Sylvestrou, 2022). The youngest known Greek lagomorph locality is the Upper Pleistocene Agios Georgios Cave, with *Ochotona pusilla* and *Lepus europaeus* (Piskoulis et al., 2023).

2. Materials and methods

2.1. Geological and palaeontological setting

The studied material comes from the Megalo Emvolon fossil locality in Central Macedonia, Greece. The site is located in the eastern shores of Thermaikos Gulf (Fig. 2A), close to the city of Thessaloniki (~20 km) (Koufos and Koliadimou, 1993) and in the center of the wider Axios-Thermaikos Basin. It was first reported by the British paleontologist Richard Owen, describing *Laophis crotaloides* (Owen, 1857). These fossils were collected by Captain Spratt from "Karabournou, on the eastern coast of the Gulf of Salonica", as mentioned by Owen (Georgalis et al., 2016 and references therein). Later, the site become well known for the large mammal, referred to as "Falaise de Karabouroun" (Arambourg and Piveteau, 1929; Koufos, 2006). Megalo Emvolon is among the limited Lower Pliocene fossiliferous sites in Greece, featuring a diverse range of vertebrate fauna, including both large and small mammals, birds, and reptiles (Koufos et al., 1991).

Koufos et al. (1991) recognized three fossil horizons in the Megalo Emvolon section. The first one, called Megalo Emvolon-1 (MEV), is at the base of the outcrop and is made up of grey argillaceous sands that are located close to sea level. The second one, Megalo Emvolon-2 (MEM), is situated 20 meters above MEV and is characterized by gravel beds scattered throughout red sands. The third level, Megalo Emvolon-3 (MEL) is located approximately 10 meters above MEM and near the top of the section (Syrides, 1990; Koufos and Koliadimou, 1993) (Fig. 2B). The herein studied material of lagomorphs comes from a recently discovered, fourth fossil spot called Megalo Emvolon-4 (MVL) (Fig. 2E).

The Axios-Thermaikos Basin is one of the three major basins in central and North Greece, corresponding to a fault-bounded sedimentary basin situated within the North Aegean region (Maravelis et al., 2015). The Axios-Thermaikos Basin is a quite broad fault-bounded sedimentary basin that lies above the eastern edge of the crystalline massif Pelagonian Zone (Maravelis et al., 2021). The Axios-Thermaikos Basin started to form during the Early Miocene and is filled with Neogene-Quaternary deposits that are over 5 km in total thickness (Syrides, 1990). According to Syrides (1990), the stratigraphical analysis of the Neogene-Quaternary sediments that were deposited revealed variations in the filling process over different locations and periods. These differences can be attributed to the diverse depositional environments. In more detail, the deposits in the Eastern part of the basin, including the studying area, can be distinguished into six lithostratigraphic formations (Fm): (1) the Antonios Fm (fluvial deposits, Lower to Middle Miocene and Upper Miocene); (b) the Triglia Fm (continental deposits and red-beds, Upper Miocene) (c) the Trilophos Fm (brackish-lacustrine deposits, latest Miocene-earliest Pliocene); (d) the Gonia Fm (fluvio-lacustrine deposits, Lower Pliocene); and (e) the Moudania Fm (continental sediments, Upper Pliocene/Lower Pleistocene and continuing onwards) (Syrides, 1990).

According to Syrides (1990), the deposits in the area of Megalo Emvolon correspond to the Gonia Fm. It is believed to have developed in a fluvial-lacustrine environment with shallow lakes and frequent river discharges, with an estimated thickness of 100 – 150 m (Syrides, 1990). The shift from the Trilophos Fm to the Gonia Fm occurs gradually. The sedimentary sequence in this area displays a pattern of

alternating lenses and lens-shaped beds consisting of various materials, including clays, marls, sands, sandstones, massive marly limestones and gravels. These deposits often exhibit lateral transitions and interchanges. Notably, within these formations, three distinct layers of massive marly limestone exhibit significant lateral extent, enabling the identification and separation of three distinct members (Mb.), namely the Silata Mb., the Rhodokipos Mb., and the Kallikratia Mb. (Vasileiadou et al., 2003).

The wider region of Megalo Emvolon can be subdivided into three well-defined lithological units that can be correlated with the Gonia Fm. (Sidiropoulou, 2017), as previously documented by Syrides (1990). The fossiliferous site of MVL is situated on the lowest unit of fine-grained horizons of 2.5 m thick composed of green-grey to brown clay, red clay, and mud materials. These materials contain significant amounts of calcareous concretions and oxides. The horizons in this area are particularly cohesive and hard in places. The numerous calcareous concretions exhibit a wide range of shapes, including nodules and irregular forms. Additionally, in certain locations, these concretions have formed distinct, tightly packed, wavy horizons known as laminar calcrete (Syrides, 1990).

A thinner horizon of 0.3 m of coarse-grained horizons that are mixed with fine-grained horizons lies above the previous unit. These layers consist mainly of gravelly sands to sandy gravels, with a notable amount of volcanic clasts in places. It is possible to differentiate between planar cross-bedding and locally coarser-grained deposits by examining cross-bedding that shows a gradual change in grain size from coarse to fine. The contact with the fine-grained horizons can be abrupt and occasionally erosional. A thin layer of pure tuffaceous material with a distinct “pink” color can is traced in the upper level and within the fine-grained materials.

It is worth noting that in Megalo Emvolon locality, there is not a clearly defined single fossil layer; instead, fossils appear in small spots/lenses of limited dimensions (from 0.5-3 m in length) dispersed along different stratigraphic levels (Koufos, 2006; Georgalis et al., 2016). Among these dispersed concentrations, the material understudied for this thesis was discovered in MVL fossil spot of a few meters in length and 0.5-1m in thickness. Almost all the MVL lagomorph remains are from a small lens of 1-2 m long and 50 cm deep (Fig. 2D).

MVL is thought to be either at the basal or middle fossiliferous level (MEV, MEM) or in between them (Kostopoulos pers. com.) (Fig. 2C). Boev and Koufos (2000) suggested that the sediments were deposited quickly, and the mammal fauna found in MEM, MEL, and MEV do not indicate any significant age differences. Based on the available data from Drakopoulou (2022), it is believed that the same applies to the MVL.

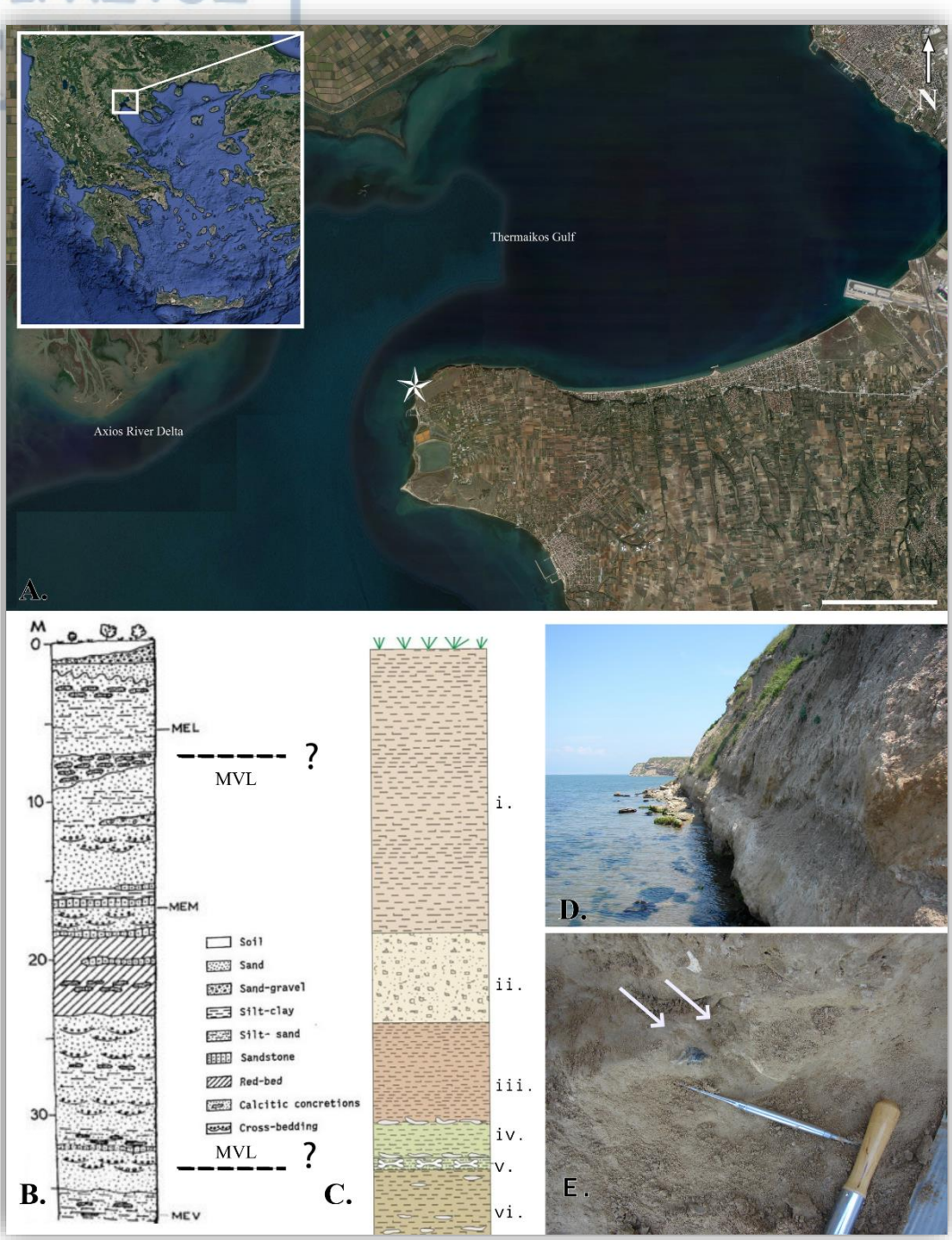

Figure 2. A) Geographic map of the location of the Megalo Emvolon localities. Images exported from Google Earth Pro © 2023. Scale bars equal 3 km; ***B)*** Synthetic stratigraphical column of Megalo Emvolon (after Koufos et al., 1991) ***C)*** Stratigraphical column of MVL [Sidiropoulou (2015) and Sylvestrou pers. data] ***i.*** Clays with calcareous concretions, ***ii.*** Coarse sand and pebbles; ***iii.*** Clay, ***iv.*** Fossil horizon of MVL, ***v.*** Silt and clay with calcareous concretions. The exact stratigraphic place of MVL is accepted as in between that of MEL and the MEV sites (after Sidiropoulou, 2017); ***D)*** The MVL site (photo courtesy DS Kostopoulos); ***E)*** in situ view of a lagomorph mandible (left arrow) and cranium (right arrow) from MVL (photo courtesy DS Kostopoulos).

The mammal fauna of Megalo Emvolon is relatively well studied, with more insights being added in recent years (Boev and Koufos, 2000; Vlachos et al., 2015; Georgalis et al., 2016; Drakopoulou et al, 2022). Apart lagomorphs it includes: the canid *Nyctereutes donnezani*, the bovids *Koufotragus bailloudi*, *Gazella borbonica*, and *Parabos macedoniae*, the cercopithecidae *Dolichopithecus ruscinensis,* the suid *Sus arvernensis*, the equid *Hipparion longipes*, as well as the rodents *Spalax odessanus* and *Microspalax odessanus* (Arambourg and Piveteau, 1929; Steffens et al.,1979; de Bruijn, 1984; Koufos et al., 1991; Koufos and Koliadimou, 1993; Koufos, 1997; Kostopoulos and Sylvestrou, 2022). Boev and Koufos (2000) report that *Pavo bravardi*, a type of peafowl, is the only bird fossil that has been discovered at the site. The reptilian fossils discovered include the giant viperid snake *Laophis crotaloides*, the tortoises *Testudo* cf. *graeca*, and *Testudo* sp., along with several other giant and small tortoises and *Varanus* (Bachmayer et al., 1980; Georgalis and Kear, 2013; Drakopoulou et al., 2022). As reported by Eronen and Rook (2004), the mammal species found in Megalo Emvolon suggests that the site was located in a semi-arid environment.

Koufos et al. (1991) and Koufos (2006 and refs. therein) suggested the fauna of the Megalo Emvolon site as Early Pliocene. *Microspalax odessanus* in Megalo Emvolon is recognized as the earliest occurrence of the genus indicating a late Ruscinian (MN15) age (De Bruijn, 1984; Koufos and Koliadimou, 1993). Additionally, the presence of *Sus arvernensis* and *Gazella borbonica*, along with the similarities between *Dolichopithecus ruscinensis* from Megalo Emvolon and Perpignan, and the stiking resemblance of the Megalo Emvolon hipparion with the larger variant discovered in Çalta, Turkey further support a late Ruscinian age (Boev and Koufos, 2000; Koufos, 2006; Koufos et al., 2022). The occurrence of the pink fine ash guide layer at the upper part of the fossiliferous sequence of Megalo Emvolon is consistent with an Early Pliocene age; these fine ash layer, observed in various locations all around Thermaikos Gulf are thought to be originating from Almopia volcanoes, which the bulk eruption occurred around 4 - 5 Ma (Syrides, 1990; Sylvestrou, 2002). In general, the Megalo Emvolon fauna dates between 4.2 and 3.2 Ma and is associated with the European Land Mammal Zone 15 (MN 15; Late Ruscinian) (Koufos et al., 1991; Koufos, 2006).

Three distinct leporid species have been so far reported from Megalo Emvolon (Steffens et al., 1979; Koliadimou and Koufos, 1993). However, the material on which these results are based is rather fragmentary. Koufos and Koliadimou (1993) attributed one left incisor, one partial left mandible with p4-m2, two partial maxillae with all cheek teeth, and one partial left mandible with p3-m3 to *T. dumitrescuae*. An additionally leporid partial left maxilla with P4-M2 is referred to by the same authors as *T.* cf. *maritsae*, in accordance with previous reports of the taxon from the same locality (Steffens et al., 1979; Vasileiadou and Sylvestrou, 2022). Thirdly, *Oryctolagus* cf. *laynensis* has been reported by Steffens et al. (1979), but no additional information is provided (Vasileiadou and Sylvestrou, 2022). Among the material collected by Arambourg at the beginning of the previous century, there are several lagomorph specimens. These include postcranial material, as well as three skulls and mandibles. This material was not included in the publication by Arambourg and Piveatau (1929) but was part of the relevant MNHN Paris collection, though never studied in detail. The material has been lost since the 70's but it has been very recently (August 2022) relocated and sent back to MNHN Paris and is currently under study by S. Sen.

2.2. Studied Material

The studied material is housed at the Museum of Geology-Paleontology-Paleoanthropology (LGPUT). Upon first studying of the dental material, it was identified as belonging to the Leporidae family. Hence, all the subsequent comparisons and discussions will be centered around leporids. According to the anatomical description, homogeneity is apparent among the MVL material. No significant differences between the various skulls, mandibles, and teeth, as well as within the postcranial material, were observed that could necessitate the division of the material into two or multiple distinct taxonomic groups. Consequently, all the specimens are considered to belong to a single taxon. The NISP (number of identified specimens) and MNI (minimum number of individuals) was determined for each skeletal group.

2.2.1 Cranial material

The cranium was measured using a digital caliper with an accuracy of 0.1 mm, following the method described by von den Driesch (1976). To avoid "metering error", all measurements were taken two times, and a mean value was calculated for it to be applied in both metrical comparisons and statistical analysis. The abbreviations and descriptions of the measurements used are given in Table 1. Complete measurements of the skull are presented in Table 9. The measurement of the facial tilt of the skull was conducted by capturing photographs of each skull from a lateral view. The skulls were set up in a sandbox in order to guarantee that the sagittal plane was at 90^{o} angle to the focal direction. The facial tilt angle was determined by analyzing the digital photos using Adobe Photoshop. It was measured as the angular difference between the occipital plane and a line parallel to the cranial diastema according to Kraatz et al. (2015).

Table 1. Skull measurements used in this study.

Abbrevation	Measurement
CL	Condylobasal length
BL	Basal length
DEL	Dental length
DIL	Diastema length
CTL	Cheektooth row length
GLN	Greatest length of the nasals
GBN	Greatest breadth of the nasals
FL	Frontal length
VL	Viscerocranium length
IFL	Incisive foramina length
GBIF	Greatest breadth of the incisive foramina
PL	Palatal length
PB	Palatal breadth
CB	Choanae breadth
LAZ	Length of the anterior root of the zygomatic arch
OZB	Oral zygomatic breadth
AZB	Aboral zygomatic breadth
GBOC	Greatest breadth of the occipital condyles
GNB	Greatest neurocranium breadth
BS	Breadth of skull
ABL	Length of auditory bullae

ABB	Breadth of auditory bullae

The cranial anatomy of the studied material was described with reference to three extensive and well-illustrated studies of extant and fossil lagomorph cranial anatomy: the CT-scanning data and analysis of *Palaeolagus haydeni* (Wolniewicz and Fostowicz-Frelik, 2021), the comparative description of *Romerolagus diazi* and *Ochotona princeps* (Wible, 2007), and the anatomical description of *Oryctolagus cuniculus* (Farag et al. 2012). Comparison was made using the descriptions of certain regions of the skull of *T. dumitrescuae* provided by Averianov (1995), which fits the chronological framework of the studied material and is one of the two previously reported leporids at the Megalo Emvolon locality (Koufos and Koliadimou, 1993). Furthermore, Sen and Geraads (2023) recently published a new species of the genus, *Trischizolagus meridionalis* Sen and Geraads, 2023, wherein certain palatal parts of the cranium have been preserved and described. Additional cranial comparisons of the studied material with *Alilepus hibbardi* White 1991, *Hypolagus balearicus* Quintana, Bover, Alcover, Agustí & Bailon, 2010, and the extant species *Lepus europaeus*, *Oryctolagus cuniculus*, and *Sylvilagus floridanus* are possible. The selection of fossil species for comparison was based on their proximity in age to the Megalo Emvolon site and their level of preservation. Measurements from the three recent species were acquired from collection of Naturalis Biodiversity Center (Appendix Table 1). Lastly, six indices were calculated to provide morphometrical guidance for the comparison for the cranium and the mandible, presented in Figure 14 (I1= FL/BL; I2=GBIF/DEL; I3=IFL/DEL; I4=PL/DEL; I5=PB/DEL; I6=dl/al, I7= ABL/BL; I8= ABB/BL; and I9= ABB/GNB); for measurements abbreviations see Table 1.

2.2.2 Dental material

The dental terminology and metrics used for describing dental structures adhere follow Palacios and López-Martínez (1980). Lower-case letters refer to the lower dentition, and upper-case letters to the upper dentition. Figures 3A-B displays the placement of enamel structures in p3 and P2, as described by White (1991), along with corresponding terminology. The general enamel p3 pattern of Leporidae is classified according to the combination of presence/absence or degree of three characteristics: 1) anteroflexid (morphotypes A0-A1), 2) morphostructures between the trigonid and talonid (morphotypes PR0-PR4), and 3) paraflexid (morphotypes Pa0-Pa2). This classification pattern is presented in Figure 3C.

The measurements were taken with the assistance of a binocular microscope with a camera lucida and ocular micrometer (electronic micrometer bounded on binocular Wild orthoscope). The material was measured twice, to minimize the "metering error". All data measurements are provided in millimeters and rounded to the 2nd decimal place for the best possible accuracy. Dental measurements were taken to determine the maximum antero-posterior or bucco-lingual dimensions of the two-dimensional dental structures in the orthogonally prismatic shaft. Table 2 provides the abbreviations and explanations for the measurements. The selected taxa for comparison based on p3 and P2 are presented in Table 3 and Table 4 respectively. The P2 and p3 measurements of the comparative material are provided in Table 22, while for MVL they are presented in Table 9.

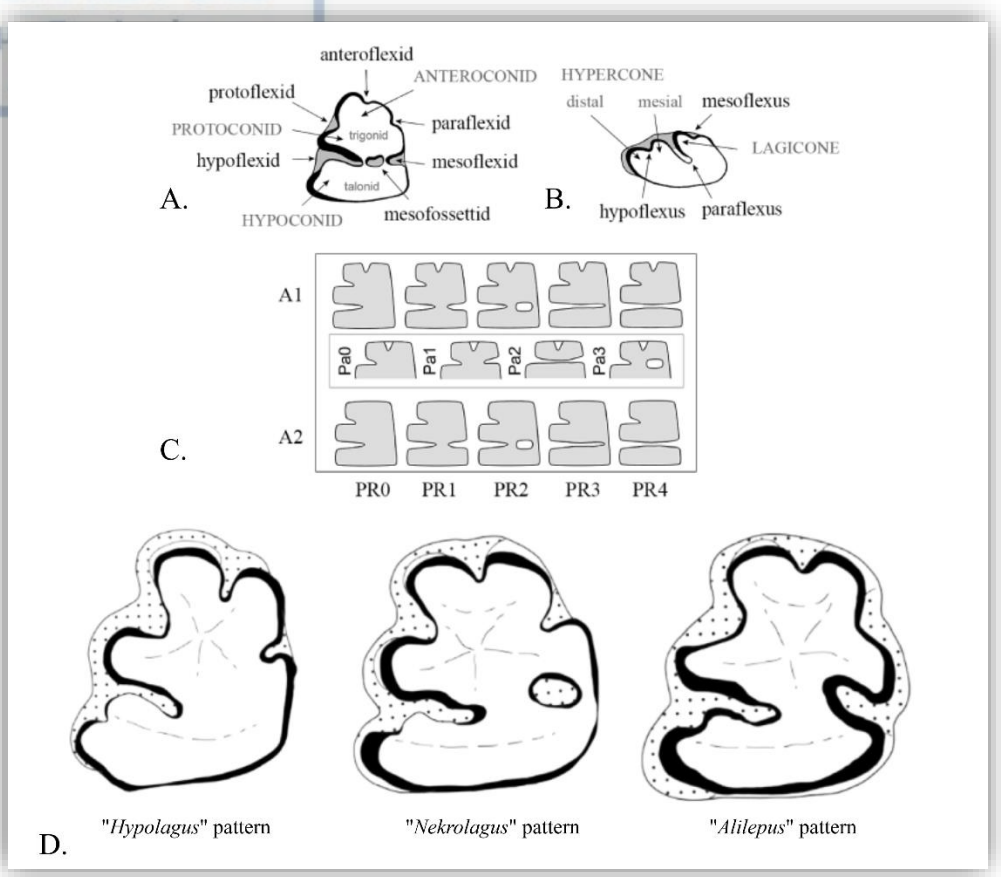

Figure 3. Dental terminology and morphology of leporid p3 and P2. ***A)*** Terminology and position of enamel structures in p3 (after Palacios and López-Martinez, 1980). ***B)*** Terminology and position of enamel structures in P2 (after Palacios and López-Martinez, 1980) ***C)*** Categorization of basis enamel p3 patterns based on the combination of **1)** the presence or absence of anteroflexid (morphotypes A0-A1), **2)** development of morphostructures between trigonid and talonid (morphotypes PR0-PR4), and **3)** development of paraflexid (morphotypes Pa0-Pa3) (after Čermak et al., 2015). ***D)*** Presentation of the "*Hypolagus*", "*Nekrolagus*", and "*Alilepus*" p3 pattern (illustrations after Sen and Geraads, 2023).

Table 2. Dental measurements used in this study.

	Abbrevation	**Measurement**
Upper dentition	I1L	Length of the first upper incisor
	I1W	Width of the first upper incisor
	I2L	Length of the second upper incisor
	I2W	Width of the second upper incisor
	P2L	Length of the second upper premolar
	P2W	Width of the second upper premolar
	P3L	Length of the third upper premolar
	P3Want	Width of the third anterior upper premolar
	P3Wpost	Width of the third posterior upper premolar
	P4L	Length of the fourth upper premolar
	P4Want	Width of the fourth anterior upper premolar
	P4Wpost	Width of the fourth posterior upper premolar
	M1L	Length of the first upper molar

	M1Want	Width of the first anterior upper molar
	M1Wpost	Width of the first posterior upper molar
	M2L	Length of the second upper molar
	M2Want	Width of the second anterior upper molar
	M2Wpost	Width of the second posterior upper molar
	M3L	Length of the third upper molar
	M3W	Width of the third upper molar
Lower dentition	iL	Length of the first lower incisor
	iW	Width of the first lower incisor
	p3L	Length of the third lower premolar
	p3W	Width of the third lower premolar
	p4L	Length of the fourth lower premolar
	p4Ltrig	Length of the trigonid of the fourth lower premolar
	p4Ltal	Length of the talonid of the fourth lower premolar
	p4Wtrig	Width of the trigonid of the fourth lower premolar
	p4Wtal	Width of the talonid of the fourth lower premolar
	m1L	Length of the first lower molar
	m1Ltrig	Length of the trigonid of the first lower molar
	m1Ltal	Length of the talonid of the first lower molar
	m1Ltrig	Width of the trigonid of the first lower molar
	m1Wtal	Width of the talonid of the first lower molar
	m2L	Length of the second lower molar
	m2Ltrig	Length of the trigonid of the second lower molar
	m2Ltal	Length of the talonid of the second lower molar
	m2Wtrig	Width of the trigonid of the second lower molar
	m2Wtal	Width of the talonid of the second lower molar
	m3L	Length of the third lower molar
	m3Ltrig	Length of the trigonid of the third lower molar
	m3Ltal	Length of the talonid of the third lower molar
	m3Wtrig	Width of the trigonid of the third lower molar
	m3Wtal	Width of the talonid of the third lower molar
	dL	Length of the lower diastema
	aL	Length of the lower alveolar

During the Late Miocene, leporids of the Old World exhibited a great degree of morphological and taxonomic variety. There are one Archaeolaginae and three Leporinae genera reported from this period in Eurasia and known by their dentition, used in the comparisons: 1. *Hypolagus* from MN13 (Averianov, 1996; Čermák, 2009); 2. *Alilepus* from MN12 (Flynn et al., 2014); 3. *Pliopentalagus* from late MN13 (Tomida and Jin, 2009); and 4. *Trischizolagus* from MN13, whose record is however questionable (López Martínez et al., 2007; Čermák and Wagner 2013). Their taxonomy has been largely based on the morphology of the lower third premolar, which has been extensively studied (Dice, 1931; López Martínez et al., 2007; Čermák and Wagner 2013).

Dental comparison with *Trischizolagus* includes the species: *T. crusafonti* (Janvier and Montenat, 1971), *T. dumitrescuae*, *T. gambariani* (Melik-Adamyan, 1986), *T. maritsae*, *T. mirificus* Qiu and Storch, 2000, *T. nihewanensis* (Cai, 1989), *T. meridionalis*, and *T. raynali* (Geraads, 1994). Furthermore, the previously reported material of *T. dumitrescuae* and *T.* cf. *maritsae* from Megalo Emvolon (Koufos and Koliadimou, 1993) is also incorporated for the purpose of comparison. Recent species

are excluded from dental comparison due to their advanced characters. For consistency only adult specimens were used for size and morphological comparisons.

Table 3. List of the comparative taxa examined for the upper dentition in this study.

Species	Reference	Location	Age
T. dumitrescuae	Koufos and Koliadimou (1993); original comparison	Megalo Emvolon (Greece)	Pliocene, late Ruscinian (MN15) (Vasileiadou and Sylvestrou, 2022)
T. cf. *maritsae*			
T. dumitrescuae	Crespo et al. (2022)	Măluşteni (Romania)	Early Pliocene (MN14/15) (Crespo et al., 2022)
T. dumitrescuae		Berești (Romania)	Early Pliocene (MN14–15) (Crespo et al., 2022)
T. dumitrescuae	Averianov and Tesakov (1997)	Novaya Andriashevka (Moldova)	Early Pliocene, early Ruscinian (MN14) (Averianov and Tesakov, 1997)
T. dumitrescuae		Grebeniki 2 (Ukraine)	Early Pliocene, early Ruscinian (MN14) (Averianov and Tesakov, 1997)
T. dumitrescuae		Lucheshty (Moldova)	Early Pliocene, late Ruscinian (MN15) (Averianov and Tesakov, 1997)
T. maritsae	Koufos and Koliadimou (1993); original comparison	Maritsa (Greece)	Late Miocene, Turolian (MN13) (Hordijk and de Bruijn 2009)
T. crusafonti	Janvier and Montenat, 1971; Koufos and Koliadimou (1993)	La Alberca (Spain)	Late Miocene, Turolian (MN13) (Sen, 2020)
T. crusafonti	Sen (2020)	Dorkovo (Bulgaria)	Early Pliocene, early Ruscinian (MN14) (Sen, 2022)
T. meridionalis	Sen and Geraads (2023)	Ahl al Oughlam (Morocco)	Late Pliocene - Early Pleistocene (MN16) (ca. 3.0-2.5 Ma)
T. gambariani	Čermak et al. (2019)	Tepe Alagöz (Turkey)	Early Pliocene, early Ruscinian (MN14) (Čermak et al., 2019)
T. mirificus	Qiu and Storch (2000)	Bilike (China)	Early Pliocene, early Ruscinian (MN14) (Qiu and Storch, 2000)

Table 4. List of the comparative taxa examined for the lower dentition in this study.

Species	Reference	Location	Age
T. dumitrescuae	Koufos and Koliadimou (1993); original comparison	MEV Megalo Emvolon (Greece)	Pliocene, late Ruscinian (MN15) (Vasileiadou and Sylvestrou, 2022)
T. cf. *maritsae*			
T. dumitrescuae	Crespo et al. (2022)	Măluşteni (Romania)	Early Pliocene (MN14/15) (Crespo et al., 2022)

T. dumitrescuae	Čermak and Wagner (2013)	Berești (Romania)	Early Pliocene (MN14–15) (Crespo et al., 2022)
T. dumitrescuae		Beremend 39 (Hungary)	Pliocene, late Ruscinian (MN15b) (Čermak and Wagner, 2013)
cf. *Trichizolagus dumitrescuae*		m ?Beremend [?4] (Hungary)	?MN 15/16 (Čermak and Wagner, 2013)
T. dumitrescuae	Averianov and Tesakov (1997)	Novaya Andriashevka (Moldova)	Early Pliocene, early Ruscinian (MN14) (Averianov and Tesakov, 1997)
		Grebeniki 2 (Ukraine)	Early Pliocene, early Ruscinian (MN14) (Averianov and Tesakov, 1997)
		Nikolskoe (Moldova)	Early Pliocene, early Ruscinian (MN14) (Averianov and Tesakov, 1997)
		Stavnichevo (Ukraine)	Early Pliocene, early Ruscinian (MN14) (Averianov and Tesakov, 1997)
		Moskovei (Moldova)	Early Pliocene, late Ruscinian (MN15) (Averianov and Tesakov, 1997)
		Lucheshty (Moldova)	Early Pliocene, late Ruscinian (MN15) (Averianov and Tesakov, 1997)
		Tatareshty (Moldova)	Early Pliocene, late Ruscinian (MN15) (Averianov and Tesakov, 1997)
T. dumitrescuae	Averianov (1995)	South Moldova	Early Pliocene
T. aff. *T. dumitrescuae*	Wu and Flynn (2017)	Yushe Basin (China)	Late Pliocene/Early Pleistocene
T. meridionalis	Sen and Geraads (2023)	Ahl al Oughlam (Morocco)	Late Pliocene - Early Pleistocene (MN16) (ca. 3.0-2.5 Ma)
T. crusafonti	Janvier and Montenat, 1971; Koufos and Koliadimou (1993)	La Alberca (Spain)	Late Miocene, Turolian (MN13) (Sen, 2020)
T. crusafonti	Sen (2020)	Dorkovo (Bulgaria)	Early Pliocene, early Ruscinian (MN14) (Sen, 2022)
T. gambariani	Čermak et al. (2019)	Tepe Alagöz (Turkey)	Early Pliocene, early Ruscinian (MN14) (Čermak et al., 2019)
T. maritsae	Koufos and Koliadimou (1993)	Maritsa (Greece)	Late Miocene, Turolian (MN13) (Hordijk and de Bruijn 2009)
T. mirificus	Qiu and Storch (2000)	Bilike (China)	Early Pliocene, early Ruscinian (MN14) (Qiu and Storch, 2000)
T. nihewanensis	Tomida and Qiu (2005)	Hebei (China)	Late Pliocene (MN16) (Tomida and Qiu, 2005)
T. rayneli	Geraads (1994)	Rhino Cave (Morocco)	Middle Pleistocene

2.2.3 Postcranial material

Leporid postcranials are abundant in MVL, with multiple specimens of several bone groups. The measurements were obtained using an electronic caliper that has an accuracy of 0.1 mm. The measurements were taken twice to avoid any metrical error. The metrics used to describe the fossilized remains in the postcranial material follow the methods outlined by Fostowicz-Frelik (2007) and Pelletier et al. (2015). The measurements and indices used are either conventional, based on the largest dimensions of bones and specific structures or considered to have functional significance. The indices were calculated using the mean values for MVL sample. Table 5 provides abbreviations and explanations for the postcranial measurements presented, while Table 6 gives used indices along with their description. Complete measurements of the postcranial material of the leporids of MVL are presented in Tables 11-21. Additionally, boxplots of the postcranial indices are shown in Figures 17–23, and the index list is included in Tables 23–29.

Comparisons were carried out with the modern skeletons of *L. europaeus*, *O. cuniculus*, *S. floridanus*, and *Pentalagus furnessi* (Stone, 1900), based on the available data by Fostowicz-Frelik (2007). The selected comparative measurements are presented in the Appendix Table 4. Additionally, photographic material as well as measurements for *L. europaeus, O. cuniculus*, and *S. floridanus* were used by the OsteoID Bone Identification database (https://boneidentification.com/). Further comparative analyses of fossilized taxa were made based on the data given for *H. beremendensis* (Fostowicz-Frelik, 2007), *T. dumitrescuae* (Averianov, 1995), and *T. meridionalis* (Sen and Geraads, 2023). Due to a lack of comparative material, the atlas, axis, and vertebra are not included in the comparative chapter.

Table 5. Postcranial measurements used in this study.

Skeletal part	Abbrevation	Measurement
Scapula	Wscapr	Proximal width
	Lnsca	Smallest length of the collum scapulae
	Lpasca	Greatest length of the processus articularis
	Bglsca	Breadth of the glenoid cavity
Humerus	Lhu	Length
	Whupr	Proximal width
	Wshu	Width of shaft
	Whud	Maximum distal width
	Dhupr	Depth of the proximal end
	Bthu	Breadth of trochlea
	Bdhu	Smallest breadth of diaphysis
	Dhud	Distal humeral anteroposterior diameter
	Dhup	Proximal humeral anteroposterior diameter
Radius	Lra	Maximum length
	Wrapr	Proximal width
	Drapr	Proximal anteroposterior diameter
	Wrash	Width of shaft
	Wrad	Maximum distal width
Ulna	Lul	Maximum length
	Wulpr	Proximal width
	Dulol	Minimum olecranon anteroposterior depth

	Lulol	Length of olecranon
	Wulraf	Width of radial articular facets
	Dulpa	Depth across the processus anconaues
Coxal	Dac	Acetabulum diameter
	Lisch	Length of ischium
	Wilb	Width of body of ilium
	Lac	Length of acetabulum
	Hac	Height of acetabulum
Femur	Lfe	Length
	Lfecph	Greatest length from caput femoris - head
	Wfepr	Proximal width
	Bfetrt	Greatest breadth of the region of the trochanter tertius
	Wfedis	Distal width
	Dfed	Distal femoral anteroposterior diameter
	Wintf	Width of intercond fossa
	Wpag	Width of patellar groove
	Hdis	Diameter of distal extremity
	Whe	Width of the head
	Wfesh	Width of the shaft
	Tfesh	Thickness of the shaft
	Dfepr	Proximal femoral transversal diameter
Tibiofibula	Lti	Length
	Wtipr	Proximal width
	Wtish	Width of shaft
	Wtidis	Distal width
	Ttidis	Distal thickness
	Dtipr	Proximal thickness
	Ttipr	Proximal diameter
	Htitu	Height of tibial tuberosity
Astragalus	Las	Length
	Was	Width of trochlea tali
	Lasn	Length of neck
Calcaneus	Lca	Length
	Wca	Width
	Lcat	Length of calcaneal tuber
	Lcab	Length of calcaneal body
	Wcat	Width of calcaneal tuber
Navicular	Lnab	Length of navicular body
	Lnat	Length of the tuberosity
	Wna	Width of navicular body
	Tna	Thickness of naviculare
Cuboid	Lcu	Length
	Wcu	Width
	Tcu	Thickness

Table 6. Postcranial indices used for this study according to Fostowicz-Frelik (2007).

Skeletal part	**Description**
Humerus	Lhu1 = Whupr/Lhu
Coxal	Ico1 = Lac/Hac
	Ico2 = Lac/Wilb
Femur	Ife1 = Wfepr/Lfe

	Ife2 = Wfedis/Lfe
	Ife3 = Wintf/Wfedis
	Ife4 = Wpag/Wfedis
	Ife5 = Wfedis/Hdis
Tibia	Iti1 = Ttipr/Wtipr
	Iti2 = Wtipr/Lti
	Iti3 = Htitu/Lti
	Iti4 = Ttidis/Wtidis
	Iti5 = Wtidis/Lti
	Iti6 = Wtish/Lti
Astragalus	Ita1 = Was/Las
	Ita2 = Las/Las
Calcaneus	Ica1 = Wca/Lca
	Ica2 = Lcat/Lca
	Ica3 = Lcab/Lca
	Ica4 = Wcat/Lcat
Navicular	Ina1 = Lnab/Lnat
	Ina2 = Wna/Tna
	Ina3 = Lnab/Wna
Cuboid	Icu1 = Lcu/Wcu
	Icu2 = Wcu/Tcu

2.2.4 3D scanning

The specimens MVL-47, MVL-48, MVL-63, and MVL-64 underwent surface scanning using Artec Micro, kindly provided by the Department of Palaeoanthropology of the University of Tübingen. Artec Micro is a fully automated desktop 3D scanner that is designed to provide high-quality scans. It employs advanced blue LED lights and twin-color cameras, synchronized within its dual-axis rotation system, encompassing swing and rotation movements.

The specimens were positioned on the circular scanning platform and subsequently scanned. Artec Micro offers high 3D accuracy, with precision as fine as 0.01 mm and a 3D resolution of up to 0.029 mm. Moreover, it supports full-color scanning and enables target-free scanning. Following scanning, the data was processed and edited using the open-source software MeshLab to further simplify them. The scans presented here have undergone a significant reduction in file size, with up to 75% compression due to their high-resolution nature. The 3D scans of these specimens can be found in the Appendix II (Figs. 1-19).

2.2.5 Estimated body mass (BM)

In the present study, a total of fourteen regressions that consistently displayed strong accuracy were employed from Moncunill-Solé et al. (2015) to assess the body size estimation. Given the inclusion of the numerus teeth, cranial, and postcranial components in the material, and that not all samples are associate with a specific individual, the intention was to attain a more comprehensive perspective of the estimation. As mentioned by Moncunill-Solé et al. (2015), it is crucial for these models to display high r^2 values and low values for both the standard error of estimate (SEE) and the high accuracy percentage (%PEE). These criteria indicate a high level of

accuracy. The regression selected for the BM estimations are presented on Table 7. In addition, comparative remarks were carried out with the recent *L. europaeus*, *O. cuniculus*, *S. floridanus*, and *Pentalagus furnessi* based on the data by Fostowicz-Frelik (2007). Due to the limited available data, for the fossil species *T. dumitrescuae*, *T. meridionalis*, *T. crusafonti*, *T. gambariani*, and *T. maritsae* mainly the dental proxy of the m1wtrig was used for the estimations.

Table 7. Teeth, skull, and postcranial regression model for the estimation of the body mass (BM) of the leporids of MVL, according to Moncunill-Solé et al. (2015). SEE (standard error of the estimation), %PEE (average absolute per cent prediction).

Bone	**Regression**	**r^2**	**SEE**	**%PEE**
Teeth	log BM = 1.778 + (2.959 * log m1wtrig)	0.832	0.115	20.201
	log BM= 0.547+(2.247 * log TRL)	0.668	0.151	29.133
Skull	log BM = - 1.526 + (4.091 * log GBOC)	0.957	0.115	21.331
Femur	log BM = - 1.110 + (2.229 * log Lfe)	0.961	0.102	19.080
	log BM = 0.498 + (2.217 * log Wfepr)	0.970	0.089	16.747
	log BM = 0.225 + (2.630 * log Dfed)	0.954	0.111	20.331
Humerus	log BM = - 1.221 + (2.418 * log Lhu)	0.949	0.117	22.749
	log BM = 0.949 + (2.191 * log Dhup)	0.876	0.086	17.080
	log BM= -0.063+(3.386 * log Dhud)	0.894	0.079	14.871
	log BM = 0.934 + (2.393 * log Whud)	0.875	0.087	15.997
Tibia	log BM= -1.271+(2.254 * log Lti)	0.930	0.136	27.826
	log BM = 0.599 + (2.265 * log Ttipr)	0.960	0.103	19.429
	log BM = 0.219 + (2.577 * log Wtipr)	0.976	0.080	14.353
	log BM = 0.461 + (2.584 * log Wtidis)	0.970	0.089	15.427

3. Systematic Paleontology

3.1. Descriptions

3.1.1 Cranium

Referred material: MVL-46, MVL-47, MVL-48, MVL-49, MVL-50, MVL-51, MVL-52, MVL-58, MVL-59, MVL-62, MVL-73a. According to the cranial material the NISP is 26. The MNI is 13.

Dorsal view of the skull. The nasals are located medially on the rostrum, whereas the maxillary corpus is located laterally. The most lateral part of the skull, the zygomatic arch, comprised of the jugal, the zygomatic process of the maxilla, and the zygomatic process of the squamosal. The lacrimal is placed on the rostral edge of the orbit. The rather long frontal is located in the center of the dorsal skull and forms prominent postorbital processes, which protrude posteriorly and have a thin thorn-like appearance. The parietal and interparietal comprise the bulbous braincase, whose most caudal portion cannot be observed in dorsal view due to poor preservation (Figs. 4 A1, B1).

Lateral view of the skull. To the lateral rostrum belong the nasal, located dorsally, the overall long premaxilla, anteroventrally, and the maxilla, posteroventrally, pierced by the infraorbital foramen. The upper tooth row consists of two incisors, three premolars, and three molars. The premaxilla carries the upper two incisors. The body of the maxilla is located between the premaxilla and the anterior orbital rim. The zygomatic arch protrudes laterally with a nearly horizontal way. The orbit is large, located nearly in the center of the skull, and is comprised of part of the frontal with its postorbital process, the lacrimal, and the orbitosphenoid. The braincase appears to have an oval shape overall. Parietal and squamosal bones create the lateral surface, whereas interparietal and supraoccipital bones seal the braincase in a caudal direction. Due to the poor preservation of the occipital area in almost all cranial specimens, the facial tilt could only be calculated for the MVL-47 and MVL-48. The angle of facial tilt was approximately 38^{o} for MVL-47, and 43^{o} for MVL-48 (Figs. 4 A3, A4, B3, B4)

Ventral view of the skull. The palatine process of the maxilla and the hard palate are visible on the rostral portion of the ventral side. The palate is long, extending to the level of the upper second molar, and is pierced by the midline palatal vacuity. This opening is bordered anteriorly by the premaxillae, laterally by the maxilla, and posteriorly by the palatines, roofed by the vomer. On the palatine process of the maxilla, and at the level of the fourth premolar opens a small premolar foramen. Each palatine is pierced by a small foramen. The area between the third molar and the alisphenoid and basiooccipital is damaged in all specimens. The posterior part of the skull is rather poorly preserved. Between the auditory bullae is the basioccipital. The auditory bullae although poorly preserved appear to be small and inflated. Also visible on the auditory bullae in some specimens is the external acoustic meatus (Figs. 4 A2, B2).

Occipital view of the skull. The occipital side of the skull is the most damaged part in all specimens. Thee inflated auditory bullae and the foramen magnum dominate the occiput. The foramen magnum is roughly sub-circular, and lateral-positioned are the occipital condyles, which are slightly medially inclined, forming a wide U-shaped morphology. Lateral to the foramen magnum are the thorn-shaped paroccipital processes of the exoccipital.

Table 8. Measurements of the MVL crania (in mm).

Abbrevation	MVL-46	MVL-47	MVL-48	MVL-49	MVL-50	MVL-51	MVL-52	MVL-73a
CL	-	78.73	81.53	-	-	-	-	-
BL	-	70.01	71.06	-	-	-	-	-
DEL	37.5	42.31	42.16	38.9	-	-	-	42.38
DIL	20.02 (dex), 20.11 (sin)	21.98 (dex), 22.1 (sin)	21.95 (dex), 22.1 (sin)	20.03 (dex), 20.15 (sin)	-	-	-	22.18 (dex)
CTL	15.3 (dex)	16.94 (dex), 16.88 (sin)	16.58 (dex)	16.31 (dex), 16.55 (sin)	16.41 (sin)	15.89 (sin)	15.69 (dex), 15.4 (sin)	16.93 (dex)
GLN	34.79	35.52	-	-	-	-	-	-
GBN	-	15.92	17.92	16.1	17.45	-	16.84	-
FL	35.77	33.23	33.17	31.19	33.65	-	-	-
VL	29.43	29.36	31.48	28.59	-	-	-	-
IFL	19.8	21.47	21.75	20.26	-	-	-	20.83
GBIF	7.5	6.72	7	7.43	6.82	-	6.65	6.04
PL	6.88	6.52	7.25	6.71	7.29	-	6.51	6.76
PB	11.33	10.55	10.51	11.51	10.15	-	10.34	10.21
CB	6	7.2	6.9	6.7	6.9	-	7.1	-
LAZ	5.7	6.45	6.7	5.55	6.5	-	6.05	-
OZB	36.58	37.08	38.6	37.11	-	-	35.26	-
AZB	35.07	34.97	40.8	39.34	-	-	-	-
GBOC	-	-	15.98	-	-	14.96	-	-
GNB	25.36	26.07	31.85	29.21	-	28.24	-	-
BS	-	-	26.92	25	-	25.93	-	-

3.1.2 The skull bones

Nasals. The paired nasals form the roof of the nasal cavity and the dorsal surface of the rostrum, extending to the level of the anterior orbit. Due to their general fragility, only the imprint of the nasals is preserved in the majority of specimens, including, MVL-46, MVL-48 and MVL-49, while the posterior portions are preserved in MVL-50 and in a rather bad condition in MVL-52. The anterior region of the skull in MVL-51, including the nasals, is destroyed. MVL-73a also has the nasals destroyed. However, the complete nasal bones can be observed in MVL-47 in excellent condition. The nasals are broadest posteriorly to their narrowest point at their straight suture with the frontal bones and taper anteriorly at the anterior nasal aperture. The muzzle can be described as overall long and wide. The suture between the nasal and frontal bones forms a forward pointing V that extends slightly beyond the zygomatic shoulders and reaches approximately the level of the P4-M1 limit. In MVL-47, the dorsal sides of the nasals are somewhat concave over the majority of their anteroposterior length, but at the base of the frontal process, they become sub-horizontal. A thin and very prominent posterodorsal process

of the premaxilla contacts the nasal bones and separates them from the premaxilla. The posterodorsal process of the premaxilla is recovered in MVL-47 and MVL-48, at the left side of MVL-49 and MVL-46, at the posterior parts of MVL-50, and at the anterior parts of MVL-73a. A field of neurovascular foramina is located at the lateral border of the dorsal surface of each nasal, arranged along the premaxilla's nasal process. Except for MVL-47, similar fenestrations are visible in the preserved nasals of MVL-46 and MVL-50.

Premaxilla. The paired premaxillae are relatively long and bear both pairs of upper incisors. It creates the anterolateral portions of the rostrum and contribute to the anterior part of the palate. In MVL-46, MVL-47, MVL-48, MVL-49, and MVL-73a, both premaxillae are overall preserved. The premaxilla of the remaining specimens has been severely damaged; thus, they cannot be evaluated for morphological descriptions. The premaxilla can be split into two parts, the corpus (body) and three processes: a nasal process, a palatine process, and a maxillary process. On the premaxillary corpus are located the alveoli for both pairs of incisors. Both pairs of incisor alveoli are situated on the premaxillary corpus. The alveolus for the anterior upper incisor (I1) is proportionally bigger and located more anteriorly and dorsally than the alveolus for the posterior upper incisor (I2). Throughout the whole anteroposterior length of the premaxillary corpus, both alveoli are posteriorly extending and dorsally curving. Dorsally located on the premaxillary corpus are multiple small neurovascular foramina present on its lateral surface. These foramina can be seen as a significant fenestration, albeit of a much smaller size than those described above. Furthermore, in lateral view, at the premaxilla and maxilla suture of MVL-46, MVL-47, and MVL-73a, a significantly larger, narrower, and longer fenestration occurs. In ventral view, the length of the premaxilla occupies approximately half of the diastema. The two premaxillae are robust, nonparallel, and form an angle of approximately 35^{o} with the first incisor roots at their apex.

In dorsal view, the nasal process of the premaxilla extends posterodorsally from the corpus. It possesses a rather sharp ventral edge and is anteroposteriorly elongated, dorsally curved, and sub-triangular in shape. The nasal process terminates anterior to the apex of the frontal process of the nasals, as seen in the available specimens. Throughout its entire anteroposterior length, the medial surface of the nasal process of the premaxilla is in contact with the lateral process of the premaxilla. The maxillary process of the frontal, which divides the premaxilla from the maxilla in dorsal view, is in touch with the ventrolateral side of the nasal process. In ventral view, the palatine process of the premaxilla is poorly preserved. It can only be observed in MVL-46, MVL-47, and MVL-73a, extending posteriorly from the anteromedial surface of the premaxillary corpus. It is slender mediolaterally and elongated anteroposteriorly. The anterior roof of the palatine process is located approximately 2 mm below the alveoli of I2. The posterior area is destroyed.

Maxilla. In the posterolateral areas of the palate and rostrum, the paired maxillae are located. In addition, they support all of the cheek teeth, form the ventral and ventromedial sections of the orbital walls, and contribute to the anterior orbital edge. In most of the specimens, the maxilla is well preserved, except for MVL-50, MVL-51, and MVL-52. MVL-50 and MVL-52 have poorly preserved anterior parts of the maxilla, and the posterior parts are abraded. In ventral view, only the medial and posterior parts of the left maxilla have been preserved in MVL-51. The maxillary corpus exhibits a roughly trihedral form. The lateral wall of the maxillary corpus is

perforated by numerus small openings. These fenestrations can be observed on the anteroventral and dorsal surfaces of the maxillary corpus. All specimens show a big, sub-circular infraorbital foramen on the lateral side of the maxillary corpus.

The anterior-ventral part of the maxillary corpus has a narrow fissure that runs from the back to the front. This fissure is surrounded by a series of long ridges and troughs that run from the front to the back. When looked at, these ridges and valleys fit tightly with a series of similar structures on the back and front of the maxillary process of the premaxilla. This makes a suture between the premaxilla and maxilla. The facial tuberosity is not well pronounced.

The palatine process of the maxilla is preserved in all specimens with the exception of MVL-51, which lacks its right side. The anterior palatine foramen is long, extending posteriorly to the limit of P2. Anteromedially and posteromedially of the palatine process, a small triangular cape is observed, which is more pronounced anteromedially. In posteroanterior view, this triangular cape creates the nearly heart-shaped impression of the anterior palatine foramen.

Palatine. The palatine bone is a solitary and unpaired anatomical structure situated at the posterior end of the maxillae, forming the posterior portion of the hard palate. In all specimens, most parts of the palatine are preserved, enabling a detailed description of its anatomy. In MVL-46, MVL-47, and MVL-48, the palatine is completely preserved; in MVL-50 and MVL-52, only the anterior parts are preserved. In MVL-51, part of the left medial side is preserved, and in MVL-73a, the right medial side. In MVL-49, the palatine is rather abraded.

In each hemipalatine, a lateral perpendicular lamina (portion) and a medial horizontal lamina can be observed. The latter forms almost the whole surface of the palatine and approximately the posterior half of each side of the hard palate. In ventral view, the walls seem to have a slight slope, and the margins seem to narrow from top to bottom. The anterior margin is located at the level of the anterior part of P4, and the posterior margin bears a very notable nasal spine, medially. The sub-circular premolar foramen is located on the maxilla-palatine suture, anterolaterally. In MVL-46 and MVL-50, the premolar foramen shows a slight posterior placement, below the suture. Posteriorly and posteromedially to the major palatine foramen, the palatine surface has several smaller additional foramina. It’s worth mentioning that MVL-46 displays an additional prominent foramen on the level of the anterior portions of M2. The presphenoid and vomer are completely damaged and hence cannot be described.

Zygomatic and squamosal. The zygomatic is a paired bone forming the middle part of the zygomatic arch. It is positioned between the maxilla and the squamosal. In the vast majority of the specimens, both of the zygomatic bones are preserved. In MVL-47, MVL-48, and MVL-49, both zygomatics are maintained in their entirety. Only the right zygomatic is intact in MVL-46, whereas the left zygomatic is preserved in MVL-50, MVL-51, and MVL-52. In the rest of the specimens, only the zygomatic process is present. Anteriorly, the maxilla's zygomatic process and the zygomatic are extensively united to form a distinct V-shaped structure that is positioned horizontally on the bone. The zygomatic is the broadest anteriorly and mediolaterally and forms a basket-handle type of arch morphology. Its dorsoventral height gradually increases posteriorly until the middle of the bone and decreases abruptly posteriorly to its end. Its mediolateral width seems to decrease posteriorly to its anterior end and remain constant throughout the remainder of its anteroposterior length, although the preservation of the specimens

is very poor due to their general fragility. The zygomatic has a concavity in both the lateral and medial ides, with the concavity on the lateral surface creating a prominent zygomatic fossa.

The internal lateral surface of the middle cranial fossa is formed by the squamosal, which resides in the lateral region of the braincase. It can be observed in all studied specimens, except MVL-73a. It consists of an anterolaterally protruding zygomatic process and the squama of the squamosal. The cranial portion of the craniomandibular joint is influenced by the posterior region of the zygomatic process. The zygomatic process of the squamosal is not as broad as the zygomatic arch and is positioned above the posterior margin of the zygoma, giving an essentially trihedral morphology with a conspicuous oblique line extending anteriorly in lateral view. Lastly, in the majority of the specimens, the squamosal and its sutures with the frontal and parietal can be observed.

Frontal. The frontal is a large, paired bone that comprises the front portion of the skull's roof and creates the nasal cavity's posterior top. Additionally, they compose the dorsal sections of the orbital walls (pars orbitalis). Except for MVL-73a, in all the specimens, both frontals are well preserved. Furthermore, MVL-47, MVL-48, MVL-49, MVL-50, and MVL-51 exhibit complete frontals. In MVL-46, the frontal bone is crashed and damaged in numerous places, particularly on its left side. In MVL-52, only the anterior portion of the frontals is recovered.

The frontal bone can be separated into an orbital portion and the frontal squama, which are divided from each other by the supraorbital rim (infraorbital margin). The anterior part of the cranial roof and the posterior part of the dorsal wall of the nasal cavity are formed by the frontal squama. The dorsal surface seems to be relatively convex on most specimens, yet in MVL-49 and MVL-50 it’s more flattened. This may be the result of pressure being applied dorsoventrally to the cranium, causing some deformation and resulting in a slight dorsoventral compaction. Pitting is present on the dorsal surface of the frontal squama. Numerous small foramina on the external surfaces of the bones of the braincase can be observed in all specimens. Furthermore, in the specimens MVL-47, MVL-49, MVL-51, and MVL-52, the pitting is very prominent. Due to bad preservation, in MVL-46, MVL-48, and MVL-50, the pitting may not be so noticeable.

The orbital portion of the frontal bone is concave medially and laterally strongly arched. MVL-47 and MVL-51 display the most arched orbital portion of the frontal bone, and the rest of the specimens have been deformed due to taphonomy. In dorsal view, the supraorbital process is very prominent, forming a thorn-like morphology and extending ventrally to form part of the orbital wall. The lacrimal, squamosal, parietal, and posterior surface of the frontal process of the maxilla are all abutted by the orbital section of the frontal anteriorly. The lacrimal is positioned on the orbit's anterior wall. Due to poor preservation, the lacrimal as well as the orbits' oblique dorsolateral view cannot be described.

Parietal. The posterior ceiling of the skull is formed by the parietal pair, with the supraoccipital and interparietal adding a small basin and a thin strip in the posterior margin, respectively, and the squamosal contributing a narrow strip in the lateral and anterior-lateral edges. In the vast majority of the specimens but MVL-52 the parietal is preserved. The anterior roof of the parietal is only preserved in MVL-48. MVL-47 and MVL-50 have only the left parietal intact, while MVL-46, MVL-49, and MVL-51 have

the paired parietal overall preserved in good condition. The pitting continues and is also visible in most specimens, especially at the lateral suture with the frontal and squamosal. However, in MVL-46, MVL-48, and MVL-50, the pitting is less prominent.

The braincase seems to be globular, although in some specimens a slight deformation of the cranium can be observed, as mentioned. It is noteworthy that the parietal width of MVL-48 is significantly larger than that of the other specimens, that may have been cause by taphonomic deformation. The posterior suture between the parietals is raised as a low sagittal crest in MVL-46 and MVL-51. The interparietal and supraoccipital regions are damaged in all specimens.

Figure 4. A) The cranium of MVL-46 in ***(1)*** dorsal, ***(2)*** ventral, ***(3)*** left lateral, and ***(4)*** right lateral view. ***B)*** The cranium of MVL-47 in ***(1)*** dorsal, ***(2)*** ventral, ***(3)*** left lateral, and ***(4)*** right lateral view. Scale bar = 10 mm.

Basisphenoid, Pterygoid, Presphenoid, Alisphenoid. The presphenoid is connected to the basal sphenoid and is located on the ventral side of the cranium. The presphenoid bone forms the ventral and anterior boundaries of the optic foramen. Only in MVL-47

and MVL-48 is the presphenoid partially preserved. It is very thin and ventrodorsally concave. Positioned anterior to the basioccipital and posterior to the presphenoid, the basisphenoid is situated near the base of the middle cranial fossa. In ventral view, the basisphenoid forms an isosceles triangular shape, as seen in MVL-47 and MVL-48. Also, in MVL-46, the anterior portion of the basisphenoid is preserved, forming the top. On the top of the basisphenoid medially, in MVL-47 and MVL-48, the small yet prominent pituitary foramen can be observed. Anterolaterally to the basisphenoid, the paired pterygoids are extending. They are only poorly preserved in MVL-48, but in a bad condition that cannot be described. Lastly, the alisphenoids, firmly united with the basisphenoid ventrally, extend into the caudal orbital wall and continue to the caudal borders of the palatine bone, where they form the pterygoid process, which is damaged in all specimens.

Ectotympanic. The ectotympanic is situated in the posteroventrolateral area of the skull and supports the auditory bulla. MVL-47, MVL-48, MVL-50, MVL-51, and MVL-62 all preserve the ectotympanic. MVL-58 and MVL-59 are isolated auditory bullae. The external auditory meatus is visible on both sides of MVL-47 and MVL-48, on the left side on MVL-50 and on the right side of MVL-51 and MVL-62, in dorsal and lateral views. It has the shape of a canal that leads within the auditory bulla and is oriented posterolaterally. The canal's opening is large and oval. The auditory bullae are round, inflated, and have a smooth surface. The front end is more rounded than its posterior counterpart, which is somewhat more pointed. They are angled slightly toward the center of the skull. The petrosal, which occupies the posterodorsal region of the skull and is bordered anteriorly by the ectotymbanic, is poorly preserved in all specimens.

Occipital complex (Basiooccipital, Exoccipital, Supraoccipital). In the back of the cranium, the occipital bone forms a bony ring around the foramen magnum. Because of its general fragility, the occipital can only be seen to some extent in MVL-46, MVL-48, and MVL-51. The occipital comprises four portions: the basioccipital, exoccipitals, and supraoccipital. The posterior section of the cranial base is occupied by the basilar portion (basioccipital). It is only observable in MVL-48, which is in a good state, and partially in MVL-47, which is quite damaged. Anteroposteriorly, it occurs as a pair of lobes, narrower anteriorly and slightly broader posteriorly, approaching the foramen magnum. The paired lateral sections (exoccipitals) comprise the lateral borders of the foramen magnum and support the main portions of the occipital condyles. They are visible in MVL-48; however, their preservation is poor in MVL-47 and MVL-51. The exoccipital creates a thin paracondylar process lateral to the dorsal part of the occipital condyle. This process continues ventrolaterally, forming a prominent V-shaped morphology with the occipital condyles. The dorsolateral margins of the foramen magnum are formed by the supraoccipital. Only in MVL-51 are fragments of the supraoccipital visible yet somewhat poorly preserved; therefore, no anatomical description can be offered. As observed in MVL-47, MVL-48, and MVL-51, the foramen magnum, which is situated inside the occipital, has a subcircular appearance that is somewhat compressed in a ventral view anteroposteriorly. MVL-48 exhibits a somewhat larger foramen magnum, with wider-spaced occipital condyles.

3.1.2 Mandibles

Referred material: MVL-55 (dex i1-p3), MVL-63 (sin i1-m3), MVL-64 (sin i1-m2), MVL-65 (dex p3-m2), MVL-66 (dex i1-m3), MVL-67 (dex p3-m2), MVL-68 (sin p3-m3), MVL-69 (dex i1-m3), MVL-70 (dex p3-m3), MVL-71 (dex p3-m3), MVL-72 (sin

i1-m3) and MVL-73b (dex i1-m3 and sin i1-m2). The NISP for the mandibles is 16, while the MNI is 8.

With the exception of the damaged posterior parts of the mandibular ramus and coronoid process, the mandibles of the vast majority of specimens are well-preserved. Seven specimens (MVL-63, MVL-64, MVL-66, MVL-69, MVL-72, and MVL-73b) maintain the body (corpus), the diastema, and most of the teeth (Figs. 5A, B), whereas four specimens are more damaged and lack either the diastema or the dentition (MVL-55, MVL-67, MVL-70, and MVL-71). Only in MVL-68 are some areas of the fossa masseterica recovered (Fig. 5C).

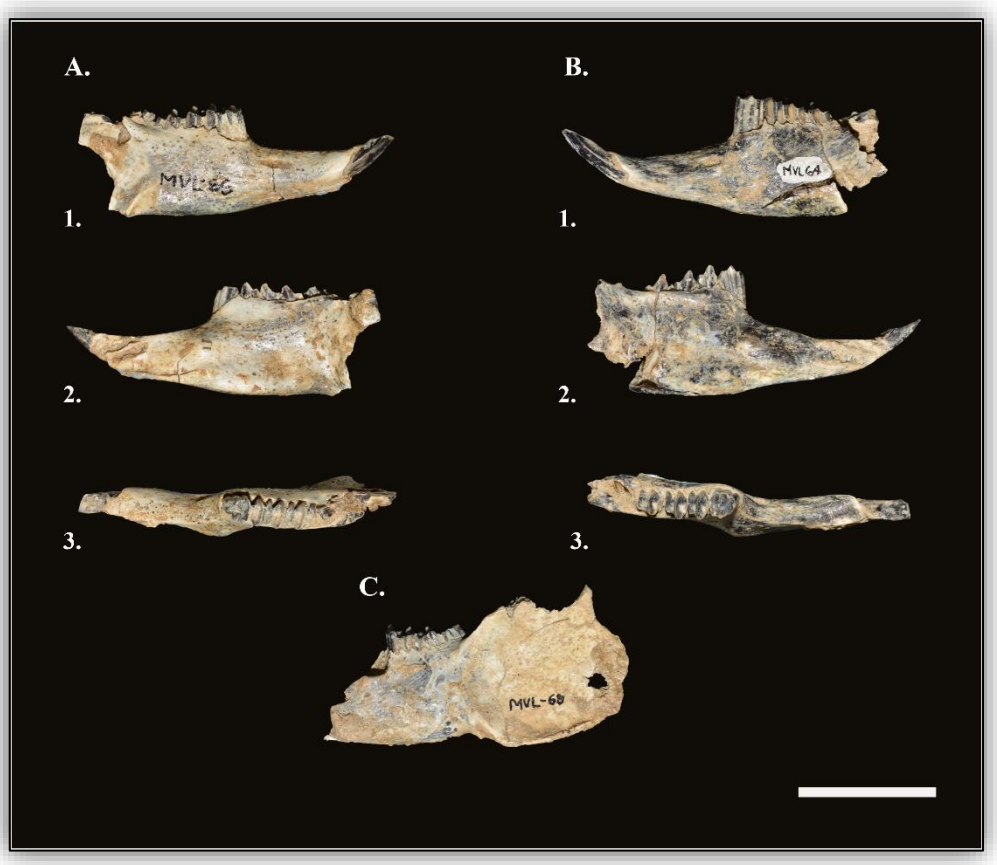

Figure 5. A) The right mandible MVL-66 in ***(1)*** lateral, ***(2)*** medial, and ***(3)*** dorsal view. ***B)*** The left mandible MVL-64 in ***(1)*** lateral, ***(2)*** medial, ***(3)*** dorsal view. ***C)*** The masseteric fossa of the left mandible MVL-68. Scale bar = 10 mm.

The two hemimandibles are united anteriorly at the mandibular symphysis to construct the mandible. MVL-73b is the only specimen with the two hemimandibles intact. The diastema is relatively long and slender, somewhat longer than the alveolar length of p3-m3. The alveolus for i1 is located anteriorly on the mandibular body. Apart from the m3 alveolus, which is noticeably smaller, the posterior dorsal side of the mandibular body contains alveoli for p3–p4 and m1–m3. These alveoli are approximately comparable in size. The dorsal side of the mandibular body is somewhat concave and contributes to the ventral half of the diastema, located posterior to the i1

alveolus and prior to the p3 alveolus. There is a mental foramen located approximately at the posterior 1/3 of the anteroposterior length of the diastema, which is likely homologous with the mental foramen in leporids located in a similar position (Wible, 2007). The buccal surface of the body is richly fenestrated. In addition, the lateral surface of the premaxillary corpus at the retromolar fossa bears a prominent and round-shaped neurovascular foramen dorsally. This foramen is only visible in MVL-63, MVL-70, MVL-73b, and partly in MVL-68. The lower incisive root protrudes from the lingual side of the body and extends posteriorly below the anterior border of p3. Lastly, for the mylohyoid muscle's insertion, the ventral side of the mandibular body has a noticeable mylohyoid line.

3.1.3 Upper teeth

Referred material: MVL-46 (dex I1-M3 and sin I1-M3), MVL-47 (dex P2-M3 and sin P2-M3) , MVL-48 (dex I1-I2, P3-M3 and sin I1-M3), MVL-49 (dex I1-I2, P3-M3 and sin I1-M3), MVL-50 (dex P2-M2 and P2-M3), MVL-51 (sin P2-M3), MVL-52 (dex P2-M3 and sin P2-M3), MVL-53 (dex P3-M2), MVL-54 (dex I1-I2 and sin I1-I2), MVL-56 (sin P3-M2), MVL-57 (dex P3-M2), MVL-73a (dex I1-M3 and sin I1-I2, P3), MVL-74 (dex I1-I2), MVL-76 (I1), MVL-80 (I2), MVL-81 (I2), MVL-85 (I1), MVL-153 (I1).

I1 and I2. In total, thirteen I1 (eight intact and five isolated) and twelve I2 (ten intact and two isolated) are preserved. The occlusal outline of the upper incisors has an asymmetrical quadrangle shape that extends anteriorly in its medial part. The anterior enamel is relatively thin with no substantial variation, with the anterior notch being shallow. It is V-shaped with widely opened walls and is not filled with cement. An anterior V-shaped notch separates the tooth into two parts of approximately equal anterior prominence. The breadth of the notch’s medial portion is narrower than its lateral halves. The second upper incisors are rounded and mediolaterally elongated. Encircling the teeth, the enamel is thin.

P2. Twelve P2 specimens are available, all of which are still intact in the maxilla. The occlusal outline of the teeth is generally oval. They display three flexa, of which the medial one, the paraflexus, is the deepest, while the hypoflexus and mesoflexus are shallower. Hypoflexus and mesoflexus are labially and anterobuccally situated. It’s to be noted that the paraflexus is well-defined in all specimens, while the mesoflexus and hypoflexus may be weak or almost absent. All flexa are filled with cement.

MVL-46 has a weak hypoflexus, with the left one being essentially nonexistent. The mesoflexus is shallow and forms a relatively wide V-shaped notch with a soft edge in both maxillae. MVL-47 likewise has a weak hypoflexus and a larger and deeper set of mesoflexus than MVL-46. The lone remaining P2 in MVL-48 has a weak hypoflexus, although not as weak as the other specimens, and a shallow and not as broad mesoflexus, as in MVL-46. In MVL-49, the hypoflexus produces a shallow and narrow notch, similar to MVL-48. The mesoflexus is shallow and broad. In comparison to the other specimens, MVL-49 exhibits the weakest mesoflexus. MVL-50, on the other hand, has a pair of well-defined hypoflexus, which are not as shallow as the rest of material, with the left being narrower than the right. The mesoflexus is shallow and broad in both maxillae. MVL-51's left maxillae have a substantially weaker hypoflexus and a shallow and narrow mesoflexus. In MVL-52, the hypoflexus is, as in MVL-51, a shallow and narrow notch, and the mesoflexus is broad and shallow, but in the right maxillae, the mesoflexus is more prominent and therefore considerably wider.

Furthermore, the hypoflexus is prominent in MVL-73a, with a shallow notch, while the mesoflexus is shallow and not as wide.

Table 9. Measurements of the upper dentition of the MVL sample (in mm).

	Diastema	Alveolar length	I1 L	I1 W	I2 L	I2 W	P2 L	P2 W	P3 L	P3 Want	P3 Wpost	P4 L	P4 Want	P4 Wpost	M1 L	M1 Want	M1 Wpost	M2 L	M2 Want	M2 Wpost	M3 L	M3 W
MVL-46 sin	20.15	-	2.29	2.85	1.40	1.45	2.03	4.00	2.55	4.20	5.00	2.40	4.55	4.66	2.30	4.50	3.79	2.35	3.70	3.30	-	-
MVL-46 dex	20.11	15.30	2.35	2.90	1.44	1.45	1.99	3.97	2.46	4.17	4.86	2.35	4.54	4.61	2.27	4.46	3.76	2.35	3.68	3.28	1.56	1.87
MVL-47 sin	22.00	17.00	-	-	-	-	2.09	3.75	2.60	4.18	5.18	2.74	4.76	4.90	2.55	4.75	4.53	2.40	4.39	3.82	1.26	2.20
MVL-47 dex	21.98	16.94	-	-	-	-	2.06	3.73	2.55	4.15	5.18	2.72	4.80	4.85	2.50	4.71	4.52	2.37	4.34	3.79	1.21	2.12
MVL-48 sin	?22	?16.66	1.79	3.18	1.17	1.65	-	-	2.58	4.29	5.09	2.53	?	?	2.40	4.40	4.42	2.30	4.02	3.50	1.03	2.10
MVL-48 dex	21.95	16.58	1.74	3.14	1.19	1.65	2.35	4.33	2.55	4.24	5.00	2.59	4.47	4.65	2.44	4.46	4.49	2.34	4.07	3.54	1.06	2.17
MVL-49 sin	19.25	16.31	2.01	2.72	1.21	1.48	1.85	3.64	2.38	4.04	4.81	2.55	4.88	4.76	2.31	4.73	4.33	2.22	3.99	3.74	1.07	1.88
MVL-49 dex	20.10	16.58	2.00	2.75	1.18	1.60	-	-	?2.45	?4.26	?5.05	?2.61	?4.5	?4.62	?2.38	?4.39	?4.4	?2.4	?4.03	?3.59	-	-
MVL-50 sin	-	?16.41	-	-	-	-	1.97	3.85	2.61	4.27	5.12	2.60	4.62	4.78	2.44	4.53	4.51	2.30	4.12	3.25	?1.04	?1.52
MVL-50 dex	-	-	-	-	-	-	1.99	3.89	2.66	4.30	5.17	2.66	4.70	4.77	2.50	4.55	4.55	2.35	4.20	3.29	-	-
MVL-51 sin	-	15.89	-	-	-	-	1.96	3.70	2.59	4.38	4.91	2.49	4.53	4.60	2.46	4.55	4.25	2.20	4.17	3.68	1.02	2.09
MVL-52 sin	-	-	-	-	-	-	1.85	3.60	2.25	4.00	4.69	2.58	4.30	4.36	2.47	4.30	4.30	2.36	3.80	3.40	-	-
MVL-52 dex	-	15.91	-	-	-	-	1.89	3.64	2.29	4.02	4.72	2.62	4.29	4.36	2.46	4.32	4.30	2.38	3.81	3.40	1.24	1.87
MVL-53 dex	-	-	-	-	-	-	-	-	2.57	-	5.19	2.46	4.80	4.86	2.26	4.65	-	2.12	4.30	3.75	-	-
MVL-54 set	-	-	-	2.99	1.20	1.55	-	-	-	-	-	-	-	-	-	-	-	-	-	-	-	-
MVL-56 sin	-	-	-	-	-	-	-	-	2.37	4.29	4.98	2.49	4.91	4.62	2.29	4.64	-	2.27	4.10	3.70	1.18	1.71
MVL-57 dex	-	-	-	-	-	-	-	-	2.67	4.32	4.86	2.40	4.73	4.62	2.24	4.61	4.36	2.21	4.17	3.82	-	-
MVL-73a dex	22.18	16.93	4.98	5.94	1.23	1.47	2.02	3.73	2.68	4.06	4.67	2.61	4.54	4.90	2.41	4.78	4.33	2.25	4.08	3.61	1.11	2.15
MVL-74 dex	-	-	2.64	2.97	1.21	1.32	-	-	-	-	-	-	-	-	-	-	-	-	-	-	-	-

The hypercone is advanced, achieving the same width development as the lagicone and postcone altogether. The latter set has a 45^{o} angle from the distal hyperloph, whereas the hypercone has a 25 to 30^{o} gradient. Following Fladerer and Reiner (1996) and Čermák (2009), the lagicone is of the B morphotype, and the hypercone is between the IV and V types of enamel structures.

Upper molariforms. The morphology of the upper molariform teeth (P3–M3) exhibit a folded hypoflexus crossing more than half of the tooth width and highly crenulated in the majority of the specimens, with extensive cement lingually. Enamel is often denser on the anterior part of the anteroloph and the lingual tips of the posteroloph. The P3, P4, M1, and M2 are of comparable size, however, the M3 is considerably smaller. M3 lacks a hypoflexus and is round-shaped. In addition, the separation between the talonid and trigonid is not easily visible. The folded hypoflexus of M2 is approximately half the breadth of the tooth crown. The degree (number and depth) of crenulation decreases from P3 to M2, with P3 and P4 exhibiting more prominent crenulations. The P3 and the plurality of P4 trigonids have a narrower width than the talonid. The situation is reversed at M1 and M2, where the trigonid has a larger breadth than the talonid.

Figure 6. Differentiation on the worn state of the enamel. In ***(a)*** MVL-48 the left side of the dentition is more worn than the right. Similarly, in ***(b)*** MVL-50 the left side of the maxillae is more affected than the right side of the dental wear. Scale bar = 10 mm.

In terms of enamel stages, MVL-49 has the most worn teeth, with nearly no enamel remaining. MVL-46 and MVL-73a have less damaged enamel than MVL-49, although they are much poorer than the remainder of the specimens. The enamel in the studied material appears to be weaker in the labial sections of the dentition while staying stronger in the buccal parts. Last but not least, an unexpected observation is that the worn state of the enamel differs significantly between the two maxillae in three specimens. In MVL-48, the left dentition is more worn than the right (Fig. 6a). In addition, in MVL-52 and not as prominently in MVL-50, the enamel on the left side of the maxillae is more worn (Fig. 6b).

3.1.4 Lower dentition

Referred material: MVL-55 (dex i1-p3), MVL-63 (sin i1-m3), MVL-64 (sin i1-m2), MVL-65 (dex p3-m2), MVL-66 (dex i1-m3), MVL-67 (dex p3-m2), MVL-68 (sin p3-m3), MVL-69 (dex i1-m3), MVL-70 (dex p3-m3), MVL-71 (dex p3-m3), MVL-72 (sin i1-m3) and MVL-73b (dex i1-m3 and sin i1-m2), MVL-82 (i1), MVL-83 (lower molariform), MVL-84 (lower molariform).

i1. In total, ten lower incisors are available in the studied material. The i1 is quadrangular and markedly prolonged anteroposteriorly. The anterior enamel wall is thick and has a constant thickness. In MVL-64, MVL-69, and MVL-72, the occlusal surface is longer anteroposteriorly, but not in MVL-63, MVL-66, and MVL-73b, where the surface is more square-shaped. The lower p3 is not reached by i1.

p3. The lower p3 is a significant element in the taxonomy and phylogeny of Lagomorpha. Among the twelve p3, only one is isolated. The majority of them are well preserved. The tooth shaft is prismatic with a rhombic occlusal outline. It is quadrangular and prolonged anteroposteriorly. The tooth can be divided into two main parts. The first is the anterior loph, the trigonid, which is divided into 4 lobes (conids), and the second is the posterior loph, the talonid, which consists of one lobe prolonged labially. The latter is approximately 1/3 of the width of the trigonid. The two lobes are connected by a dentine isthmus that is overall quite wide and short. The development of the anteroflexid also shows variations among the specimens. It can be distinguished in three main morphologies: a V-shaped, a narrow U-shaped, and a wide U-shaped anteroflexid. In the first category, MVL-55, MVL-64, MVL-67, MVL-71, and MVL-73b sin have this shallow and narrow anteroflexid. MVL-63, MVL-66, MVL-69, MVL-70, and MVL-73b dex have a narrower U-shaped anteroflexid (Fig. 7a, d), which is slightly less shallow than the previous category and quite wider. MVL-65 has the widest anteroflexid, which is also rather deep (Fig. 7b). It should be noted that MVL-72 has a bilobal anteroconid with dual anteroflexids that are wide and short (Fig. 7c).

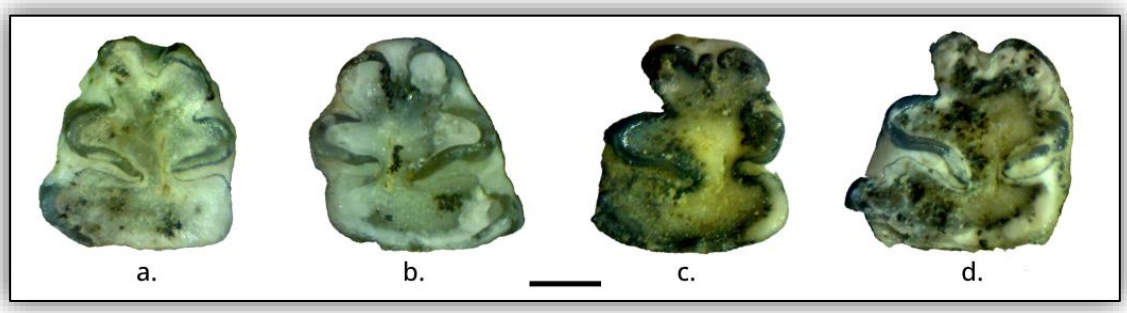

Figure 7. Occlusal surfaces of p3 in the MVL. ***a)*** MVL-63 (sin), ***b)*** MVL-65 (dex), ***c)*** MVL-72 (sin), ***d)*** MVL-73b (sin). Scale bar= 1 mm.

The hypoflexid and the mesoflexid are the deepest flexids, dividing the tooth into the trigonid and talonid parts, buccally and lingually, respectively. In the majority of the samples, it can be seen that the two flexids have the same development. However, in MVL-69, MVL-72, and MVL-73b, it's clear that the mesoflexid is not as deep as the hypoflexid and shorter. The mesoflexid is nearly half developed in MVL-72, while the hypoflexid is much deeper and the mesoflexid is quite shallow. In MVL-69 and MVL-73b, the mesoflexid is approximately 2/3 of the hypoflexid. The angle of the hypoflexid

shows variations in the studied material. The hypoflexid exhibits a slope of about 45° towards the talonid. The gradient is more prominent in MVL-73b and of lower significance in MVL-55, MVL-66, MVL-69, and MVL-71.

Table 10. Measurements of the lower dentition of the specimens of MVL (in mm).

	il	iw	p3l	p3w	p4l	p4l trig	p4l tal	p4w trig	p4w tal	m1l	m1l trig	m1l tal
MVL-55	?4.193	?2.947	3.50	3.80	-	-	-	-	-	-	-	-
MVL-63	2.69	2.96	3.41	3.42	2.78	1.53	1.35	3.28	2.94	2.86	1.50	1.26
MVL-64	4.54	2.87	3.55	3.58	2.95	1.31	1.42	3.55	2.87	3.15	1.59	1.68
MVL-65	-	-	3.32	3.46	3.01	1.65	1.17	3.35	2.96	3.06	1.64	1.24
MVL-66	2.81	2.91	3.34	3.43	2.77	1.42	1.15	3.35	2.89	2.86	1.55	1.14
MVL-67	-	-	3.18	-	-	-	-	-	-	-	-	-
MVL-68	-	-	-	-	2.94	1.56	1.17	3.49	2.91	2.98	1.64	1.30
MVL-69	3.92	3.24	3.71	3.67	2.88	1.47	1.06	3.59	3.19	2.97	1.65	1.13
MVL-70	-	-	3.76	3.51	3.09	1.75	1.42	3.54	3.08	3.12	1.63	1.36
MVL-71	-	-	3.33	3.18	2.81	1.42	1.20	3.27	2.86	2.93	1.58	1.19
MVL-72	4.22	3.05	3.62	3.31	2.94	1.37	1.23	3.46	3.11	2.85	1.39	1.23
MVL-73b dex	3.83	2.90	3.50	3.33	2.98	1.60	1.18	3.49	2.79	3.14	1.60	1.31
MVL-73b sin	3.92	3.29	3.44	3.61	2.75	1.46	1.21	3.36	3.01	2.89	1.57	1.16
MVL-82	3.57	3.14	-	-	-	-	-	-	-	-	-	-
	m1w trig	m1w tal	m2l	m2l trig	m2l tal	m2w trig	m2w tal	m3L	m3l trig	m3 L tal	m3Wtrig	m3W tal
MVL-55	-	-	-	-	-	-	-	-	-	-	-	-
MVL-63	3.09	2.66	2.85	1.57	1.26	3.40	-	1.98	1.01	0.95	1.81	1.13
MVL-64	3.43	2.65	3.33	1.44	1.56	3.32	2.49	-	-	-	-	-
MVL-65	2.93	2.53	3.12	1.51	1.40	3.23	2.62	-	-	-	-	-
MVL-66	3.30	2.63	2.73	1.34	1.01	3.93	2.53	2.03	-	1.02	-	1.17
MVL-67	-	-	-	-	-	-	-	-	-	-	-	-
MVL-68	3.44	2.89	2.93	1.49	1.30	3.38	2.68	2.14	1.06	1.07	2.15	1.39
MVL-69	3.39	3.01	3.01	1.72	1.24	3.51	2.64	-	-	-	-	-
MVL-70	3.45	2.95	3.05	1.54	1.54	3.54	2.84	2.31	1.09	1.13	1.97	1.25
MVL-71	3.24	2.63	3.15	1.61	1.28	3.29	2.59	-	-	-	-	-
MVL-72	3.43	2.78	3.01	1.54	1.18	3.00	2.55	-	-	-	-	-
MVL-73b dex	3.46	2.97	-	-	-	-	-	-	-	-	-	-
MVL-73b sin	3.74	2.92	3.05	1.63	1.19	3.71	2.90	2.30	1.33	1.12	1.91	1.08

The protoflexid also exhibits a variety of different developments in the material. It can be distinguished in two main morphotypes. The first one shows a shallow and wide V-shaped flexid. This type of protoflexid is shown in MVL-63, MVL-65, MVL-70, MVL-71, and MVL-73b. On the other hand, a narrow and shallow L-shaped flexid is seen in MVL-55, MVL-66, MVL-67, MVL-69, MVL-72, and MVL-73b. Lastly, the hypoconid is relatively massive and rectangular. The buccal side of the hypoconid shows a small, rounded notch with very thin enamel. According to Fladerer and Reiner (1996) and Čermák (2009), the hypoconid is of the "a morphotype" in MVL-55, the "b morphotype" in MVL-70 and MVL-72, and the "c morphotype" in MVL-63, MVL-65, MVL-66, MVL-69, and MVL-71. An in-between stage of the "morphotype b and c" can be seen in MVL-66 and MVL-73b. The hypoflexid shows the "A morphotype" in MVL-71, the "C morphotype" in MVL-65, MVL-66, MVL-69, and MVL-73b, and the "D morphotype" in MVL-55, MVL-70, and MVL-72. An in-between stage of the "C and D morphotype" is shown in MVL-63.

Lower molariforms. The two cylindrical shafts united by a small bridge at the lingual side characterize the morphology of all teeth, which is typical of the great majority of leporid species. In contrast to the very variable molariform p3, the lower molariforms (p4, m1, m2, and m3) in Lagomorpha are rather consistent and do not display any remarkable traits. In comparison with the talonid, the trigonid is larger (both in length and width). The anterobuccal corner of trigonids is small and smooth. Anterolabially, the labial portion of the talonid is convex. The isthmus joining the trigonid and talonid is lengthy and narrow. The flexid between the trigonid and talonid is smooth, and the enamel on the labial portion of the trigonid's posterior edge is extremely thick. The p3, p4, and m1 are of comparable size, however, the m2 is considerably smaller. In addition, the entire m3 shape is cylindrical, and the talonid portion is round, as opposed to the cylindrical shape of the remainder of the lower molariforms. No crenulations are noticeable.

Regarding the overall tooth wear, the enamel is more damaged or even completely absent on the lingual side of the tooth, as in the upper dentition. The most worn one is that from MVL-67 and MVL-65. MVL-69, MVL-70, and MVL-72 show the most undamaged enamel development. It's also clear that p3 is less worn than the other molariforms, therefore the enamel is thicker and more prominent.

3.1.5 Postcranial material

Atlas, axis and vertebrae

Referred material: MVL-190, MVL-191 MVL-192, MVL-193, MVL-194, MVL-195, MVL-196, and MVL-198.

Only two atlas specimens (MVL-191 and MVL-192) have been preserved in the MVL material. While MVL-192 has the left transverse process damaged, MVL-191 is well preserved. Its morphology is comparable to a signet ring. In an anterior view, the neural spine is thin, and the neural arches are pointed. The facets for the occipital condyles have a broad, concave morphology and are well developed. It has two substantial faces for the articulation, with the axis in the posterior view. They have a teardrop-like overall outline. The transverse process appears thin, horizontal, and wing-like from the dorsal aspect, with the most lateral portion being straight. The neural spine exhibits a rudimentary morphology.

In addition, four axis specimens have been preserved in the MVL material (MVL-193, MVL-194, MVL-195, MVL-196, and MVL-198a), all in good condition. MVL-198a is articulated with the third cervical vertebra. In general, the axis is sturdy with sharp edges and processes. The neural spine exhibits a tall and crest-like morphology, with a flattened lateral aspect and an elongated anteroposterior dimension. The transverse processes are relatively small, oriented towards the posterior aspect, and possess basal perforations through which the vertebral canals traverse. Anteriorly, the centrum bears a long, pointed, peg-like odontoid process.

MVL-198a comprises an articulation involving the axis as well as the third and fourth cervical vertebrae. The two latter exhibit a greater width in comparison to the axis and possess a dorsal morphology reminiscent of a trapezoidal shape. The third and fourth vertebrae of the cervical region exhibit a relatively diminutive neural spine and a substantial neural arch in general. The centrum, which is solely perceptible in the fourth cervical, exhibits a reduced and somewhat compressed morphology. The centrum's epiphysis exhibits a tilted and arched configuration. The bifurcated transverse processes are penetrated by a vertebraterial canal, which unfortunately remains imperceptible due to poor preservation. A single thoracic vertebra (MVL-190) can also be described. The neural spine has sustained damage. The morphology of the neural canal is characterized by a curved structure that approximates a semi-circle, featuring a centrally located, oval-shaped, abbreviated, and moderately robust centrum. Horizontally oriented, the transverse processes exhibit a stout and truncated morphology, with each process featuring a facet for the tuberculum of a rib. MVL-198b consists of a set of five thoracic vertebrae that are very poorly preserved, rendering them unsuitable for detailed description. Lastly, MVL-198c consists of three poorly preserved lumbar articulated vertebrae. The centrum seems to be well developed.

Scapula

Referred material: MVL-143. MVL-144, MVL-145, MVL-151, and MVL-199.

There are five incomplete specimens, all of which have poor preservation. All specimens still have their column and coronoid process intact. Unfortunately, the acromion and the top portions of the scapula are damaged. MVL-161 is the only scapula with a somehow fully but poorly preserved bone (Fig. 8 A.1,2). The glenoid cavity has a distinctly irregular oval shape, forming an approximately 30^{o} angle to the anteroposterior axis. The coronoid process is overall long and has a soft tip, extending beyond the development of the glenoid cavity (Fig. 8 A.3,4). The area connecting the glenoid cavity with the coronoid process, known as the tuberculum supraglenoidale, is triangular and flat. The neck of the scapula is broad, and the superior border is very pronounced and crested. Lastly, MVL-199 belongs most likely to a young individual. Apart from the difference in the overall size, the coronoid process is not articulated with the fossa articularis. The latter is also flatter in comparison to the rest of the scapulars.

Table 11. Measurements of the scapula specimens of MVL. The measurements are presented in mm.

Specimen	Wscapr	Lnsca	Lpasca	Bglsca
MVL-143	12.11	5.07	11.56	8.35
MVL-144	11.56	5.58	11.32	8.21
MVL-145	11.25	4.97	10.7	8.08
MVL-151	11.84	5.63	10.88	8.09

mean	11.69	5.31	11.12	8.18

Humerus

Referred material: MVL-107, MVL-108, MVL-109, MVL-110, MVL-111, MVL-112, MVL-113, MVL-114, MVL-158, MVL-159, MVL-160, and MVL-161.

Five out of the twelve humeri discovered (MNI=5), are well preserved (MVL-107, MVL-108, MVL-109, MVL-110, and MVL-167), and one (MVL-160) features only the proximal portion. The remaining five humeri primarily consist of the distal portion of the bone (MVL-111, MVL-112, MVL-114, MVL-158, and MVL-159), while one is solely the shaft, lacking both epiphyses. The bone exhibits a slender morphology with proximal edges that are rounded and distal edges that are pointed. The length of the humerus ranges from 66.51 mm to 71.86 mm. In anterior view (Fig. 8 B.1), the proximal region of the humerus displays a laterally positioned greater tuberosity that exhibits a triangle shape and appears flat when observed from a lateral viewpoint. A shallow oval notch can be observed on the greater tuberosity in a medial position. Medially, the lesser tuberosity has a triangular shape and is discernible from the neighboring head of the humerus by a conspicuously shallow line (Fig. 8 B.2,4). The greater tuberosity displays a comparable form of line but more prominent. The head of the humerus is bulbous and smooth in appearance. From a proximal perspective, the head of the humerus is oval. There is a very prominent cavity that extends towards the articular surface adjacent to the lesser tuberosity (Fig. 8 B.5).

On the shaft of the humerus the deltoid ridge is very prominent. Anteriorly, it forms a very sharp triangular formation along the upper part of the shaft, while it occupies the almost half of the length of the bone and disappears abruptly (Fig. 8 B.3). Distally, the humerus exhibits narrow and sharp-edged articulation. Anteriorly, the trochlea exhibits a slight yet noticeable mediolaterally angle. In addition, the trochlea is relatively wide, and the crests show a light acute outline (Fig. 8 B.6). The radial fossa covers a small shallow triangular area in comparison to the deeper olecranon fossa which has a more oval shape. A small circular foramen supratrochlear is observable laterally on both fossae.

Table 12. Measurements of the humerus specimens of MVL. The measurements are presented in mm.

Specimen	Lhu	Whupr	Wshu	Whud	Dhupr	Bthu	Bdhu	Dhud	Dhup
MVL-107	67.73	11	4.9	10.77	15.19	7.37	5.59	7.13	14.12
MVL-108	66.51	10.58	4.76	11.02	15.05	7.46	5.78	7.92	14.26
MVL-109	66.56	10.37	5.23	10.41	-	7.44	5.35	7.29	14.72
MVL-110	-	10.4	4.4	10.14	15.25	-	5.13	7.36	-
MVL-111	-	10.27	-	10.37	-	7.65	5.23	7.82	-
MVL-112	-	10.38	-	10.66	-	7.49	5.43	7.38	-
MVL-113	-	10.49	4.4		-	7.65	5.08	-	-
MVL-114	-	-	-	-	-	-	4.82	-	-
MVL-158	-	10.02	-	10.23	-	7.55	-	7.01	-
MVL-160	-	-	-		-	-	-	-	13.5
MVL-161	71.86	-	5.1	10.77	15.6	8.29	5.56	7.69	-
mean	68.17	10.44	4.80	10.55	15.27	7.613	5.33	7.45	14.15

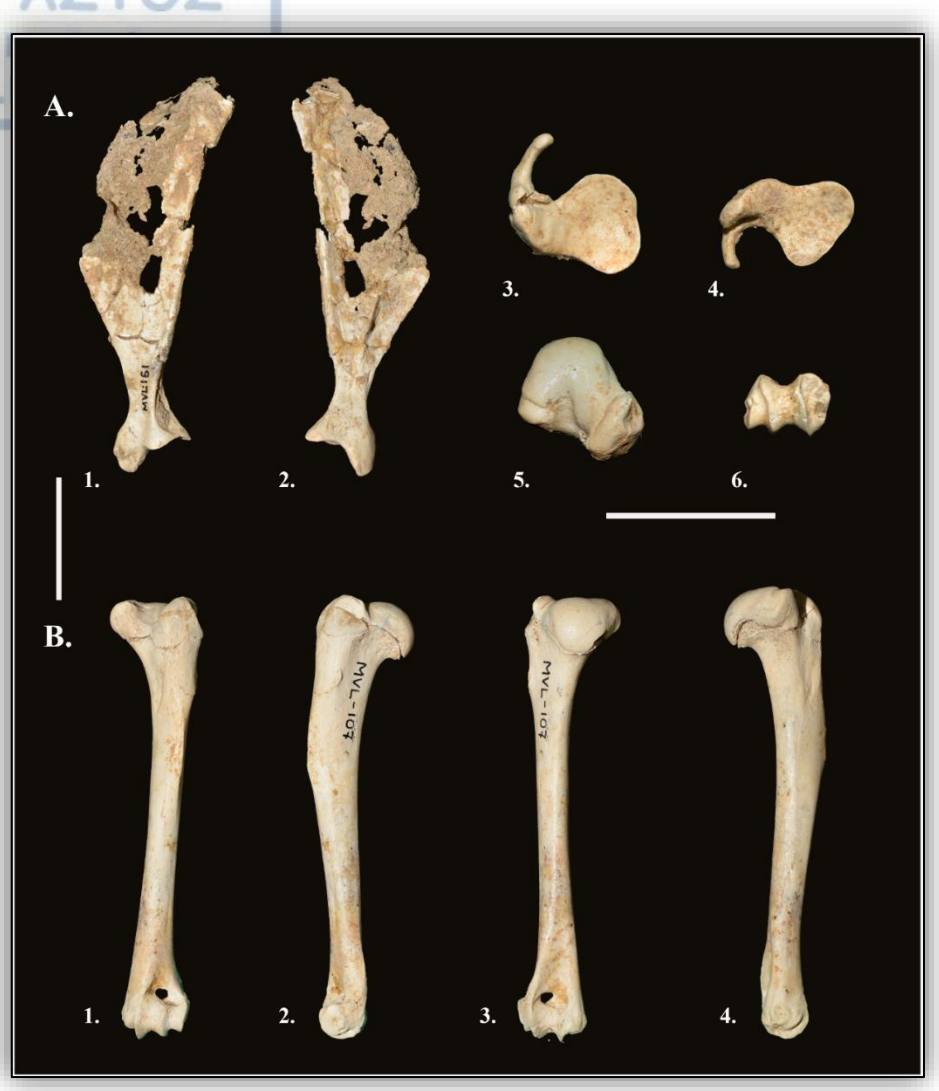

Figure 8. ***A)*** The left scapula of MVL-161 in ***(1)*** medial and ***(2)*** lateral view. The distal part of ***(3)*** MVL-143 and ***(4)*** MVL-144. ***B)*** The right humerus of MVL-107 in ***(1)*** anterior, ***(2)*** medial, ***(3)*** posterior, ***(4)*** lateral, ***(5)*** proximal, and ***(6)*** distal view. Left scale bar = 10 mm and right scale bar = 5 mm.

Ulna and Radius

Referred material: MVL-115, MVL-116, MVL-117, MVL-118, MVL-119, MVL-120, MVL-121, MVL-162, MVL-163, and MVL-235.

Five ulnae specimens in all have been obtained (MNI=3). Only one is complete (MVL-115) (Fig. 9 A. 1,2), while the others have either the whole (MVL-116 and MVL-117) or sections (MVL-118 and MVL-235) of the proximal extremity preserved (Fig. 9 A.3,4). Overall, the ulna bone is slender, highly delicate, and arched, with a length of 84.53 mm. The coronoid process produces a wide trochlear notch that is wide, especially on the distal end. The anconeal process is quite sharp and prominent and has a tilted triangle form on a cranial view. On the cranial side of the shaft, there is a noticeable shallow line. The styloid process, which is short and rounded on the distal end, is present on MVL-115.

There are five radii in MVL (MNI=3), one of which is complete (MVL-119) (Fig. 9 B.5,6), two have solely the upper end and part of the shaft intact (MVL-120 and MVL-162), and the remaining two have the distal end and part of the shaft preserved (MVL-121 and MVL-165). The radius is a thin, extremely fragile bone that has a more robust and rounded distal end and a sharp, pointed upper end, like the ulna. The length measured from MVL-119 is 64.35 mm. The bone's posterior side has an elongated groove, and the shaft is more arched than the ulna. The styloid process of the radius exhibits a comparatively acute morphology in comparison to the ulna, but it is smaller. Lastly, the distal ends exhibit a shallow concave morphology, overall oval in outline.

Table 13. Measurements of the radius specimens of MVL. The measurements are presented in mm.

Specimen	**Lra**	**Wrapr**	**Drapr**	**Wrash**	**Wrad**
MVL-119	64.35	6.85	6.83	4.46	6.99
MVL-120	-	-	7.03	4.7	7.3
MVL-121	-	6.8	-	4.79	-
MVL-162	-	-	7.04	4.7	-
MVL-163	-	6.51	-	4.73	7.22
mean	64.35	6.72	6.97	4.68	7.17

Table 14. Measurements of the ulna specimens of MVL. The measurements are presented in mm.

Specimen	**Lul**	**Wulpr**	**Dulol**	**Lulol**	**Wulraf**	**Dulpa**
MVL-115	84.53	6.73	7.77	9.02	6.69	8.73
MVL-116	-	6.74	8.09	8.88	6.77	8.33
MVL-117	-	6.72	-	-	6.7	7.93
MVL-118	-	6.45	-	-	6.5	-
MVL-235	-	-	7.32	-	-	8.3
mean	84.53	6.66	7.73	8.95	6.67	8.32

Figure 9. A) The left ulna of MVL-115 in ***(1)*** anterior and ***(2)*** medial view. The left ulna of MVL-116 in ***(3)*** posterior and anterior ***(4)*** view. ***B)*** The radius of MVL-119 in ***(5)*** anterior and ***(6)*** posterior view. Scale bar = 10 mm.

Os coxae

Referred material: MVL-136, MVL-137, MVL-138, MVL-139, MVL-140, MVL-141, MVL-142, MVL-146, MVL-147, MVL-148, MVL-149, MVL-150, MVL-152, MVL-154, and MVL-155.

A total of fifteen specimens of the pelvic bone have been recovered from the available material (MNI=11). Unfortunately, only one partially complete coxal was found (MVL-146) (Fig. 10 A1, 2). In greater detail, two have parts of the ilium, acetabulum, and ischium preserved (MVL-136 and MVL-137). Additionally, seven specimens have been discovered that feature only the ilium bone, either with or without the acetabulum (MVL-139, MVL-140, MVL-141, MVL-147, MVL-150, MVL-159, and MVL-192) (Fig. 10 A3, 4). Lastly, five specimens exhibit preserved portions of the acetabulum and ischium (MVL-138, MVL-142, MVL-148, MVL-149, and MVL-155). The available coxals do not display any particular distinguishing characteristic and are overall the same in morphology. Regrettably, a complete measurement of the pelvis length was unattainable. The ilium, which represents the foremost aspect of the coxal bone, is the most well-preserved component of the pelvis. It is overall robust, and a distinct wing morphology is formed. A crested line is observable along the midsection

of the ilium's wing. The crest line exhibits notable prominence in MVL-139, MVL-140, and MVL-152. The visibility of the crista iliaca is limited in MVL-136, MVL-139, and MVL-154, where it develops as a slender crest-like structure on the wing's anterior regions.

The acetabulum appears nearly circular on a lateral view and exhibits a noticeable incisura acetabuli, which is wide and lacks acute pointedness. However, the part of the acetabulum connected with the ischium is slightly more elongated and oval in contrast to the anterior extremity. The observed facies lunata exhibits notable breadth and robustness. Proximal to the acetabulum, a bulge, known as area m. recti femoris, is noticeable with a triangular morphology with smooth edges. The ischium is relatively slender in comparison to the wider ilium. Posterior to the acetabulum on the medial side, a wide notch can be observed; it is elongated along the anteroposterior axis and is mediolaterally suppressed. However, it should be noted that the part of the incisura acetabuli connecting the ischium with the fossa acetabuli is open and deep (Fig. 10 A.5), in MVL-137, but closed in MVL-136 (Fig. 10 A6). On the pubic bone, the emimentia iliopupica is fully visible in MVL-146, and only the uppermost parts are visible in MVL-136 and MVL-137. The foramen obturatum is only visible in MVL-146 and has an oval shape, exhibiting a wider base and a slightly pointed apex. The most lateral part of the pelvis, the ischial tuberosity (tuber ischiadicum), is only preserved in MVL-146. In ventrolateral view, is prominently triangular shaped, similar to a wave, with soft lateral edges.

Table 15. Measurements of the coxal specimens of MVL. The measurements are presented in mm.

Specimen	Dac	Lisch	Wilb	Lac	Hac
MVL-136	9.14	-	8.4	8.73	9.82
MVL-137	10.14	-	8.51	9.77	10.36
MVL-139	-	40.44	8.79	-	-
MVL-140	-	-	8.22	-	-
MVL-141	-	-	8.1	-	-
MVL-146	9.2	-	8.25	8.93	9.44
MVL-147	9.68	-	8.37	9.35	8.93
MVL-148	9.28	-	-	9.1	9.42
MVL-149	9.23	-	-	8.5	8.85
MVL-150	9.37	-	-	8.8	9.54
MVL-152	9.94	-	8.31	9.25	9.64
MVL-155	9.12	-	-	8.93	8.44
mean	9.46	40.44	8.37	9.04	9.38

Femur

Referred material: MVL-122, MVL-123, MVL-124, MVL-125, MVL-126, MVL-127, MVL-130, MVL-131, MVL-132, MVL-133, MVL-134, and MVL-135.

Out of the total 13 specimens (MNI=7), a subset of four (MVL-122, MVL-123, MVL-124, and MVL-125) are complete, while five specimens (MVL-126, MVL-127, MVL-129, MVL-130, and MVL-131) are derived from the proximal end, and the remaining four (MVL-132, MVL-133, MVL-134, and MVL-135) are from the distal

portion of the bone. The length could be measured from a limited sample of two, with values 94.14 mm and 94.45 mm respectively. The femur's morphology displays similarities to that observed in rabbits. The anterior aspect of the bone is relatively elongated and slender, featuring a proximal end with sharp edges. In the proximal extremity of the femur in MVL, the caput femoris is bulbous and is retained by an overall short and wide neck. The fovea capitis is oval and small, yet prominently positioned mediolaterally on the caput femoris. The first trochanter is preserved only in MVL-123 and MVL-125. It exhibits a medial curvature and has a smooth appearance (Fig. 10 B2). However, in MVL-125, it displays a slight greater angularity at the most cranial part. The third trochanter shows a significant prominence and is situated in a proximal position, resulting in a morphology resembling that of a fin, with the upper tip pointing medially. The MVL-126 specimen exhibits a comparatively narrower extension of the third trochanter. Trochanter minor is not as developed in comparison to trochanter third and resembles the shape of an amblygon triangle, featuring a coarse anterior surface. In addition, trochanter minor terminates at a lower point than trochanter third. In a posterior view, it becomes apparent that the groove separating the first trochanter and the neck displays a significant depth and spaciousness.

Apart from the diaphysis, the distal extremity is the most preserved part of the femur. Anteriorly, a shallow and straightly developed trochlea intercondylaris separates the two condyles, medialis and lateris. The condylus medialis exhibits a solitary shallow concavity in its medial aspect, whereas the condylus lateralis develops a comparable shallow groove on a more extensive surface in its lateral side. Posteriorly, the prominence of the epicondylus lateralis is greater than that of the epicondylus medialis. In a similar manner, condylus lateralis is more developed than condylus medialis and terminates at a lower point. Lastly, in distal view, a small circular foramen can be seen on the lateral side of the facies patellaris, which is known as the fossa extensoria.

Table 16. Measurements of the femur specimens of MVL. The measurements are presented in mm.

Specimen	Lfe	Lfecph	Wfepr	Bfetrt	Wfedis	Dfed	Wintf	Wpag	Hdis	Whe	Wfesh	Tfesh	Dfepr
MVL-122	-	86.23	19.16	18.3	16.26	16.32	4.31	6.54	17.33	8.4	7.56	6.21	18.99
MVL-123	94.45	90.07	18.8	-	15.77	14.46	3.55	-	20.13	8.33	8.13	6.26	18.85
MVL-124	-	84.29	18.66	17.35	16.67	15.16	3.86	5.5	19.15	7.77	7.2	6.47	18.4
MVL-125	94.19	87.58	19.12	17.02	-	13.11	3.88	5.67	-	8.5	7.57	6.4	19.21
MVL-126	-	-	18.76	17.05	-	-	-	-	-	7.82	7.46	6.2	18.8
MVL-127	-	-	17.76	17.19	-	-	-	-	-	7.85	-	6.5	18.2
MVL-129	-	-	-	17.8	-	-	-	-	-	-	7.6	6.55	-
MVL-131	-	-	-	-	-	-	-	-	-	-	7.46	6.18	-
MVL-132	-	-	-	-	17	15.84	3.88	6.12	18.5	-	-	-	-
MVL-133	-	-	-	-	15.86	14.29	3.47	-	-	-	-	-	-
MVL-134	-	-	-	-	-	13.87	-	5.95	-	-	-	-	-
mean	94.32	87.04	18.71	17.45	16.31	14.72	3.83	5.96	18.78	8.11	7.57	6.35	18.74

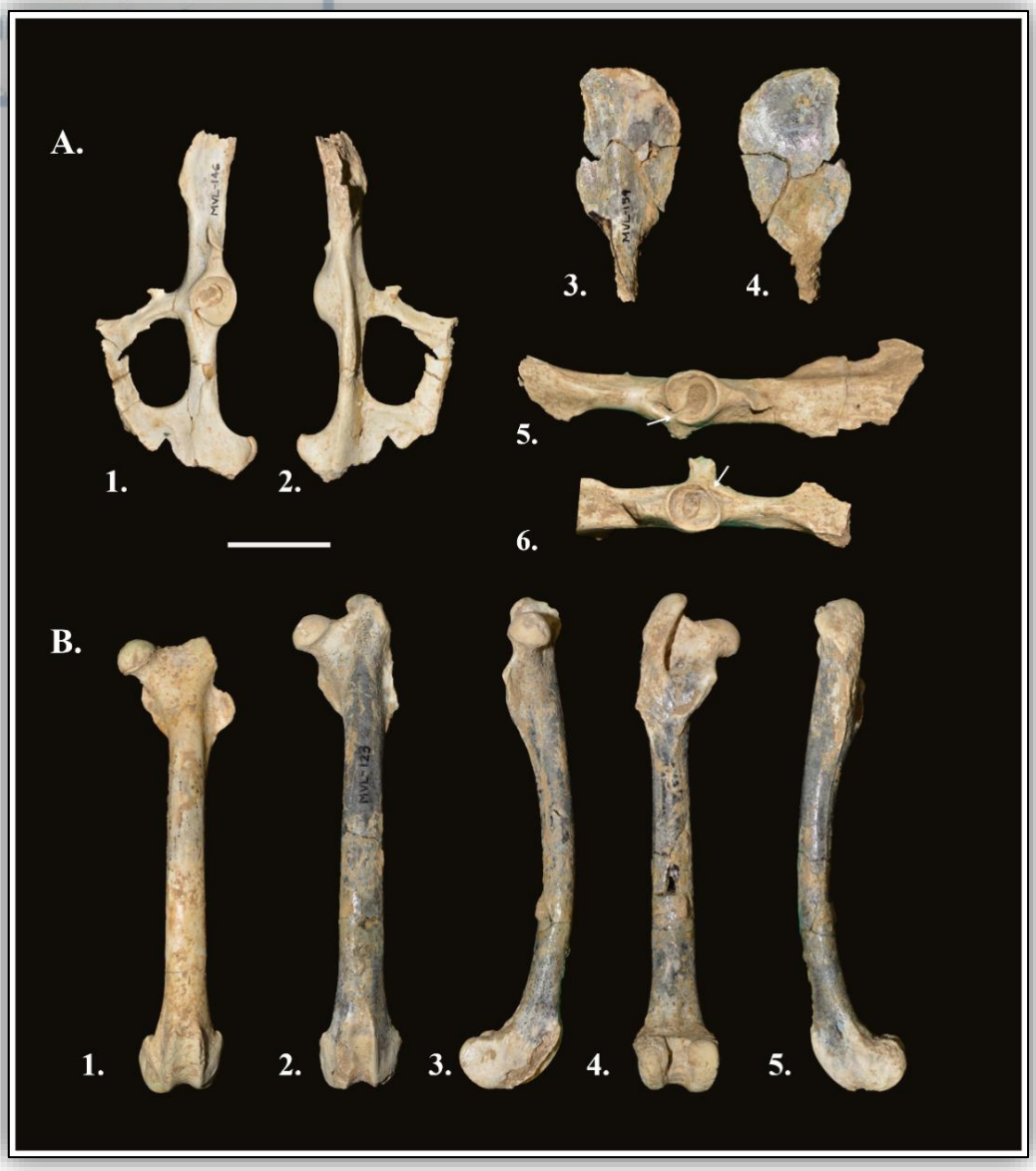

Figure 10. A) The os coxae of MVL-146 in ***(1)*** medial and ***(2)*** lateral view. The ilium of the coxal of MVL-154 in ***(3)*** and ***(4)*** view. The acetabulum; The arrows point to the incisura acetabuli, which is closed in ***(5)*** MVL-137 and open ***(6)*** in MVL-136. ***B)*** The femur of MVL-122 in ***(1)*** anterior view; The femur of MVL-123 in ***(2)*** anterior, ***(3)*** medial, ***(4)*** posterior, and ***(5)*** lateral view. Scale bar = 10 mm.

Tibiofibula

Referred material: MVL-86, MVL-87, MVL-88, MVL-89, MVL-90, MVL-91, MVL-92, MVL-93, MVL-94, MVL-95, MVL-96, MVL-97, MVL-98, MVL-99, MVL-100, MVL-101, MVL-102, MVL-103, MVL-104, MVL-105, MVL-106, MVL-156, MVL-157, and MVL-200.

The hind limb of a lagomorph contains a zeugopodial part that is comprised of a fused tibia and fibula, resulting in a single bony structure. In total, 24 specimens of the tibiofibula bone have been preserved in the MVL material, which makes them the second most numerous bone group after the calcaneus. Nine of them are fairly complete

(MVL-86, MVL-87, MVL-88, MVL-89, MVL-90, MVL-91, MVL-92, MVL-93, and MVL-106), thirteen have only the distal part and the shaft (MVL-94, MVL-95, MVL-96, MVL-97, MVL-98, MVL-99, MVL-100, MVL-101, MVL-103, MVL-104, MVL-105, MVL-106, MVL-156, and MVL-157), while only two specimens (MVL-102 and MVL-200) have only the fragment of the proximal edge preserved (Fig. 11). The tibia and fibula are conjoined for approximately half of their extent, creating a shared distal articulation facet for the tarsal constituents (Fig. 11). In the majority of the specimens, the complete fusion is observable, albeit the fibula's delicate morphology prevents its full extension from being fully visible. However, only in MVL-90 and MVL-92 are parts of the anterior part of the fibula preserved (Figs. 11 5-6). Overall, the morphology of the tibia exhibits a slender appearance, characterized by a relatively thin diaphysis. The total length ranges from 102 mm to 109.63 mm, exhibiting relative variability. The crest of the tibia's tuberosity is highly developed and runs parallel to the shaft, resulting in a conspicuous tubercle. A distinctive feature of the plantar side of the shaft in all specimens, situated below the proximal extremity, is the presence of a well-pronounced s-shaped linear muscle attachment known as the linea musculi poplitei, which serves as an attachment for the popliteus muscle.

On a proximal view, the proximal segment of the bone has a triangular shape, forming a near-heart-shaped type of morphology. On the anterior side, the condylous medialis and condylous lateralis are concave areas, with the latter being marginally larger and more angular. A deep notch known as the sulcus muscularis is noticeable above the condylous lateralis. At the most posterior edge of the proximal extremity, the crista tibiae is noticeably projecting in a slender oval morphology and bent laterally. The sulcus malleolaris lateralis on the distal epiphysis is trihedral and deep. On the lateral side, the malleolaris lateralis exhibits a small bulge. The medial malleolus exhibits a significant and profound sulcus malleolaris medialis and has a more tetrahedral appearance. On the lateral side, malleolaris lateralis also exhibits a bulge, more profound than the one occurring on the medial side and similar in appearance to a fin. Additionally, a comparatively less deep sulcus is present in a more medial position. Lastly, on a distal view, the furrows in the cochlea tibiae are shallow, with the lateral one being flatter and rectangle-shaped and the medial one being more deep and oval-shaped with angular anteroposterior edges.

Table 17. Measurements of the tibiofibular specimens of MVL. The measurements are presented in mm.

Specimen	Lti	Wtipr	Wtish	Wtidis	Ttidis	Dtipr	Ttipr	Htitu
MVL-86	?107.05	17.57	6.77	-	7.56	16.23	17.8	20.68
MVL-87	109.63	-	6.15	13.37	7.34	-	-	19.72
MVL-88	108.89	-	6.55	14.12	7.56	-	-	21.16
MVL-89	-	-	6.52	13.71	7.48	-	-	17.3
MVL-90	107.72	16.76	6.39	13.67	7.43	16.31	18	-
MVL-91	104.16	18.08	6.42	13.67	7.27	-	-	-
MVL-92	-	16.86	6.31	-	-	15.88	18.75	20.61
MVL-93	102	16.93	6.45	13.55	-	15.42	17.17	-
MVL-94	-	-	6.1	13	6.71	-	-	-
MVL-95	-	-	6.24	13.93	7.66	-	-	-
MVL-96	-	-	6.54	13.51	7.33	-	-	-
MVL-98	-	-	6.28	13.72	7.04	-	-	-
MVL-99	-	-	6.29	13.42	7.17	-	-	-

MVL-100	-	-	6.38	13.31	6.73	-	-	-
MVL-101	-	-	-	13.81	7.67	-	-	-
MVL-102	-	17.03	-	13.43	7.22	15.37	17.78	-
MVL-103	-	-	-	13.69	7.4	-	-	-
MVL-106	-	-	6.2	-	7.56	-	-	-
MVL-156	-	-	6.32	12.17	7.16	-	-	-
MVL-157	-	-	-	13.95	7.57	-	-	-
mean	106.58	17.21	6.37	13.53	7.33	15.84	17.9	19.90

Figure 11. The tibiofibula of MVL-86 in ***(1)*** anterior, ***(2)*** medial, ***(3)*** posterior, and ***(4)*** lateral view. The tibiofibula of MVL-92 with the anterior parts of the fibula preserved in ***(5)*** lateral and ***(6)*** posterior view. Scale bar = 10 mm.

Astragalus

Referred material: MVL-202, MVL-203, MVL-204, MVL-205, MVL-206, MVL-221, MVL-222, MVL-223, MVL-224, MVL-225, MVL-226, MVL-227, MVL-228, and MVL-229.

A total of 14 astragali specimens have been well preserved (MNI=8), with the exception of one specimen (MVL-229) that has incurred distal damage. The specimen exhibits no major size variation, with a range of 13.43 mm to 14.4 mm in its medial length and display an overall similar morphology (Fig. 12A). When viewed in a proximal view (Fig. 12A 5), the trochlea exhibits a wider breadth in comparison to its anteroposterior dimension and is situated at a slight angle. The trochlea's medial aspect exhibits a concave morphology. The length of the neck (collum tali) is relatively short and displays a minor bulge on the outline that is more visible in certain specimens (i.e., MVL-204, MVL-224, and MVL-226). The connection between the astragalus and the calcaneus happens on three surfaces. One of these surfaces is located at the back (known

as facies articularis calcanea posterior) and consists of two circular regions of different sizes positioned within the lower part of the trochlea's concavity. The medial one (facies articularis media) is situated on the underside of the trochea/collum border. It has a stretched-out oval shape and is linked to the talus head's articular surface via a narrow isthmus. The facies articularis calcanea anterior is the most undersized and furthest one of all. It is situated on the medial side of the caput tali. Its shape can range from elongated in the plantar to dorsally direction to almost circular. Finally, the area where it connects with the navicular bone (facies articualaris navicularis) is present at the top of the talus. The outline oval to nearly round and forms dorsally a triangular concave morphology that is positioned at a mediolateral angle on the caput tali.

Table 18. Measurements of the astragalus specimens of MVL. The measurements are presented in mm.

Specimen	**Las**	**Was**	**Lasn**
MVL-202	14	7.38	6.98
MVL-203	13.43	7.15	5.73
MVL-204	13.91	7.34	7.24
MVL-205	13.72	7.38	7.26
MVL-206	14.4	7.16	6.26
MVL-221	14.15	7.21	6.89
MVL-222	14.4	6.79	6.84
MVL-223	14.14	6.81	6.94
MVL-224	14.07	7.28	6.15
MVL-225	14.38	7.24	6.25
MVL-226	13.94	7.13	6.15
MVL-227	14.31	7.17	6.15
MVL-228	13.57	6.77	6.2
MVL-229	-	6.56	-
mean	14.03	7.10	6.54

Figure 12. A) The astragalus of MVL-204 in ***(1)*** anterior, ***(2)*** medial, ***(3)*** posterior, ***(4)*** lateral, ***(5)*** proximal, and ***(6)*** distal view. ***B)*** The calcaneus of MVL-189 in ***(1)*** anterior, ***(2)*** medial, ***(3)*** posterior, ***(4)*** lateral, ***(5)*** proximal, and ***(6)*** distal view. Scale bar = 10 mm.

Calcaneus

Referred material: MVL-164, MVL-165, MVL-166, MVL-167, MVL-168, MVL-169, MVL-170, MVL-171, MVL-172, MVL-173, MVL-174, MVL-175, MVL-176, MVL-177, MVL-178, MVL-179, MVL-180, MVL-181, MVL-182, MVL-183, MVL-184, MVL-185, MVL-186, MVL-187, MVL-188, MVL-189, and MVL-201.

In total, 27 specimens of calcaneus can be documented from the MVL, which makes them the most common preserved bone (MNI=15). Overall, the vast majority are well preserved, apart from a few specimens that are damaged on the proximal and distal parts. Apart from the variations in maximum length, which range from 24.7 to 27.3 mm, there are no apparent morphological distinctions within the samples (Fig. 12B). Proximally, the corpus calcanei exhibits a curved surface in its upper region, featuring a raised medial upper proximal extremity. The observed elevation, depicted from a lateral viewpoint, shows a sub-square morphology lacking sharp or angular features.

It is noteworthy that the body of the calcaneus is situated at a slight angle in comparison to the anteroposterior axis. The facies articularis talaris posterior is located in the middle portion of the trochlea, closer to the body, and can be differentiated from the astragalus's anterior surface (facies articularis talaris media) by the noticeable crest on the medial side of the trochlea. The most inner part of the bone is known as the sustentaculum tali, and it serves as the third surface where the astragalus is attached. It is flat, round, and inclined towards the plantar aspect. It is slightly concave on its dorsal

aspect, which accommodates the surface for the astragalus. Facies articularis tibialis is the most lateral extension of the bone that inclines towards the lateral aspect. Its morphology is concave. Finally, facies articularis cuboidea, which is located on the distal end of the bone, can only be observed from a medial perspective. It is concave with a clustered bean-shaped morphology. Facies articularis navicularis is situated above facies articularis cuboidea.

Table 19. Measurements of the calcaneus specimens of MVL. The measurements are presented in mm.

Specimen	**Lca**	**Wca**	**Lcat**	**Lcab**	**Wcat**
MVL-164	26.85	9.6	13.53	9.65	6.8
MVL-165	26.37	8.91	11.79	9.75	6.61
MVL-166	26.35	8.73	11.6	9.9	6.7
MVL-167	27.21	10	-	10.37	6.69
MVL-168	26.7	10.5	13.07	10.29	6.94
MVL-169	25.33	9.85	12.75	10.18	6.8
MVL-170	25.73	10.14	-	10.48	-
MVL-171	26.87	10.09	13.7	10.38	6.71
MVL-172	27.08	9.83	13.56	10.75	6.86
MVL-173	26.42	10.22	13.67	9.98	6.67
MVL-174	27.06	9.54	13.61	10.71	6.76
MVL-175	26.78	10.23	-	10.74	-
MVL-176	26.73	10.5	13.95	10.08	-
MVL-177	27.32	10.47	14.4	10.06	6.78
MVL-178	-	9.83	-	9.77	-
MVL-180	24.73	9.9	12.23	9.86	6.52
MVL-181	26.13	10.25	13.8	9.87	6.69
MVL-182	25.71	9.65	13.07	9.98	6.6
MVL-183	26.82	10.27	13.12	10.57	6.58
MVL-184	27.03	10.3	13.72	10.58	6.69
MVL-185	26.53	9.7	-	9.92	-
MVL-186	-	-	-	10.21	-
MVL-187	26.35	9.84	13.28	9.58	6.44
MVL-188	-	10.05	-	10.45	-
MVL-189	25.76	9.75	12.93	9.4	6.47
MVL-201	27.27	10.45	13.78	10.35	6.81
mean	26.48	9.93	13.24	10.15	6.69

Navicular

Referred material: MVL-207, MVL-208, MVL-209, MVL-210, MVL-211, MVL-212, MVL-213, MVL-214, MVL-215, MVL-216, MVL-217, MVL-218, MVL-219, and MVL-220.

In total, 14 specimens of the navicular bone are preserved, all of which in excellent preservation (MNI=9). The navicular bone is situated in the middle area between the astragalus (which is towards the top) and the cuneiform bones (which are towards the bottom). It consists of a body and an elongated, extended plantar process called the process plantaris ossis navicularis. The length ranges from 5.01 mm to 6.01

mm. The shape of the body is like an asymmetrical cube with a flattened proximo-distal aspect and a concave proximal face. The proximal face contains a single oval-shaped surface that is used for articulating with the head of the astragalus. The shape of the surface closely approximates that of a circle. The plantar process has a flattened morphology on its underside and includes a shallow groove oriented vertically in a planto-medial direction. The edges of this process are notably angular and rough, and its overall shape resembles that of a rectangle. It must be noted that the length of the body of the navicular is particularly reduced in proportion to its width (Fig. 13A).

Table 20. Measurements of the navicular specimens of MVL. The measurements are presented in mm.

Specimen	**Lnab**	**Lnat**	**Wna**	**Tna**
MVL-207	5.84	9.45	6.63	9.71
MVL-208	6.01	9.38	6.71	9.81
MVL-209	6.01	9.51	7.06	10.09
MVL-210	5.31	9.31	6.94	9.55
MVL-211	5.47	9.63	6.9	10.19
MVL-212	5.2	9.49	6.68	10.5
MVL-213	5.63	9.5	6.89	10.24
MVL-214	5.01	9.48	6.9	10.23
MVL-215	5.03	9.88	7.2	10.3
MVL-216	5.49	9.83	7	10
MVL-217	5.14	9.3	6.86	10
MVL-218	5.11	9.54	6.86	10.03
MVL-219	5.44	9.71	6.85	10.4
MVL-220	5.66	9.35	6.51	10.35
mean	5.45	9.53	6.86	10.1

Cuboid

Referred material: MVL-230, MVL-231, MVL-232, and MVL-233.

The MVL material comprises four specimens of the cuboid bone, ranging in length from 7.05 mm to 8.15 mm. All of the available cuboid material does not display any major differences and are fairly the same in morphology. The cuboid bone is located on the outer side of the ankle's lower row of bones and has a rhombus-like shape. It also has a prominent bulge on the underside, known as the plantar tuberosity, which creates a horizontal ridge running across the bone's underside. At a proximal view, the articulation surface of the bone with the calcaneus (facies articularis calcanea) is quite large and convex, resembling the shape of a trapezoid, while it extends onto the dorsal side of the bone. The facies articularis navicularis, which articulates the navicular with the cuboid bone, is trihedral in shape and extends in both plantar and lateral directions. The cuboid bone connects distally with the fourth and fifth metatarsal bones displaying a pear-shaped surface and a smaller oval-shaped surface, respectively (Fig. 13B).

Table 21. Measurements of the cuboid specimens of MVL. The measurements are presented in mm.

Specimen	**Lcu**	**Wcu**	**Tcu**
MVL-230	8.15	8.26	6.96
MVL-231	8.09	7.69	6.6
MVL-232	8.05	7.84	6.5
MVL-233	7.05	7.7	6
mean	7.84	7.87	6.52

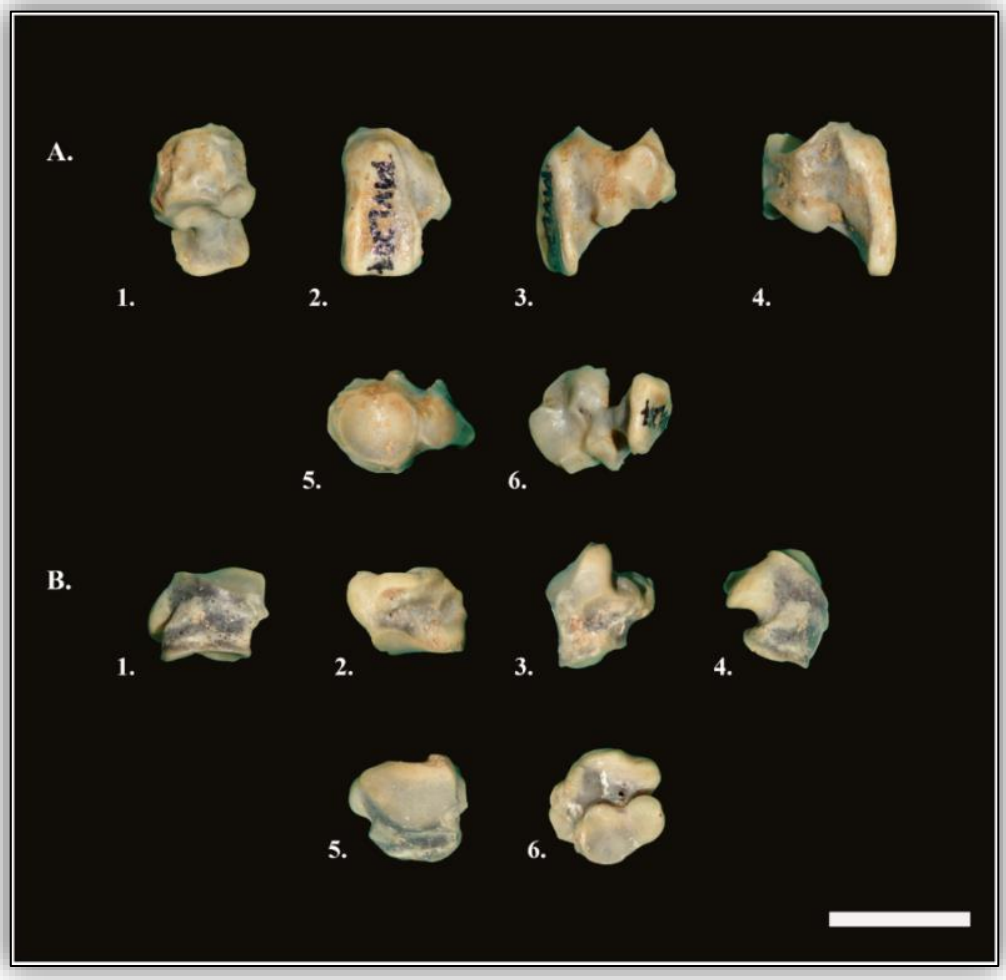

Figure 13. A) The navicular of MVL-207 in ***(1)*** anterior, ***(2)*** medial, ***(3)*** posterior, ***(4)*** lateral, ***(5)*** proximal, and ***(6)*** distal view. ***B)*** The cuboid of MVL-230 in ***(1)*** anterior, ***(2)*** medial, ***(3)*** posterior, ***(4)*** lateral, ***(5)*** proximal, and ***(6)*** distal view. Scale bar = 5 mm.

4. Comparisons

4.1. Cranium

4.1.1. Comparison with extant leporid crania

Although none of the studied MVL crania is lengthwise fully preserved, the condylobasal and basal length indicate a large cranium, very close to that of *Lepus*. *Oryctolagus* and *Sylvilagus* exhibit in general quite smaller sized skulls. MVL also share a similar robustness of the cranium as *Lepus* and *Oryctolagus*, while *Sylvilagus* appears to have a frailer cranial built. The nasal-frontal suture in MVL is triangular-shaped, while in *Lepus* and sometimes in *Sylvilagus* is rather rounded. *Oryctolagus* shares a similar angular development as MVL. In addition, the snout region in MVL is more similar to that of *Oryctolagus* and *Sylvilagus*, whereas *Lepus* displays a broader snout, especially in the anterior portions of the bone. Dorsally, the inclination of the nasal bones to the front of the cranium in *Lepus* is not that prominent, making the nasals to appear more horizontally positioned in contrast to that observed in MVL and *Oryctolagus*. *Sylvilagus* appears to have both inclined and straight nasals. Variations in the posterior suborbital process can also be observed. MVL exhibit a supraorbital process that is thin, narrow and triangular, resembling a thorn, similar to that seen in *Sylvilagus* and *Oryctolagus*, but not that robust. The two latter species exhibit a posterior supraorbital process that is more extended but not as sharp as that of MVL. In contrast to the delicate state of MVL, the shape of the supraorbital process in *Lepus* is significantly broader, triangular and wing shaped. The frontal bone in MVL is similar to that observed in *Lepus*, which is overall short compared to the elongated nasals. *Oryctolagus* and *Sylvilagus* display a greater extension of the frontal bone (Fig. 14A). The dorsal fenestration is equally noticeable in MVL as in *Lepus*, *Oryctolagus*, and *Sylvilagus*. The placement of the fenestration is not limited in the maxilla and can be observed in the nasal, frontal, and parietal regions in all this set of taxa.

In ventral view, the incisive foramen of MVL shows a relatively narrow structure. However, when compared the width of the incisive foramen in relation to the dental length (index I2) it appears that MVL shares a similarly developed incisive foramen as that of *Lepus*; *Oryctolagus* and *Sylvilagus*, exhibit a narrower one (Fig. 14B). In addition, the incisive foramen in MVL has a greater extension (index I3) compared to *Lepus*, *Sylvilagus*, and *Oryctolagus*. *Lepus* is closer to MVL (Fig. 14C). The posterior spine of the incisive foramen of MVL shares the same development with *Sylvilagus*, which is slender and thorn-like, while in *Oryctolagus* it is more prominent and robust; in *Lepus* it is not so tall and sometimes not present. MVL exhibit a slightly subcircular upper dental arch on the buccal side, similar to *Oryctolagus*, whereas *Lepus* maintains a comparatively straighter orientation. Furthermore, the length of the palatine relatively to the breadth of the choane (index I4) in MVL is comparable to that of *Oryctolagus* and *Sylvilagus*, while in *Lepus* the choanae is significantly broader (Fig. 14D). *Lepus* has the shortest palatine among the examined taxa. Additionally, the breadth of the palatine in relation to the dental length (index I5) in MVL is close to *Sylvilagus* and *Lepus*, while *Oryctolagus* possesses the narrowest palatine (Fig. 14E). In addition, the position of the paired premolar foramen relative to the maxilla-palatine suture in the majority of the specimens of MVL is placed on the level of the middle of P4, as in *Sylvilagus* and *Oryctolagus*. In *Lepus* they are slightly more posteriorly positioned, in between P4 and M1. It must be noted that in MVL-46 and MVL-50 the foramina show a slight posterior placement, below the suture, like that observed in *Lepus*. Regarding their overall development, the leporid of MVL displays small and

subcircular foramen in contrast to the extant species, which have more oval-shaped and larger foramen. However, this could be biased due to taphonomy and preservation.

The anterior regions of the zygomatic process of the maxilla attain the level of P2-P3 in MVL. In *Lepus* and *Oryctolagus,* it varies; however, it is either lower or on the same level as in MVL, whereas in *Sylvilagus*, it is situated in the middle of P2 or slightly higher. The zygomatic arches display a slight inclination, diverging posteriorly in MVL, as in *Lepus* and *Oryctolagus.* In comparison to *Lepus* and *Oryctolagus,* which possess large and circular auditory bullae, the bullae of MVL appear to be oval-shaped and inflated. The auditory bullae of MVL are characterized by a greater anterior-posterior extension, resulting in a more rounded frontal end and a relatively pointed posterior end, while their position is almost parallel to the anteroposterior axis of the skull; in *Sylvilagus*, the bullae form a stronger angle with the sagittal plane and are rounder. The length of the auditory bullae in relation to the basal length of the cranium of MVL (index I7) is closer to the values of *Oryctolagus*. The value of I7 for *Lepus* and *Sylvilagus* is significantly lower than in MVL. Regarding the breadth of the auditory bullae relative to the basal length (index I8) and the greatest neurocranium breadth it is clear that the auditory bullae of MVL are similar in breath to those of *Oryctolagus.* Unfortunately, due to the poor preservation not much can be added for the foramen magnum.

In lateral view, the nasals of MVL-47 are similar to those of *Sylvilagus* and *Oryctolagus*. They have a flatter appearance, and they are not as inflated as in *Lepus. Lepus* also displays a thinning in the anterior region of the zygoma, making the eye region seem larger. This thinning of the zygoma is not observed in MVL. In MVL the zygoma in that area share the more robust development observed in *Oryctolagus*. Moreover, the V-shaped structure on the jugal is more prominent in *Oryctolagus* as in MVL, while in *Lepus* it is not that broad. Another aspect worth noting is the angle of facial tilt. According to the reports of Kraatz et al. (2015), the facial tilt angle for *S. floridanus* varies from 31.6^{o} to 43.9^{o}, whereas for *O. cuniculus* it is between 24^{o} and 35^{o}, and for *Lepus* it is more obtuse of above 40^{o}. The MVL specimens have an estimated range of facial tilt of 38^{o} to 43^{o} (mean=40.5^{o}, N=2) which is in between the upper range of *Sylvilagus* and in the lower of *Lepus*.

The maxillary fenestration is very prominent and equally noticeable in MVL as in *Lepus*. *Sylvilagus* and *Oryctolagus* display a tamer fenestrated maxilla. The frontal of MVL, when viewed laterally, shares a similar development to *Oryctolagus*. *Lepus* exhibits a more lifted and arched frontal (due to the wing-shaped supraorbital process), allowing the eye socket to appear large. In *Oryctolagus* this development is not so prominent, and the frontal appears flatter. The posterior suture between the parietals is raised as a low sagittal crest in MVL-46 and MVL-51. This type of crested line can also be observed in *Sylvilagus* and *Oryctolagus*. The tympanic bulla seems to be overall similar in both MVL and in the recent leporids. Unfortunately, regarding their development, not much can be said due to poor preservation. However, it can be observed that the placement of the external auditory meatus in MVL is similar to that of *Lepus* and *Oryctolagus,* which in contrast to *Sylvilagus*, exhibit a more laterally positioned meatus. This placement allows the opening of the external auditory meatus to be visible in lateral view. *Sylvilagus* does not have the opening of the meatus visible when viewed laterally. The most visible meatus can be observed in *Lepus,* while in *Oryctolagus* it is slightly more tilted. MVL shares and intermediate position to the latter taxa for its external auditory meatus.

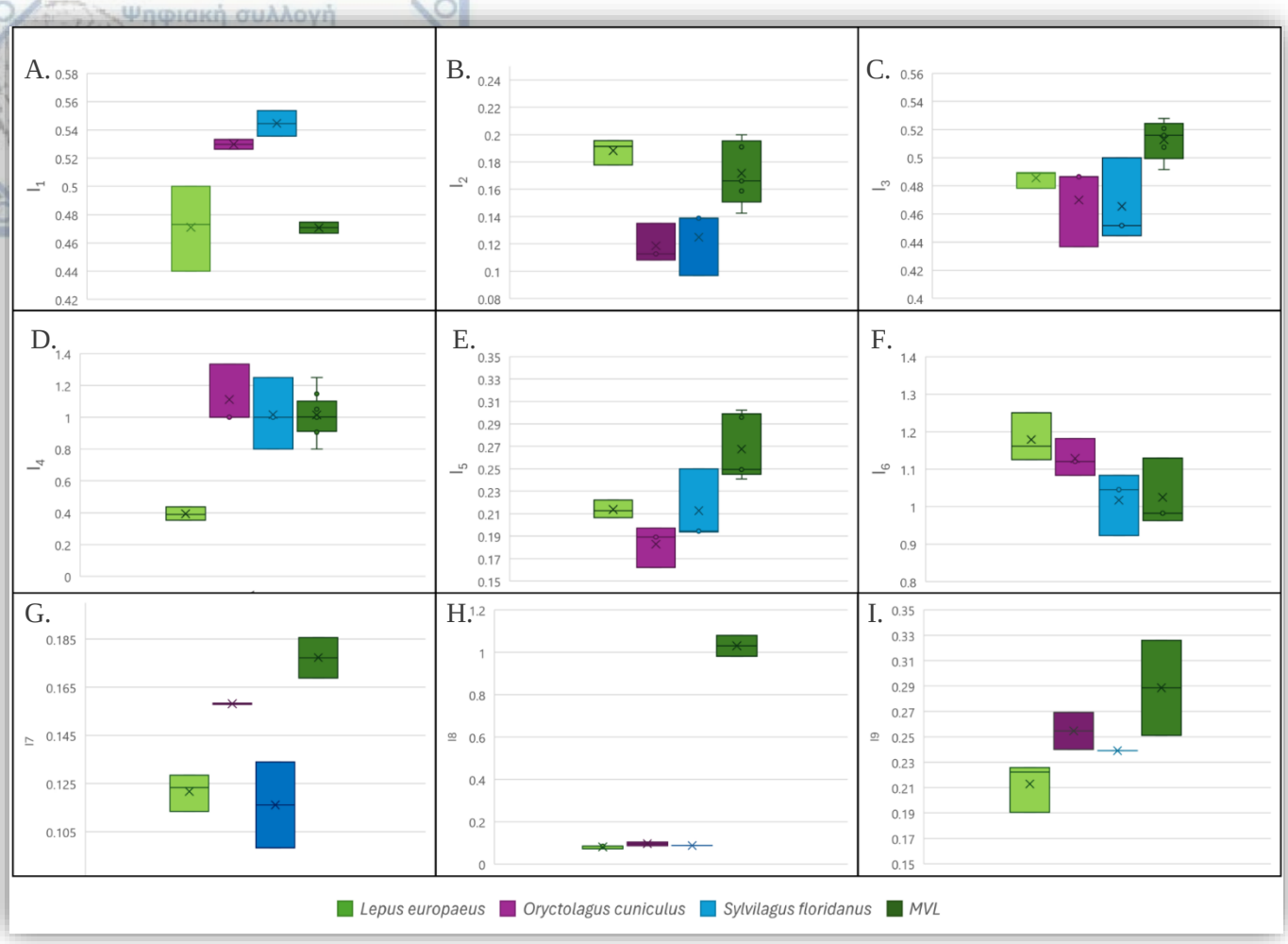

Figure 14. Box plots of the cranial and mandibular indices for *Lepus europaeus*, *Oryctolagus cuniculus*, *Sylvilagus floridanus*, and MVL. ***A)*** **I1** (FL/BL) ***B)*** **I2** (GBIF/DEL) ***C)*** **I3** (IFL/DEL) ***D)*** **I4** (PL/DEL) ***E)*** **I5** (PB/DEL) ***F)*** **I6** (dl/al) ***G)*** **I7** (ABL/BL) ***H)*** **I8** (ABB/BL) ***I)*** **I9** (ABB/GNB).

Finally, the mandibles of MVL have only the corpus preserved. Compared to the three extant taxa, they do not display any significant morphological difference. However, the diastema in relation to the alveolar length (index I6) in MVL is closer to that in *Sylvilagus*, while *Oryctolagus* and *Lepus* exhibit higher values (Fig. 14F). The mental foramen in MVL is overall prominent and oval-shaped, as in the extant species. Lastly, the mental fenestration of MVL shares the same placement as in the extant taxa; they are located on the dorsal as well as the posteroventral surface of the mandible and are similarly numerus and prominent.

4.1.2. Comparison with fossil leporid crania

Alilepus hibbardi's (IMNH 38695) complete skull, recovered from the Late Miocene in North America (White 1991), exhibits cranial dimensions that are in close proximity to those of MVL. In ventral view, *A. hibbardi* shows a shorter premaxilla in comparison to the more elongated one in MVL. The degree of fenestration observed in the maxilla and premaxilla of *A. hibbardi* is notably less than MVL. The toothrow length of *A. hibbardi* is similar to the higher values observe in MVL (MVL-47 and MVL-73a). The position of the toothrow has a straighter orientation in *A. hibbardi* in contrast to the slightly more curved one in MVL. The diastema's length in *A. hibbardi* falls within the range of MVL. According to the available illustrations, the development of the incisive foramen is similar in both MVL and *A. hibbardi*. The length of the palatal bridge of *A. hibbardi* is close to MVL-48 and MVL-50. The breadth of the choanae of

A. hibbardi is also within the MVL range. In addition, the index I4 in *A. hibbardi* is close to the value of MVL, but slightly lower (I4= 0.96). *A. hibbardi* exhibits a zygomatic breadth close to that of MVL-48, which falls in the higher size range of MVL. White's (1991) illustrations indicate that the zygomatic arches exhibit a similar level of inclination in comparison to those observed in MVL. Nevertheless, when viewed laterally, the posterior end of the zygomatic arches is situated at a higher position in *A. hibbardi* relative to that of MVL, resulting in comparatively smaller eye sockets. In dorsal view, the anterior portion of the nasals in *A. hibbardi* appear to be wider compared to MVL. The subraorbital process of the frontal bone in *A. hibbardi* shows greater development; it is more rounded and laterally extended, thereby leading to a posterior flexid that is wider and deeper in comparison to the sharper, smaller, and more medially positioned state in MVL. Regarding the mandible, the diastema of *A. hibbardi* falls within the range of MVL and is close to the values obtained for MVL-69, MVL-72, and MVL-73b sin, which are of slightly larger size. The diastema area seems to be more concave in *A. hibbardi*. The length of the alveoli is notably larger in *A. hibbardi* than in MVL.

Hypolagus balearicus Quintana, Bover, Alcover, Agustí & Bailon, 2010 from the Early Pliocene locality of Ses Fontanelles (Eivissa) (Balearic Islands, Western Mediterranean Sea) (Cardona and Moncunill-Solé, 2014), is one of the few Eurasian fossil species known by its skull. The specimen is poorly preserved and lacks dentition. However, certain morphological characteristics that can be observed are intriguing when compared to the leporid of MVL. The palate as well as the choanae are narrower in comparison to MVL, yet the length of the palate fits within the MVL range. As in MVL-46 and MVL-50, the premolar foramen of *H. balearicus* are situated slightly below the maxilla-palatine suture. The length across the facial tubers is significantly smaller than that measured in the studied leporid. The zygomatic process of the maxilla in MVL has a narrower root, while in *H. balearicus* the root is more laterally elongated. In both cases, the overall morphology of this process is similarly angular and arched. The fenestration observed in the mandibular body of *H. balearicus* is similar to that of MVL.

According to Averianov (1995), the remains of *T. dumitrescuae* skull are limited to two small fragments of the frontal and occipital bones. Regrettably, only sketches are accessible for the descriptions, as no photographs are provided. Thus, we'll settle for the author's own descriptions. Specifically, the median portion of the preserved right frontal does not differ from the condition seen in *L. europaeus*, similar to MVL. Averianov (1995) highlights that the foramen magnum displays resemblance to that of *L. europaeus*, wherein it is positioned more superiorly. This description appears to be inconsistent with the foramen magnum of the studied leporids, and specifically the specimens MVL-47, MVL-48, and MVL-51, where the foramen magnum is preserved. As previously stated, the placement of the foramen magnum in MVL is relatively more posterior and can only be fully observed from an occipital viewpoint. Averianov (1995) concluded that the auditory bullae of *T. dumitrescuae* are presumably smaller in comparison to extant species and similar in size as *Pentalagus*. The auditory bullae observed in the material of MVL are close in size to *Oryctolagus*. Finally, regarding the mandible, *T. dumitrescuae* (ZIRAS 80457) exhibits slightly greater length in the mandible’s diastema and the alveoli compared to MVL, whereas the rest of the mandible do not show any major dissimilarities worth discussing.

The palatal parts of *T. meridionalis* were recently described by Sen and Geraads (2023). Similar to MVL, the posterior end of the incisive foramen produces two rounded grooves that are separated by a pointed mesial palatal spine and extend posteriorly to the mid-level of the P2s. In contrast to MVL, the premolar foramen is not situated on the maxilla-palatine suture. In *T. meridionalis*, the palatal length in relation to the breadth of the choanae exhibits significantly lower values than MVL. It is also noteworthy that the absence of the posterior spine of the palate in *T. meridionalis* is a distinguishing characteristic between the MVL specimens and the majority of leporids (Sen and Geraads, 2022). The inter-zygomatic width in *T. meridionalis* measures 34.7 mm between the antero-external borders of the zygomatic arches, falling below the range of the MVL specimens, yet in close proximity to MVL-52. Like *T. meridionalis*, the zygomatic arches of MVL exhibit a slight posterior divergence. The zygomatic process of the maxilla in MVL forms a sharp V-shaped structure positioned horizontally on the bone. Conversely, in *T. meridionalis*, this feature is less developed and not as arched and sharp.

4.2. Dentition

Hypolagus is a widely distributed and well-understood genus of Archaeolaginae that exhibits quite a diversity in tooth structures (Fladerer and Reiner, 1996). Nevertheless, the p3 of *Hypolagus* lacks an anteroflexid and a mesoflexid (A0/PR0 type), thus differing from the studied material (Čermák and Wagner, 2013; Čermák et al., 2015). On the other hand, *Alilepus* represents one of the most primitive Leporinae forms. *Alilepus* entered Eurasia through Beringia during the Late Miocene (Čermák et al., 2015). It possesses a mesoflexid or a mesofossetid on p3 (A0/PR1-2) but lacks an anteroflexid, which is in contrast to MVL morphology. *Pliopentalagus* differs from the MVL taxon in the greatly crenulated flexids in the lower teeth (Tomida and Jin, 2005). Moreover, *Pliopentalagus* has a p3 with the "*Alilepus*" pattern, yet the anterior enamel of its talonid shows crenulations that are inconsistent with the much simpler enamel of MVL. In addition, the enamel of the anterior edge of the talonid in the m2 is also crenulated in contrast to MVL.

It is evident that, by its dental features and especially p3 morphology, the studied leporid material from MVL belongs to the genus *Trischizolagus* in the following diagnostic features: 1) the presence of a three-folded trigonid in p3, also known as the "*Alilepus*" pattern; 2) the rhombic outline of p3 with a broad lingual anteroconid and a well-developed anteroflexid 3) the presence of simple and uncrenulated enamel; 4) the general pattern of the lower and upper check teeth; and 5) the overall size of the upper and lower check teeth (Averianov and Tesakov, 1997; López-Martínez et al., 2007; López-Martínez, 2008; Čermák and Wagner, 2013). Čermák and Wagner (2013) presented a comprehensive review of *Trischizolagus* and recognized six species: *T. crusafonti* (Janvier and Montenat, 1971), *T. dumitrescuae* Radulesco and Samson, 1967; *T. gambariani* (Melik-Adamyan, 1986); *T. maritsae* De Bruijn, Dawson, and Mein, 1970; *T. mirificus* Qiu and Storch, 2000; *T. nihewanensis* (Cai, 1989); and *T. raynali* (Geraads, 1994). One more species, T. *meridionalis* has been recently described by Sen and Geraads (2023) from Morocco.

T. crusafonti was originally described from the latest Miocene (MN 13) site of La Alberca in the Fortuna Basin, southern Spain (Janvier and Montenat, 1971). Sen (2020) also described some specimens of *T. crusafonti* from the Early Pliocene of Dorkovo in Bulgaria. The overall teeth dimensions from MVL are significantly greater than those from La Alberca and Dorkovo (Table 22, Fig. 15). Regarding its

morphology, the p3 of *T. crusafonti* is attributed to the "*Hypolagus*" pattern, in contrast to the "*Alilepus*" pattern shown in MVL. *T. crusafonti* p3 displays a deep hypoflexid that exceeds half the width of the occlusal surface, and it is curved backward in some specimens; in MVL, the hypoflexid is not so deep and a thin enamel connection between the trigonid and talonid on the lingual side is observed. In the La Alberca specimens, the mesofossetid is missing, while in one Dorkovo specimen it is present (Sen, 2020). From the illustrations in Sen (2020), *T. crusafonti* follows a mainly A1/PR0 pattern in p3, while one specimen in Dorkovo displays a PR2 pattern in difference from the A1/PR1 pattern of MVL. The P2 of *T. crusafonti* displays three flexa, which is consistent with MVL. Like the MVL specimens, in *T. crusafonti* the level of enamel crenulation observed from the third premolar to the second molar is reduced.

The dimensions of *T. gambariani* from the Early Pliocene (MN14) of Nurnus in Armenia and Tepe Alagöz in Turkey (Čermák et al., 2019), indicate a smaller size compared to the MVL specimens (Table 22, Fig. 15). The lower molariforms are also smaller. In comparison to the leporids of MVL, the p3 of *T. gambariani* exhibits the "*Nekrolagus*" pattern and is primarily limited to the PR2 pattern, which is characterized by the presence of mesofossetid, and the A1 pattern, which is characterized by the presence of anteroflexid (Čermák et al., 2019). This differs significantly from MVL, where such patterns are not observed. P2 of *T. gambariani* displays no significant differences and presents the same range of morphological variation as that seen in MVL. In addition, the P2 size range (Table 22, Fig. 16) of *T. gambariani* are much smaller than in the studied specimens. Apart from the dimension, no noteworthy distinctions were detected between the lower and upper check teeth of the two taxa.

T. maritsae, originating from the Greek island of Rhodos, represents the earliest documented species of *Trischizolagus* in eastern and south-eastern Europe, dated to Late Miocene and Early Pliocene (de Bruijn et al., 1970; Vasileiadou and Sylvestrou, 2022). *T. maritsae* is the smallest species recorded so far into this genus. The type mandible is poor for displaying the pattern of p3, and only in one p3 of Maritsa is the mesoflexid well-defined, and the paraflexid displays a deep fold, a very different morphology from MVL. According to Čermák and Wagner (2013), the "*Hypolagus*" pattern predominates in *T. maritsae*, characterized by a crescent-shaped outline. It must be noted that, all known p3s from Maritsa apparently come from subadult individuals (d e Bruijn et al. 1970), and therefore their comparison to other taxa may be problematic. Furthermore, Koufos and Koliadimou (1993) assigned three upper molariforms from the Megalo Emvolon 1 locality (MEV-1005) to *Trischizolagus* cf. *maritsae*. The size of MEV-1005 falls within the known size range of *T. maritsae* (Table 22, Fig. 15). Considering that no p3 has been found, the authors suggested that it is unclear whether MEV-1005 meets the criteria to be assigned to *T. maritsae* or is a smaller individual of *T. dumitrescuae*, which is the second species reported in the site. In our opinion, *T.* cf. *maritsae* is still the most appropriate reference for MEV-1005 based on the available data, including the new ones from MVL, which show that MEV-1005 falls well outside the size range of *T. dumitrescuae*.

T. mirificus was described from the Lower Pliocene (MN14) locality of Bilike in Inner Mongolia, China (Qiu and Storch, 2000). The p3 of this species exhibits a discernible dissimilarity from the MVL taxon, as it displays a significantly less complex "*Hypolagus*-like" morphology of the third premolar (PR0 pattern), characterized by less prominent folds on the trigonid. The P2 of *T. mirificus* exhibits a simplified

occlusal outline, in contrast to MVL, causing the mesoflexus and hypoflexus in *T. mirificus* to be nearly undeveloped. *T. mirificus* was also smaller compared to the MVL taxon (Table 22, Figs. 15, 16) (Qiu and Storch, 2000).

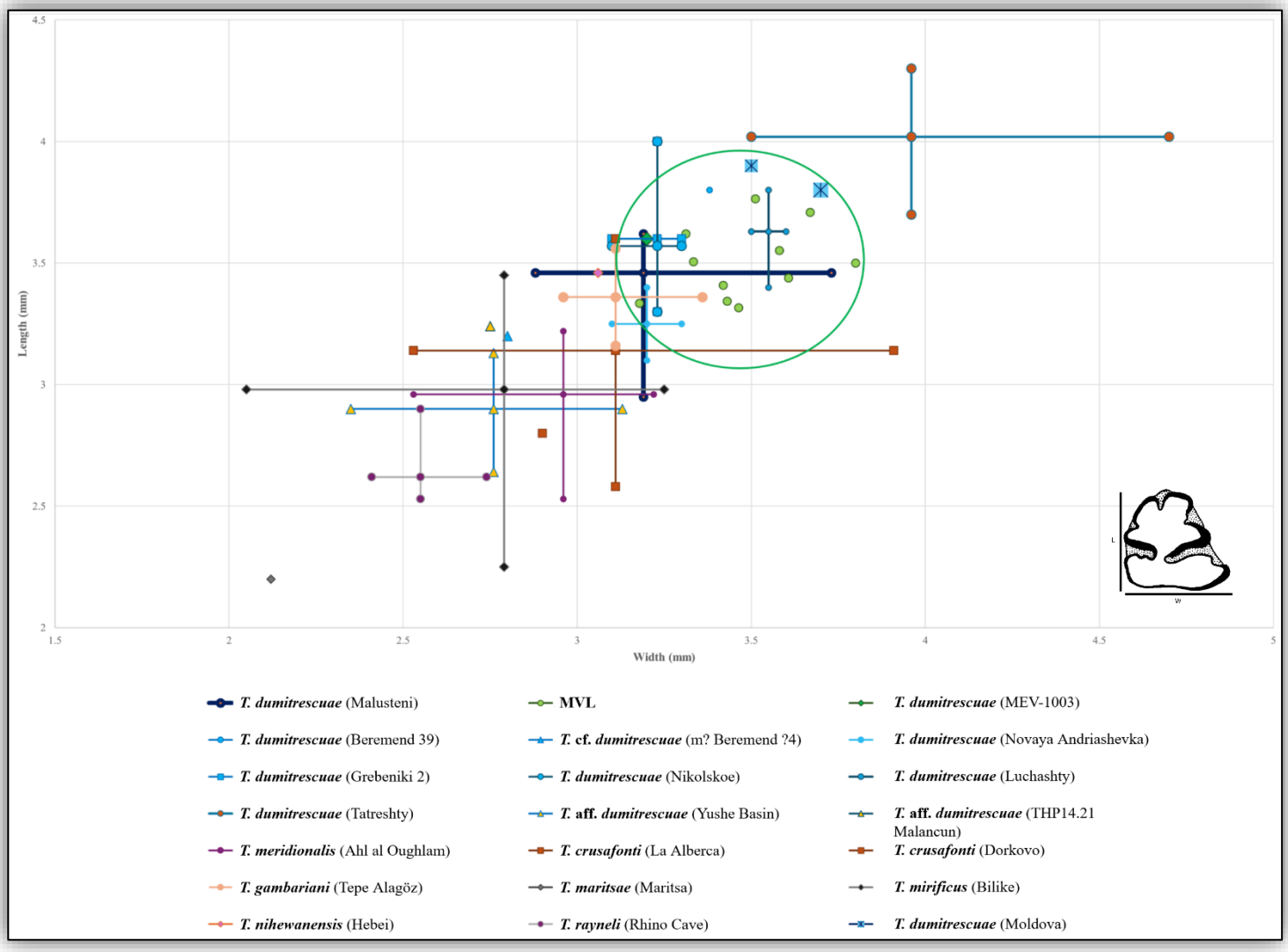

Figure 15. Scatter diagrams showing the width (x-axis) against the length (y-axis) of the p3 of the leporid of MVL and the species: *T. dumitrescuae* from Măluşteni (Romania) (Koufos and Koliadimou, 1993; Crespo et al., 2023); *T. dumitrescuae* (MEV-1003) from Megalo Emvolon MEV (Greece) (Koufos and Koliadimou, 1993); *T. dumitrescuae* from Moldova (Averianov, 1995), *T. dumitrescuae* from Beremend 39 and *T.* cf. *dumitrescuae* from m ?Beremend [?4] (Čermak and Wagner, 2013); *T. dumitrescuae* from Novaya Andriashevka, Grebeniki 2, Nikolskoe, Stavnichevo, Moskovei, Lucheshty, Tatareshty (Averianov and Tesakov, 1997); *T.* aff. *T. dumitrescuae* from Yushe and THP 14.217 Malancun (Wu and Flynn, 2017); *T. meridionalis* from Ahl al Oughlam (Morocco) (Sen et al., 2023); *T. crusafonti* from La Alberca (Spain) (Janvier and Montenat, 1971; Koufos and Koliadimou, 1993) and Dorkovo (Bulgaria) (Sen, 2020); *T. gambariani* from Tepe Alagöz (Turkey) (Čermak et al., 2019); *T. maritsae* from Maritsa (Greece) (Koufos and Koliadimou, 1993); *T. mirificus* from Bilike (China) (Qiu and Storch, 2000); *T. nihewanensis* from Hebei (China) (Tomida and Qiu, 2005); *T. rayneli* from Rhino Cave (Morocco) (Geraads, 1994). Within the green circle is the samples from MVL.

Another species from China, *T. nihewanensis*, is from the lower part of the Daodi Formation (MN16) of Yangyuan and Yuixian (Hebei Province) (Tomida and Qiu, 2005). *T. nihewanensis*, originally described as *Pliopentalagus*, was reviewed based on one p3 and two lower molariform teeth. In the view of Tomida and Jin (2005), the leporid is not referable to *Pliopentalagus* due to the simple morphology of the lower molariform teeth, associated fauna, and evolutionary trends. The only available p3 (GMC V 2008-1) shares the same "*Alilepus*" pattern with the MVL specimens while exhibiting clear infolded walls of posterior tooth structures. MVL-72, as previously described, exhibits a bilobal anteroconid with dual anteroflexids that are wide and short, similar to the two folds in the anteroconid of *T. nihewanensis*. The isthmus connecting the trigonid to the talonid is rather small in *T. nihewanensis*, while in the MVL specimens it is much wider. Tomida and Jin (2005) reported that the p3 of *T. nihewanensis* has the most complicated enamel pattern among the species of the genus, in contrast to the much simpler and uncrenulated enamel in the leporid of MVL. Nevertheless, the p3 of *T. nihewanensis* falls within the dimensional variability of MVL sample (Table 22, Fig. 15), especially, the length of MVL-73b and MVL-63. However, the p3 in *T. nihewanensis* is narrower than in MVL (Table 22, Fig. 15). The p4/m1 also shows weak crenulation on the thin enamel of the anterior edge of the talonid in *T. nihewanensis*, which is not observed in any of the specimens MVL. The remaining specimen of *T. nihewanensis*, a left m2, exhibit no significant differences from the MVL ones and are comparable in size (Tomida and Qiu, 2005).

T. raynali was previously described as *Serengetilagus raynali* from the Pleistocene locality of Rhino Cave in Morocco (Geraads, 1994). López-Martinez et al. (2007) transfered this species into *Trischizolagus*. Based on the illustrations presented by Geraads (1994), it differs from the MVL taxon in the presence of the "*Nekrolagus*" pattern in p3, which displays a mesofossetid (A1/PR2). Additionally, it is noticeably smaller in size (Geraads, 1994), significantly lower than the p3 range observed in MVL (Table 22, Fig. 15).

T. meridionalis from the Plio-Pleistocene locality of Ahl al Oughlam, Morocco was recently described (Sen and Geraads, 2023). The most notable difference between *T. meridionalis* and the studied material is, as shown in Table 22, its substantially smaller dimensions (Figs. 15, 16). Additionally, its p3's may be of the "*Alilepus*", "*Hypolagus*", or "*Nekrolagus*" pattern (Sen and Geraads, 2023). While certain specimens of *T. meridionalis* exhibit the "*Alilepus*" trait as in the leporid of MVL, the Moroccan species differs from MVL in the presence of a deep and narrow anteroflexid in its p3, which separates the anteroconid into two almost equal-sized parts. Contrary to the MVL material, the buccal anteroconid does not protrude, and nearly half of p3s have a mesofossetid or lack a mesoflexid. Regarding the mandible, the specimens from Ahl al Oughlam exhibit the buccal face of the body to be perforated by many foramina, primarily under the p3 and along the ventral side of the corpus below the diastema. This type of fenestration is rather prominent and common as observed from the available photographs provided (Sen and Geraads, 2023). Only in MVL-65 and MVL-73b a fenestration of that kind can be observed, while in the rest of the available MVL specimens the fenestration is not so prominent. The P2s of the MVL leporid are less compressed, exhibiting a straighter position in contrast to the more anteroposterior compressed P2 of *T. meridionalis*, causing the hypoflexus and mesoflexus to be shallow and prominent. However, the development of the three flexa, hypoflexus, paraflexus, and mesoflexus, is varied in both *T. meridionalis* and the specimens analyzed. The size

of the P2 is significantly larger in MVL than in *T. meridionalis* (Table 22, Fig. 16). The rest of the upper molariform teeth do not show any major dissimilarities.

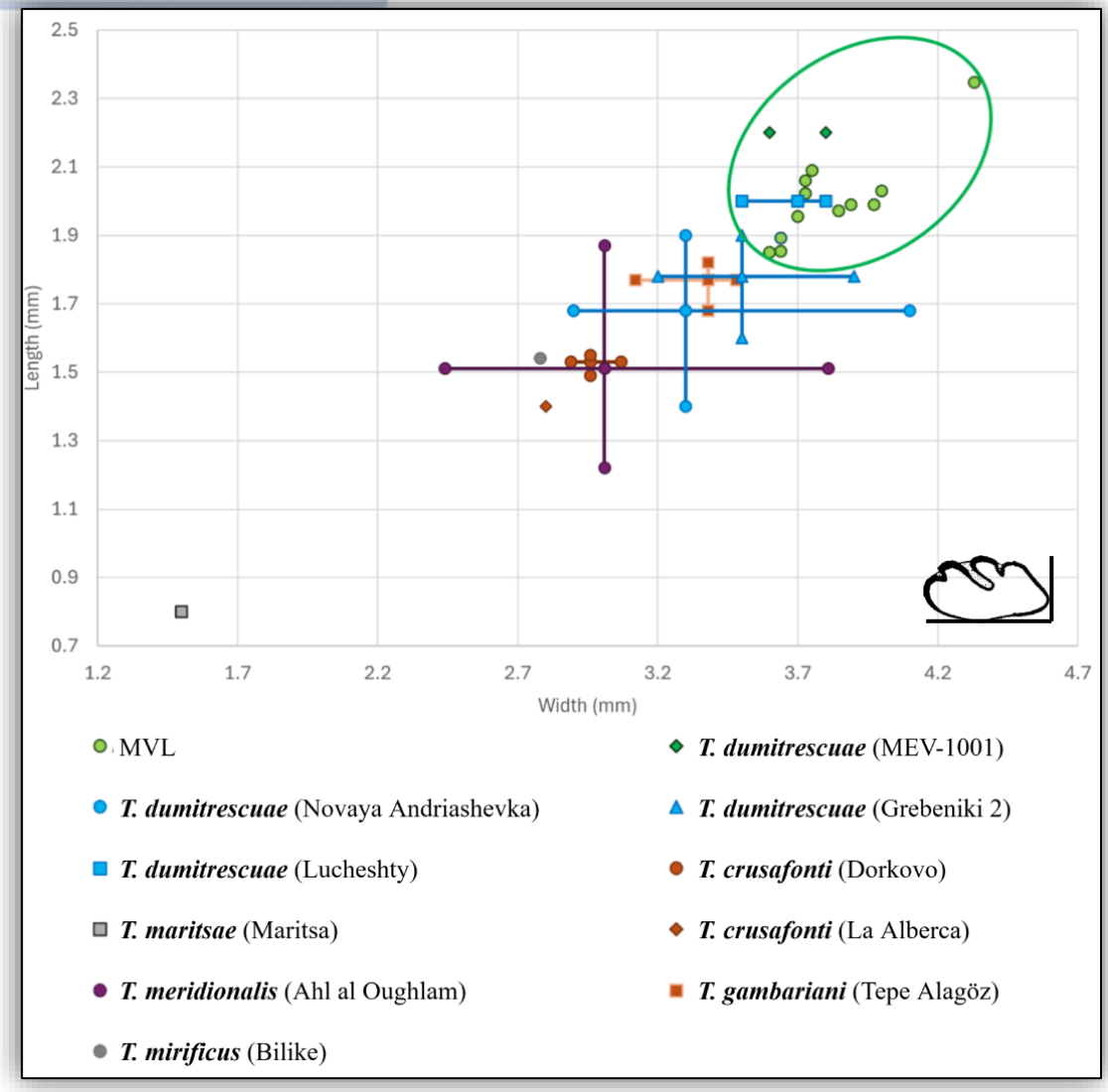

Figure 16. Scatter diagrams showing the length (y-axis) against the width (x-axis of the P2 of the leporid of MVL and the species: *T. dumitrescuae* (MEV-1001 sin/dex) from Megalo Emvolon MEV (Greece) (Koufos and Koliadimou, 1993); *T. dumitrescuae* from Novaya Andriashevka, Grebeniki 2, Lucheshty, (Averianov and Tesakov, 1997); *T. meridionalis* from Ahl al Oughlam (Morocco) (Sen et al., 2023); *T. crusafonti* from La Alberca (Spain) (Janvier and Montenat, 1971; Koufos and Koliadimou, 1993); *T. gambariani* from Tepe Alagöz (Turkey) (Čermak et al., 2019); *T. maritsae* from Maritsa (Greece) (Koufos and Koliadimou, 1993); *T. mirificus* from Bilike (China) (Qiu and Storch, 2000).

Table 22. p3 and P2 size comparison among *Trischizolagus* species. Measurements in mm.

Comparative material	**Locality**	**p3l**	**p3w**	**P2 L**	**P2 W**	**Data source**
T. dumitrescuae	MEV (Megalo Emvolon-1)	3.6	3.2	2.2 (N=2)	3.7; 3.6-3.8 (N=2)	Koufos and Koliadimou (1993)

T. dumitrescuae	Măluşteni (Romania)	3.46; 2.95-3.62 (N=10)	3.19; 2.88-3.73 (N=10)	-	-	Crespo et al. (2022); Averianov and Tesakov (1997); Radulesco and Samson (1967)
T. dumitrescuae	Beremend 39	3.8	3.38	-	-	Čermak and Wagner (2013)
cf. *Trichizolagus dumitrescuae*	m ?Beremend [?4]	3.2	2.8	-	-	
T. dumitrescuae	Novaya Andriashevka	3.25; 3.1-3.4 (N=2)	3.2; 3.1-3.3 (N=2)	1.68; 1.4-1.9 (N=4)	3.3; 2.9-4.1 (N=4)	Averianov and Tesakov (1997)
	Grebeniki 2	3.6; 3.2-4.1 (N=4)	3.23; 3-3.5 (N=4)	1.78; 1.6-1.9 (N=14)	3.5; 3.2-3.9 (N=12)	
	Nikolskoe	3.57; 3.3-4 (N=3)	3.23; 3.1-3.3 (N=3)	-	-	
	Stavnichevo	3	2.7	-	-	
	Moskovei	3.7	3.9	-	-	
	Lucheshty	3.63; 3.4-3.8 (N=3)	3.55; 3.5-3.6 (N=2)	2 (N=3)	3.7; 3.5-3.8 (N=3)	
	Tatareshty	4.02; 3.7-4.3 (N=5)	3.96; 3.5-4.7 (N=5)	-	-	
T. dumitrescuae	South Moldova	3.85; 3.8-3.9 (N=2)	3.6; 3.5-3.7 (N=2)	-	-	Averianov (1995)
T. aff. *T. dumitrescuae*	Yushe (China)	2.9; 2.64-3.13 (N=3)	2.76; 2.35-3.13 (N=3)	-	-	Wu and Flynn (2017)
	THP14.217 Malancun	3.24	2.75	-	-	
T. meridionalis	Ahl al Oughlam (Morraco)	2.96; 2.53-3.22 (N=28)	2.96; 2.53-3.22 (N=28)	1.51; 1.22-1.87 (N=17)	3.01; 2.44-3.81 (N=17)	Sen et al. (2023)
T. crusafonti	La Alberca (Spain)	2.8	2.9	1.4	2.8	Janvier and Montenat, 1971; Koufos and Koliadimou (1993)
	Dorkovo (Bulgaria)	3.14; 2.58-3.6 (N=4)	3.11; 2.53-3.91 (N=4)	1.53; 1.49-1.55 (N=3)	2.96; 2.89-3.07 (N=3)	Sen 2020

T. gambariani	Tepe Alagöz (Turkey)	3.36; 3.16-3.56 (N=15)	3.11; 2.96-3.36 (N=15)	1.77; 1.68-1.82 (N=4)	3.38; 3.12-3.48 (N=4)	Čermak et al. (2019)
T. maritsae	Maritsa (Greece)	2.2	2.12	0.8	1.5	Koufos and Koliadimou (1993)
T. mirificus	Bilike (China)	2.98; 2.25-3.45 (N=28)	2.79; 2.05-3.25 (N=28)	1.54	2.78	Qiu and Storch (2000)
T. nihewanensis	Hebei (China)	3.46	3.06	-	-	Tomida and Qiu (2005)
T. rayneli	Rhino Cave (Morocco)	2.62; 2.53-2.9 (N=4)	2.55; 2.41-2.74 (N=4)	-	-	Geraads (1994)

4.3 Dental variation within *T. dumitrescuae*

According to Čermak and Wagner (2013), sixteen Early Pliocene (MN 14-15) localities in Bulgaria, Greece, Germany, Hungary, Moldova, Romania, and southern Ukraine contain evidence of *Trischizolagus* in Europe that can be referred to *T. dumitrescuae*. *T. dumitrescuae* is widely recognized from its type locality in Măluşteni, Romania, as well as its neighboring locality of Beresti (Radulesco and Samson, 1967, 1995). It must be mentioned that Wu and Flynn (2017) describe *Trischizolagus* aff. *dumitrescuae* from northern China. The "*Alilepus*" pattern is the prevailing one in all sites where *T. dumitrescuae* is present, with the "*Nekrolagus*" pattern is following in frequency (Čermak and Wagner, 2013).

In more detail, the holotype of *T. dumitrescuae* p3 (I.S. 6001), consisting of an incomplete right maxilla with p3-m1, exhibits the "*Alilepus*" pattern and is characterized by an A1/Pa1/PR1 p3 morphology, which is consistent with the MVL specimens (Averianov, 1995; Čermak and Wagner, 2013). The anteroflexid of I.S. 6001 exhibits a comparable degree of development to that observed in the specimens from MVL, as evidenced by the sketches presented by Radulesco and Samson (1967) and Crespo et al. (2023). In both the type specimen and MVL (especially in MVL-69, MVL-72, and MVL-73) the anteroflexid divides the anteroconid into two nearly equal halves. The paraflexid is relatively narrow and shallow, whereas the protoflexid is wider and deeper in both MVL and the I.S. 6001. On the p3, the hypoflexid and mesoflexid of I.S. 6001 are compatible with those from MVL. In addition, the trapezoidal shape of the talonid remains consistent in both the Romanian type specimen and the majority of the MVL samples, albeit certain MVL specimens display reduced enamel on the buccal side of the hypoconid and lack of the characteristic notch observed due to possible wear stage of the enamel.

Additional specimens of *T. dumitrescuae* recovered from Măluşteni exhibit a comparable level of development in their p3 with both the holotype and the MVL leporids. It is important to highlight that the "*Nekrolagus*" pattern has been observed in a single specimen from Măluşteni (I.S. 6008) in contrast to the more common "*Alilepus*" pattern. Based on the measurements provided by Crespo et al. (2023), the p3 size range of the species at this Romanian locality falls within the size range measured

for the MVL specimens (Table 22, Figs. 15, 16). Regarding the mandible, the length of the diastema is only available from one specimen (I.S. 6008) and is measured 19.5 mm (Radulesco and Samson, 1967), which exceeds the measured range of 15.56 to 18.01 mm (N=8) in the MVL material. The maxillary fenestration is in both the MVL specimens and the specimens from Măluşteni prominent on the buccal side of the maxillary corpus at the level of the premolars and in the lower region where the mental foramen is located. As observed in MVL, this type of fenestration is visible on the lingual side, particularly along the lower mandible.

T. dumitrescuae has also been retrieved in Beresti. Regrettably, the dimensions of the p3 were not ascertainable, and the evaluation is predominantly grounded on the illustrations presented by Radulescu and Samson (1967), which portrayed two p3 specimens (I.S. 6006 and I.S. 6007). As indicated into the Măluşteni and Beresti revision reported by Crespo et al. (2023), a significant number of specimens were lost. However, the morphology of these two specimens is similar to that of the specimens under study. The second upper premolar is lost. No distinct size variation was provided for P3 and only a size range of the upper molariform (P4, M1, and M2) is available (Crespo et al., 2023). Nevertheless, the size range of the upper molariforms of MVL is in overall agreement with those from both Beresti and Măluşteni.

Averianov and Tesakov (1997) described a rich material from Moldova and Ukraine, the vast majority of which was attributed to *T. dumitrescuae*. Unfortunately, the available information for this material is poor. However, as in the MVL leporid, the East European sample shows the rhombic-rectangular p3 outline, which is accompanied by a relatively short and wide anteroconid in all cases. The "*Alilepus*" pattern is the most commonly observed, as reported by Averianov and Tesakov (1997) and Čermak and Wagner (2013). These traits are consistent with the MVL leporid.

In their study, Čermak and Wagner (2013) documented two records of *T. dumitrescuae* from the Beremend 39 location in Hungary (MN15b). The first specimen comprises a lower mandible encompassing p3 to m2. It displays the "*Nekrolagus*" pattern in p3, in contrast to the MVL specimens. In addition, it exhibits a bilobal anteroflexid that is similar to that observed in MVL-72. In terms of physical dimensions, the Hungarian specimen has a large p3, close to the length measurements of MVL-69 and MVL-70. However, the latter specimens demonstrate a slightly greater breadth. The remaining molariforms fall within the size spectrum of the MVL specimens, albeit on a larger scale. The dimensions of both the diastema and the alveolar region are significantly larger in the Hungarian specimens compared to those from MVL. In more detail, the length of the diastema in MVL ranges from 15.56 to 18.01 mm versus 21.11 mm in Beremend 39, while the length of the alveoli region ranges from 15.13 to 16.78 mm in MVL versus 18.2 mm in the Hungarian specimen. Conversely, the second Hungarian specimen has been attributed to cf. *Trischizolagus dumitrescuae* and comprises a single fragment of the left mandibular body bearing p3-p4. The pattern of p3 corresponds to that of "*Alilepus*". The anteroconid exhibits a broad morphology, defined by an undulating enamel pattern that shows resemblance to that of MVL-65.

As mentioned previously, Wu and Flynn (2017) described *Trischizolagus* aff. *T. dumitrescuae* from Yushe Basin, China, while acknowledging certain differences, such as the constant and stronger postero-internal reentrant. The Yushe specimens display the "*Alilepus*" pattern and an A1/PR1/Pa1 type of morphology, fully compatible with the leporids from MVL. It must be noted that according to the sketches by Wu and

Flynn, the isthmus between the trigonid and talonid seems to have crenulated enamel (specimens V11226.1 and V11226.3), which is not observed in the leporid of MVL. However, the development of the protoflexid and paraflexid are similar in both the Chinese and MVL samples. The p3 in Yushe are within the lower size range of MVL or slightly below (Table 22, Fig. 15).

4.4 Comparison with previous records from Megalo Emvolon

The previously discovered and studied specimens of *T. dumitrescuae* from the Megalo Emvolon-1 site (MEV) are also being compared with the newly discovered ones of MVL. The four available specimens, MEV-1001 (lower left and right upper maxillae with P2-M3), MEV-1002 (left mandibular fragment with p4-m2), MEV-1003 (lower left mandibular fragment of p3-m3), and MEV-1004 (lower left incisor), fully match those described in the present study. In more detail, both P2 of MEV-1001 share the same oval outline of the occlusal surface, overall size, and the same three flexa, with the middle paraflexus being the deepest as in MVL (Table 22, Fig. 16). Koufos and Koliadimou (1993) reported that the hypoflexus and mesoflexus exhibit significant development, whereas the paraflexus is comparatively larger and extends nearly halfway over P2. The aforementioned characteristics were also observed in the MVL samples. In line with Fladerer and Reiner (1996) and Čermák (2009), the lagicone of the MEV sample is of the B morphotype, and the hypercone follows the V type of enamel structure, the same as previously described for the MVL specimens in this thesis. The rest of the upper molariforms described by Koufos and Koliadimou (1993) have a close resemblance to the MVL ones and do not reveal any significant dissimilarities worth mentioning. P2 measurements of MEV are more comparable to MVL-47, MVL-48, and MVL-50, while the rest are also in close range. MVL-48 has the greatest P2 of all the material. Although the length of P2 in MVL specimens varies between 3.6 and 3.9 mm, only the width of MVL-48 is substantially larger. The morphology of the upper molariform teeth from MEV also displays the same development as shown in the MVL material, while the size is within the range of the understudied material.

Regarding the p3 morphology, only MEV-1003 has the p3 intact at the left lower toothrow, but it is severely eroded, and only the occlusal outline can be seen, with the enamel completely gone. In light of that, no detailed morphological observations can be made. Nevertheless, the fundamental anatomy of the p3 closely mirrors that of the MVL specimens. In more detail, the hypoflexid of MEV p3s apart from the poor preservation seems to be deep and rather broad, in close resemblance with all MVL specimens. The mesoflexid of MEV seems to be lingually closed while retaining the appearance of a fold. Although none of the MVL specimens have a mesoflexid that is closed, in MVL-70, MVL-73dex, and MVL-73sin, the mesoflexid is close to shutting but not completely closed. The protoflexid of MEV is shallow and relatively wide, resembling the previously described “V-shaped” flexids of MVL-63, MVL-65, MVL-70, MVL-71, and MVL-72b. The anteroflexid of MEV-1003 is close to MVL-63, MVL-66, MVL-69, MVL-70, and MVL-73b dex, revealing a U-shaped anteroflexid that is narrower, and less shallow, and somewhat broader than in the other specimens. As in MVL-73, the paraflexid is quite broad and open. According to Fladerer and Reiner (1996) and Čermák (2009), the hypoconid of MEV-1002 is either of an “e” or “d morphotype”, and the hypoflexid shows an “A” or “C morphotype”. Although none of the MVL specimens show a similar hypoconid to MEV-1002, the hypoflexid is like MVL-71, MVL-65, MVL-66, MVL-69, and MVL-73b. The size of

the p3 is also in agreement in both MEV and MVL (Table 22, Fig. 15). Similar to the upper molariforms, the lower molariforms share a strong resemblance with the MVL specimens and indicate no major differences worth discussing.

4.5 Postcranial comparisons

It is rare to come across complete or nearly complete skeletons of fossil leporids, but there have been some notable findings in recent years. For instance, Averianov (1995) reported on a partial skeleton of *T. dumitrescuae* (ZIRAS 80457) discovered in South Moldova. Similarly, Sen and Geraads (2023) described parts of the skeleton of *T. meridionalis* found in Morocco. Fostowicz-Frelik (2007) described the hind limb of *H. beremendensis* in comparison to those of currently existing species *L. europaeus*, *O. cuniculus*, and *S. floridanus*. Although complete skeletons of fossil leporids are scarce, these discoveries have provided valuable insight into the anatomy and evolution of leporids.

Scapula

The neck of the scapula in MVL is not as broad, as in *L. europaeus* and *T. dumitrescuae* from Moldova, likely resembling the state observed in *O. cuniculus*, *S. floridanus*, and *P. furnessi* (Averianov, 1995). In *T. meridionalis*, the proximal width is slightly broader than that observed in MVL. The coracoid process in MVL is not as narrow and closely located from the glenoid cavity as in *O. cuniculus*, resembling the condition of *L. europaeus* and *S. floridanus*. Averianov (1995) mentioned that this area for *T. dumitrescuae* from Moldova, resembles that of *Lepus*, as is the case in MVL.

Humerus

In proximal view, the head of the humerus in MVL is oval, like in *T. dumitrescuae* from Moldova, (Averianov, 1995). In *L. europaeus*, *O. cuniculus*, and *S. floridanus*, the humeral head is more rounded than that of MVL. The proximal width of the bone in MVL is considerably narrower than that of *T. dumitrescuae* from Moldova, and close to that of *S. floridanus*. The greater tuberosity in MVL is smaller than in *L. europaeus* but larger than in *S. floridanus*. In the latter feature, MVL resembles *T. dumitrescuae* from Moldova, and *O. cuniculus*. In comparison to *O. cuniculus* and *S. floridanus*, the lesser tubercle in MVL is not as well developed. It resembles the weaker state observed in *L. europaeus* and *T. dumitrescuae* from Moldova. Between the greater and lesser tuberosities, the proximal bicipital groove of MVL has converging, indistinct borders, similar to those of *O. cuniculus*, *T. meridionalis*, and *T. dumitrescuae* from Moldova. Like *T. dumitrescuae* from Moldova and *O. cuniculus*, the deltoid crest in MVL is very strongly developed and extends further distally. In *L. europaeus* and *T. meridionalis*, the deltoid crest is weaker, and it is nearly absent in *S. floridanus*. The distal width is broader in *S. floridanus*, while the lateral epicondyle is slightly more prominent in comparison to MVL. Unfortunately, no more comparisons could be made for the distal epiphysis of the humerus due to lack of comparative material.

Ulna and Radius

In MVL, only one complete ulna has been recovered. Compared to *T. meridionalis* and *S. floridanus*, the ulna of MVL is longer. *L. europaeus* has the longest ulna, resulting in an excessively thin distal part of the shaft, unlike MVL, which has the broadest shaft midpoint and comparable proximal and distal widths, similar to that

observed in *S. floridanus* and *O. cuniculus*. Regarding the proximal end, the length of the olecranon in MVL is slightly shorter than that of *T. dumitrescuae* from Moldova and *L. europaeus*. The olecranon process in MVL also exhibits an inside curve across the medial and lateral aspects like that in *O. cuniculus*, and unlike *L. europaeus* and *S. floridanus,* where it is flat. In MVL and *T. dumitrescuae* from Moldova, the lateral olecranon tuber is weaker developed than in *L. europaeus*, *O. cuniculus*, and *S. floridanus*. The width of the radial articular facets in MVL is also slightly narrower than that of *L. europaeus*, and close to that of *T. dumitrescuae* from Moldova. Moreover, the coronoid process is relatively weak, as in *T. dumitrescuae* from Moldova, *L. europaeus*, and *S. floridanus*. The radial notch in MVL is slightly less pointy than in *L. europaeus*, following the weaker condition observed in *S. floridanus*, *O. cuniculus*, and *T. dumitrescuae* from Moldova.

Only one specimen of radius is complete in MVL. The length of the radius in MVL is shorter than that of *T. meridionalis*. *L. europaeus* exhibits a much longer and rather robust radius in comparison to that of MVL. According to Averianov (1995), the ratio of the anteroposterior diameter to the width is 0.67 in *T. dumitrescuae* from Moldova, identical to that of MVL, while it is higher in *O. cuniculus*, and lower in *L. europaeus*. As in *T. dumitrescuae* from Moldova, *L. europaeus*, and *S. floridanus,* the arching of the shaft occurs mostly in the proximal portion of the MVL, and the distal part of the shaft remains essentially straight. The proximal end in MVL shares the same robustness with *T. meridionalis*, while in *S. floridanus* it is much slenderer. There are no apparent morphological differences in the upper epiphysis. However, the distal width in MVL is larger than in *T. meridionalis*. Only the width of the distal end is recorded for the Moldavian *T. dumitrescuae* and is slightly above the size range of MVL. The shape of the distal articulation strongly resembles that of *T. meridionalis*, *L. europaeus,* and *S. floridanus*, which is more rectangular.

Pelvis

The length of the acetabulum in contrast to its height (Ico1; Fig. 17; Table 23) is generally similar in all the studied taxa, while in MVL it has the lowest value. According to Fostowicz-Frelik (2007), in rabbits, the acetabulum is slightly more round in comparison to *L. europaeus,* and the insisura acetabuli is very narrow and almost fused. In MVL, the acetabulum is oval-shaped, and the notch is similarly narrow, but its tip is not as pointy in comparison to *H. beremendensis*. Also, in MVL-137, the acetabular notch is closed, as in *T. meridionalis* (AaO-2494) (Sen and Geraads, 2023).

The ischial tuberosity is only preserved in MVL-146 and partially in MVL-136, and it appears to be mediolaterally broader in comparison to *O. cuniculus*, *S. floridanus*, and similar to that observed in *L. europaeus. Lepus* exhibits a more isometric shape for this area. The ischial tuberosity of MVL appears to be similar to that of the ZIRAS 80457 of *T. dumitrescuae* from Moldova (Averianov, 1995). The diameter of the acetabulum is shorter in *T. meridionalis* in comparison to MVL. The ilium is not fully preserved in the material. However, the width of the wing of the ilium seems to be intermediate between *Lepus*, which has the broadest one, and *Sylvilagus* and *Oryctolagus,* which have the narrowest. The width of the body of the ilium relative to the length of the acetabulum (Ico2; Fig. 17; Table 23) is smaller in MVL than in *H. beremendensis* and *P. furnessi*. The robustness of the coxal of MVL is analogous to that of *O. cuniculus,* with the latter being slightly more heavily built.

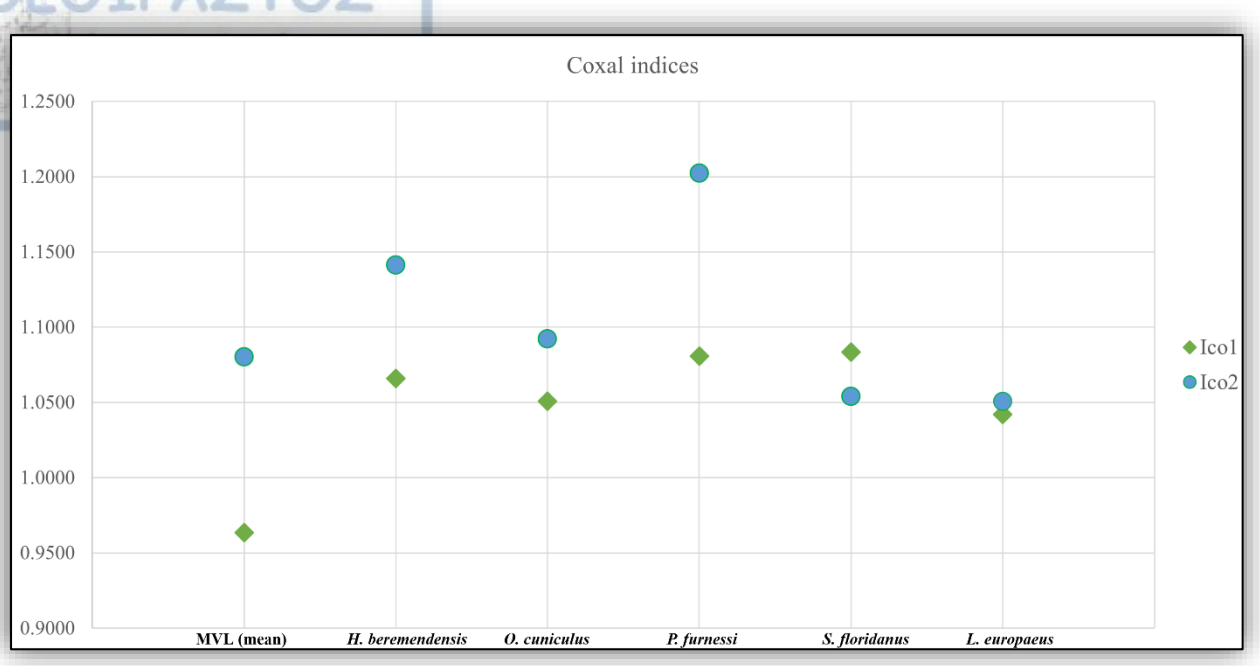

Figure 17. Indices of the coxal: **Ico1** (Lac/Hac) and **Ico2** (Lac/Wilb). Indices were calculated based on Fostowicz - Frelik (2007) (with references therein) for *H. beremendensis*, *O. cuniculus*, *P. furnessi*, *S. floridanus*, and *L. europaeus.*

Table 23. List of the iIndices of the coxal. Indices were calculated based on Fostowicz - Frelik (2007) (with references therein) for *H. beremendensis*, *O. cuniculus*, *P. furnessi*, *S. floridanus*, and *L. europaeus.*

Taxa	**Ico1 – Lac/Hac**	**Ico2 – Lac/Wilb**
MVL mean	0.9635 (N=9)	1.0802 (N=5)
H. beremendensis	1.0659 (N=41)	1.1412 (N=41)
O. cuniculus	1.0506 (N=9)	1.0921 (N=9)
P. furnessi	1.0808 (N=4)	1.2022 (N=4)
S. floridanus	1.0833 (N=5)	1.0541 (N=5)
L. europaeus	1.0420 (N=10)	1.0508 (N=10)

Femur

The proportions and shape of the MVL femur reveal an overall rabbit-like morphology with an estimated mean length of 94.32 mm. MVL has a femoral length that is comparable to that of *H. beremendensis*, whereas *T. dumitrescuae* from Moldova is somewhat longer. *P. furnessi* and *T. meridionalis* have slightly shorter femoras in contrast to MVL, whereas in *O. cuniculus* and *S. floridanus*, the femur length is significantly shorter than MVL. *L. europaeus* has the longest femur of them all.

Considering the proximal end, MVL is similar to *T. meridionalis* and *H. beremendensis*; *O. cuniculus*, *S. floridanus*, and *L. europaeus* show a more robust upper femoral end, while *P. furnessi* has the heaviest build of them all. The third trochanter

(trochanter tertius) in MVL has a round shape. However, as mentioned on the previous chapter, in MVL-126, trochanter tertius is shorter. The third trochanter of *O. cuniculus* and *H. beremendensis* is more angular, not as extended as in MVL, and shaped like an isosceles triangle. *P. beremendensis*, *S. floridanus,* and *L. europaeus* share a similar level of extension of this trochanter but it is more angular.

The second trochanter (trochanter minor) in MVL is also much rounder and placed closer to the femoral head, like in *H. beremendensis* and *S. floridanus*. In *T. meridionalis*, as pointed out by Sen and Geraads (2023), the trochanter minor is fully visible, as the head of the femur is directed more cranially. The trochanter minor in MVL follows the direction of *L. europaeus* with a more medially directed head. The position of the third trochanter in MVL is the same as in *O. cuniculus, S. floridanus, L. europaeus,* and *T. dumitrescuae* from Moldova which is above the lower limits of the trochanter minor. *P. furnessi* has a lower position for the trochanter minor. The width of the head in MVL is similar to that of *H. beremendensis*, whereas in *O. cuniculus* and *S. floridanus* it is slenderer. *P. furnessi* shows a slightly broader head than in MVL, and *L. europaeus* the broadest of them all. In addition, the notch between the head and the trochanter primus is more profound in MVL, as in *O. cuniculus*, *P. furnessi*, and *T. meridionalis*, while *T. dumitrescuae* from Moldova, *S. floridanus,* and *L. europaeus* display a straighter line. The neck of the femur in MVL is a little shorter and wider than in *P. furnessi*, like the condition found in *L. europaeus*, *O. cuniculus,* and *S. floridanus*. In addition, the distal surface between the lesser trochanter and the trochanteric fossa is rounder and shorter in MVL in comparison to *L. europaeus*.

Regarding the shaft, MVL is as broad as in *H. beremendensis* and slightly similar to *P. furnessi*. *O. cuniculus,* and *S. floridanus* have a slender shaft, while the shaft width in *L. europaeus* is considerably broader than in MVL. However, the thickness of the shaft in *S. floridanus* and *O. cuniculus* has similar values to MVL, yet the thickness of the shaft is thicker in *H. beremendensis, P. furnessi*, and *L. europaeus.*

The distal end is more robust in MVL in comparison to *H. beremedensis, O. cuniculus, S. floridanus,* and *T. meridionalis*. *L. europaeus* has the slenderest distal end, and *P. furnessi* has the most robust femoral distal build. In MVL, the width of the intercondylar fossa compared to the width of the end of the fossa (Ife3; Fig. 18; Table 24) is the smallest compared to the other genera. *H. beremendensis* shows a slightly higher value than MVL. Moreover, the width of the patellar groove in relation to the distal width (Ife4; Fig. 18; Table 24) in MVL is quite close to that of *L. europaeus*, which is slightly lower. *H. beremendensis*, *O. cuniculus*, and *S. floridanus* display lower values in comparison to MVL, while *P. furnessi* has the highest value of them all. Lastly, the diameter of the distal extremity in relation to the distal width (Ife5; Fig. 18; Table 24) in MVL is similar to *H. beremendensis*. In comparison to MVL, *O. cuniculus, P. furnessi*, *S. floridanus*, and *L. europaeus* show considerably higher values.

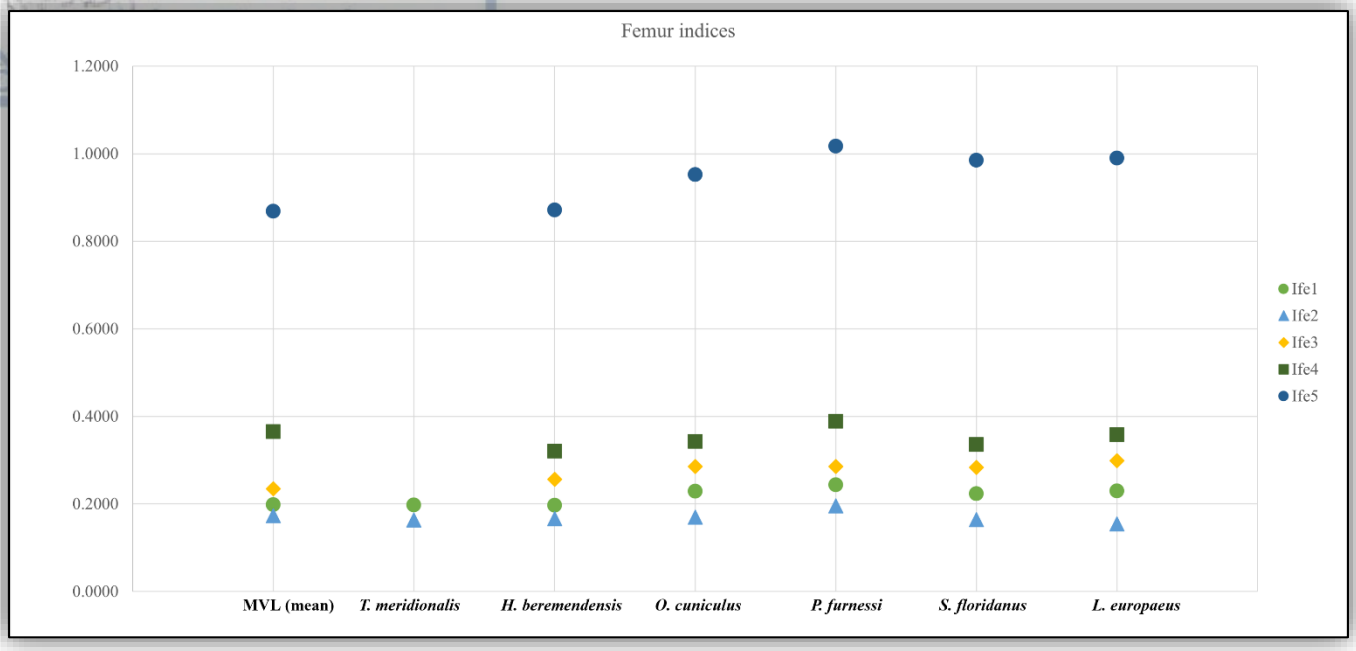

Figure 18. Indices of the femur: **Ife1** (Wfepr/Lfe), **Ife2** (Wfedis/Lfe), **Ife3** (Wintf/Wfedis), **Ife4** (Wpag/Wfedis), and **Ife5** (Wfedis/Hdis). Indices were calculated based on Fostowicz - Frelik (2007) (with references therein) for *H. beremendensis*, *O. cuniculus*, *P. furnessi*, *S. floridanus*, and *L. europaeus*, and according to Sen and Geraads (2023) for *T. meridionalis*.

Table 24. List of the calculated indices of the femur. Indices were calculated based on Fostowicz - Frelik (2007) (with references therein).

Taxa	Ife1 – Wfepr/Lfe	Ife2 – Wfedis/Lfe	Ife3 – Wintf/Wfedis	Ife4 – Wpag/Wfedis	Ife5 – Wfedis/Hdis
MVL mean	0.1984 (N=2)	0.1729 (N=2)	0.2345 (N=5)	0.3651 (N=3)	0.8687 (N=4)
T. meridionalis	0.1977 (N=2)	0.1634 (N=5)	-	-	-
H. beremendensis	0.1968 (N=1)	0.1660 (N=1)	0.2564 (N=60)	0.3205 (N=27)	0.8715 (N=13)
O. cuniculus	0.2288 (N=8)	0.1695 (N=)	0.2857 (N=7)	0.3429 (N=8)	0.9524 (N=8)
P. furnessi	0.2436 (N=4)	0.1955 (N=4)	0.2857 (N=3)	0.3886 (N=4)	1.0174 (N=4)
S. floridanus	0.2237 (N=4)	0.1638 (N=4)	0.2836 (N=5)	0.3358 (N=5)	0.9853 (N=5)
L. europaeus	0.2296 (N=10)	0.1541 (N=10)	0.2990 (N=10)	0.3578 (N=10)	0.9903 (N=10)

Tibiofibula

The tibia of MVL is overall slender and somewhat delicate, with a relatively thin shaft. Its total length is measured at 106.58 mm, similar to the state reported in *H. beremendensis*. The ratio of MVL's proximal diameter to its proximal width (Iti1; Fig.

19; Table 25) is most like that of *H. beremendensis* and *O. cuniculus*, sharing a similar proximal build, and is slightly smaller than that of *L. europaeus*. MVL has a slightly robuster proximal end than *S. floridanus* and *T. dumitrescuae* from Moldova. On the other hand, the ratio of the width of the proximal end to the total length (Iti2; Fig. 19; Table 25) is identical to that of *O. cuniculus* and very close to that of *S. floridanus. T. meridionalis, L. europaeus*, and *H. beremendensis* show slightly lower values. In comparison to *P. furnessi*, MVL has a low Iti2. On a proximal view, the lateral condyle in MVL is not as extended as in *S. floridanus* and *L. europaeus*, sharing the slightly more clustered state observed in *T. dumitrescuae* from Moldova. An S-shaped linear muscle attachment (linea musculi poplitei) for the popliteus muscle can be observed on the caudal side, just below the proximal extremity. This line is well pronounced, significantly longer, and more distinct in MVL, compared to *O. cuniculus* and *S. floridanus*, resembling that of *H. beremendensis*.

The tuberosity of the tibia is significantly prominent in MVL, like that observed in *S. floridanus*. Moreover, the tuberocity of the tibia in MVL is slightly shorter in relation to total tibia length (Iti3; Fig. 19; Table 25) than in *H. beremendensis* and *L. europaeus*. It3 in MVL most closely resembles the proportions observed in *O. cuniculus* and *S. floridanus*. *P. furnessi* exhibits considerably larger values of Iti3 in contrast to MVL and the rest of the studied taxa. Averianov (1995) reports that the tibial tuberosity of *T. dumitrescuae* from Moldova is relatively low compared to that of *L. europaeus*. Unfortunately, there are no photos available to corroborate this. *T. dumitrescuae* from Moldova most likely resembles in this aspect MVL due to the fact that *L. europaeus* and MVL share a similar size on this tubercle.

Regarding the shaft of the tibiofibula is more flattened cranio-caudally in MVL than in *L. europaeus*, resembling that of *H. beremendensis* and *T. meridionalis*. Moreover, the minimal width of the shaft in relation to the total bone length (Iti6; Fig. 19; Table 25) resembles that of *H. beremendensis* and *T. meridionalis. O. cuniculus* exhibits slightly higher values in comparison to MVL, and *L. europaeus* lower values.

The distal width in relation to the total length (Iti5; Fig. 19; Table 25) in MVL is relatively similar in all studied genera. Only compared to *P. furnessi*, Iti5 is considerably lower in MVL. The distal extremity of the tibiofibula in MVL is relatively thicker than that of *O. cuniculus* and *P. furnessi*. In greater detail, the relative thickness of the articular surface of the tibiofibula (Iti4; Fig. 19; Table 25) is high in MVL, somewhat identical to that of *L. europaeus*. *H. beremendensis* and *S. floridanus* exhibit slightly lower values than MVL. The lateral malleolus in MVL is pronounced, resembling the condition seen in *S. floridanus*, while in *L. europaeus* it is slightly more prominent.

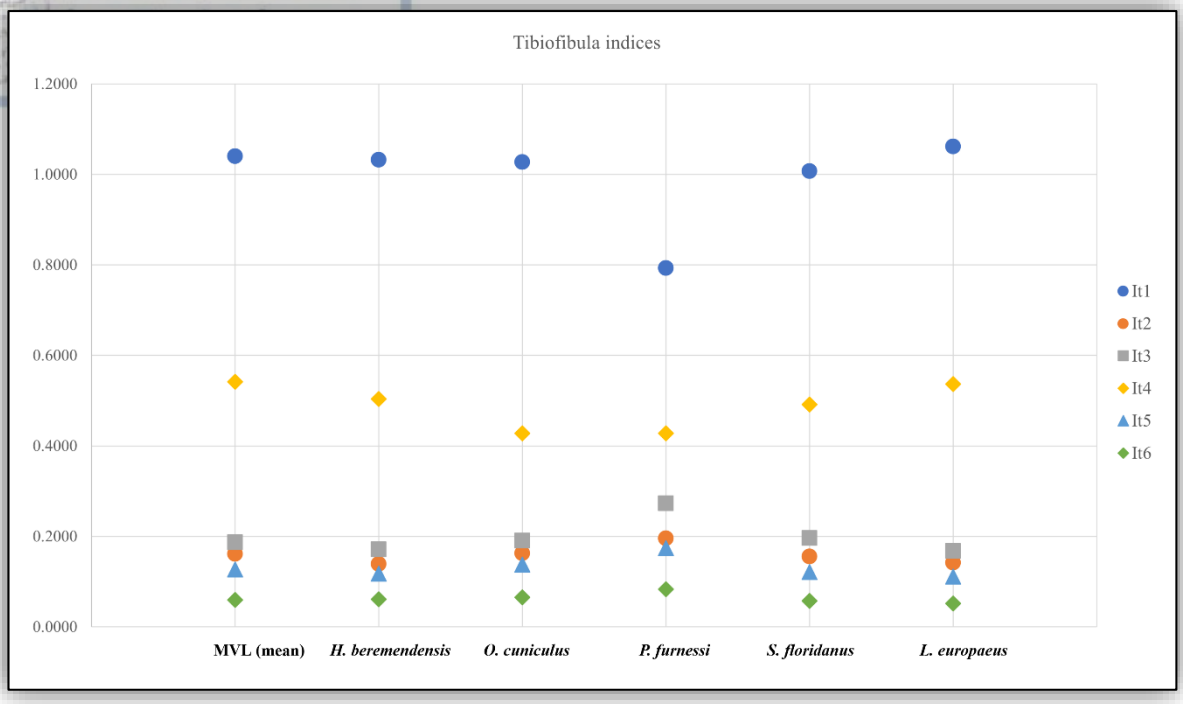

Figure 19. Indices of the tibia: **Iti1** (Ttipr/Wtipr), **Iti2** (Wtipr/Lti), **Iti3** (Htitu/Lti), **Iti4** (Ttidis/Wtidis), **Iti5** (Wtidis/Lti), and **Iti6** (Wtish/Lti). Indices were calculated based on Fostowicz - Frelik (2007) (with references therein) for *H. beremendensis*, *O. cuniculus*, *P. furnessi*, *S. floridanus*, and *L. europaeus*.

Table 25. List of indices for the tibiofibula. Indices were calculated based on Fostowicz - Frelik (2007) (with references therein).

taxa	Iti1 – Ttipr/Wtipr	Iti2 – Wtipr/Lti	Iti3 – Htitu/Lti	Iti4 – Ttidis/Wtidis	Iti5 – Wtidis/Lti	Iti6 – Wtish/Lti
MVL mean	1.0404 (N=5)	0.1614 (N=4)	0.1867 (N=)	0.5414 (N=3)	0.1270 (N=5)	0.0598 (N=6)
H. beremendensis	1.0323 (N=25)	0.1391 (N=1)	0.1715 (N=1)	0.5038 (N=70)	0.1176 (N=1)	0.0610 (N=1)
O. cuniculus	1.0272 (N=8)	0.1626 (N=7)	0.1903 (N=7)	0.4274 (N=8)	0.1372 (N=7)	0.0653 (N=7)
P. furnessi	0.7933 (N=3)	0.1956 (N=3)	0.2732 (N=3)	0.4277 (N=3)	0.1738 (N=3)	0.0831 (N=3)
S. floridanus	1.0069 (N=4)	0.1553 (N=4)	0.1963 (N=3)	0.4911 (N=4)	0.1208 (N=4)	0.0572 (N=4)
L. europaeus	1.0619 (N=10)	0.1417 (N=10)	0.1673 (N=10)	0.5366 (N=10)	0.1107 (N=10)	0.0513 (N=10)

Astragalus

The astragalus of MVL is longer than that of *O. cuniculus*, *S. floridanus*, and *T. meridionalis*. The length of the bone in MVL is similar to that of *T. dumitrescuae* from Moldova, *H. beremendensis*, and *P. furnessi*. The greater length of the bone in comparison to the width of the trochlea, however, indicates that the astragalus appears to be relatively robust in MVL. In more detail, the ratio of trochlear width to the length of the talus (Ita1; Fig. 20; Table 26) is high in MVL, close to the value for *O. cuniculus* and *S. floridanus*. *T. dumitrescuae* from Moldova shows slightly lower values of a slenderer bone, similar to *H. beremendensis* and *L. europaeus*. *P. furnessi* displays the most robust astragalus of the examined taxa. The length of the neck of the astragalus corresponding to the entire bone (Ita2; Fig. 20; Table 26) in MVL is generally similar to that of *S. floridanus*, while *H. beremendensis*, *O. cuniculus*, *P. furnessi*, and *L. europaeus* exhibit slightly higher values. In proximal view, the lips of the trochlea in *T. meridionalis* are less unequal and not as defined as in MVL. The medial side of the trochlea is somewhat concave, a condition that can be somewhat observed in MVL. In addition, the lateral outline in *T. meridionalis* is rounded, while in MVL it is slightly more angular, closer to an L-shaped border, similar to that described for *T. dumitrescuae* from Moldova (Sen and Geraads, 2023). A small elevation can be observed halfway until reaching the facies articularis navicularis in MVL.

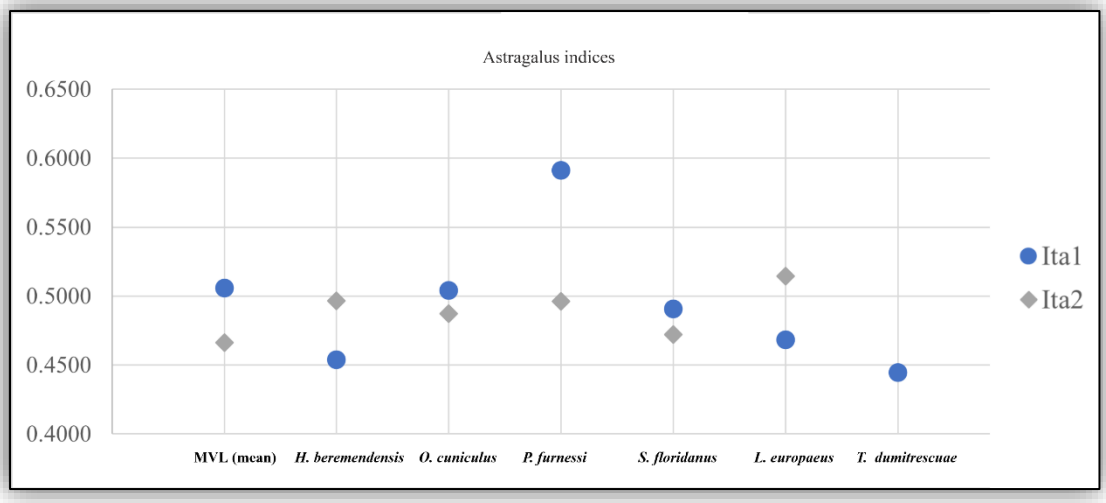

Figure 20. Indices of the astragalus: **Ita1** (Was/Las) and **Ita2** (Las/Las). Indices were calculated based on Fostowicz - Frelik (2007) (with references therein) for *H. beremendensis*, *O. cuniculus*, *P. furnessi*, *S. floridanus*, and *L. europaeus*, *T. dumitrescuae* based on Averianov (1995) and according to Sen and Geraads (2023) for *T. meridionalis.*

Table 26. List of indices for the astragalus. Indices were calculated based on Fostowicz - Frelik (2007) (with references therein).

Taxa	**Ita1 – Was/Las**	**Ita2 – Ltas/Las**
MVL mean	0.5058 (N=13)	0.4662 (N=13)
H. beremendensis	0.4539 (N=80)	0.4965 (N=80)
O. cuniculus	0.5042 (N=4)	0.4874 (N=4)
P. furnessi	0.5912 (N=2)	0.4964 (N=2)

S. floridanus	0.4907 (N=3)	0.4722 (N=3)
L. europaeus	0.4682 (N=10)	0.5145 (N=10)
T. dumitrescuae	0.4444 (N=2)	-

Calcaneus

MVL displays an overall longer calcaneus compared to that of *O. cuniculus* and *S. floridanus. T. meridionalis* has slightly shorter bone length, closer to the minimum values of the size range seen in MVL. The length of MVL calcanei is comparable to that of *P. furnessi* and *H. beremendensis*. *T. dumitrescuae* from Moldova shows a slightly longer calcaneus compared to MVL, closer to the maximum values of the size range reported for MVL. MVL calcaneus is overall slenderer than in *P. furnessi*, and its width is similar to that of *H. beremendensis*. In more detail, the maximum width of the calcaneus in relation to the total length of the bone (Ica1; Fig. 21; Table 27) in MVL is similar to that of *H. beremendensis*, *O. cuniculus*, and *S. floridanus*. *P. furnessi* displays a higher rate of Ica1 in comparison to MVL, while *L. europaeus* shows the lowest value from all previously mentioned taxa (Fig. 21; Table 27).

On the other hand, the length of the tuber calcanei in relation to the total bone length (Ica2) in MVL is slightly higher than that of *H. beremendensis* (Fig. 21; Table 27). *S. floridanus* has also a lower value of Ica2 than MVL. *O. cuniculus, P. furnessi*, and *L. europaeus* have similar values of Ica2 in comparison to MVL. In contrast to *P. furnessi,* the body of the calcaneus in relation to the total bone length (Ica3; Fig. 21; Table 27) is higher in MVL. Ica3 in *H. beremendensis* is the same as in MVL, whereas *S. floridanus* has a slightly higher value. *O. cuniculus* and *L. europaeus* show a slightly lower value of Ica3 than MVL. The width of the calcaneal tuber agains the length of the calcaneal tuber (Ica4; Fig. 21; Table 27) has the same value in MVL as in *H. beremendensis* and is close to that of *L. europaeus*; *O. cuniculus*, *P. furnessi,* and *S. floridanus* have a higher Ica4 than MVL.

Anteriorly, the two crest of the trochlea (trochlea peronealis) for the articulation with the fibular portion of the tibiofibular in MVL are not of similar in size, with the lateral one being more prominent, like the condition described for *L. europaeus*. *H. beremendensis* exhibit similar size crests. On the medial side of the bone, a distinct transverse ridge in MVL divides the facis articularis talaris anterior and the facies articularis navicularis into two parts. In leporids, these two surfaces could be merged or separated. In *H. beremendensis,* they are frequently fused, whereas in *L. europaeus* and *T. dumitrescuae* from Moldova they are separated (Averianov, 1995; Fostowicz-Frelik, 2007). In MVL as in *L. europaeus*, *H. beremendensis*, *O. cuniculus*, and *T. dumitrescuae* from Moldova the proximal calcaneoastragalar facet (facies articularis talaris) are divided into two parts by a distinct transverse ridge, whereas in *P. furnessi* it is undivided (Averianov, 1995). Lastly, the calcaneus's distal surface is obliquely orientated, with its longer edge positioned dorsally, same as in *H. beremendensis*.

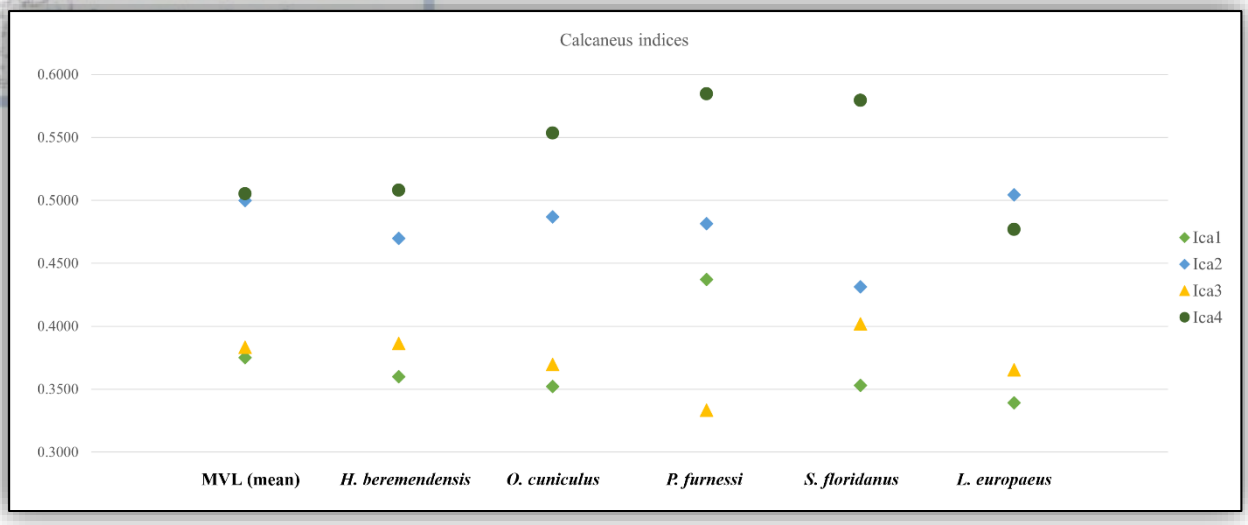

Figure 21. Indices of the calcaneus: **Ica1** (Wca/Lca), **Ica2** (Lcat/Lca), **Ica3** (Lcab/Lca), and **Ica4** (Wcat/Lcat). Indices were calculated based on Fostowicz - Frelik (2007) (with references therein) for *H. beremendensis*, *O. cuniculus*, *P. furnessi*, *S. floridanus*, and *L. europaeus.*

Table 27. List of indices for the calcaneus. Indices were calculated based on Fostowicz - Frelik (2007) (with references therein) for *H. beremendensis*, *O. cuniculus*, *P. furnessi*, *S. floridanus*, and *L. europaeus.*

Taxa	Ica1– Wca/Lca	Ica2– Lcat/Lca	Ica3– Lcab/Lca	Ica4 – Wcat/Lcat
MVL mean	0.3750 (N=23)	0.4999 (N=23)	0.3832 (N=23)	0.5053 (N=18)
H. beremendensis	0.3598 (N=69)	0.4697 (N=69)	0.3864 (N=69)	0.5081 (N=66)
O. cuniculus	0.3522 (N=4)	0.4870 (N=4)	0.3696 (N=4)	0.5536 (N=4)
P. furnessi	0.4370 (N=3)	0.4815 (N=3)	0.3333 (N=3)	0.5846 (N=3)
S. floridanus	0.3529 (N=2)	0.4314 (N=2)	0.4020 (N=2)	0.5795 (N=2)
L. europaeus	0.3391 (N=10)	0.5043 (N=10)	0.3652 (N=10)	0.4770 (N=10)

Navicular

The navicular bone of MVL is longer than those of *H. beremendensis*, *O. cuniculus*, *P. furnessi*, and *S. floridanus*. *L. europaeus*, however, has a navicular that is nearly twice as large. The length of the navicular body in relation to the length of the tuberosity (Ina1; Fig. 22; Table 28) is also notably greater in MVL, with the exception of *L. europaeus*. *H. beremendensis* and *S. floridanus* have lower values than MVL, whereas *O. cuniculus* and *P. furnessi* have extremely low values of Ina1. The width of the navicular body in relation to the thickness of the bone (Ina2; Fig. 22; Table 28) is comparable to that of *H. beremendensis*, *S. floridanus*, and *L. europaeus*. Surprisingly, *O. cuniculus* possesses the highest value of Ina2. Lastly, the length of the navicular

body relative to its width (Ina3; Fig. 22; Table 28) in MVL is close to that of *S. floridanus*, with the latter holding a slightly higher value. This index has an exceedingly low value in *H. beremendensis*, *O. cuniculus*, and *P. furnessi*.

Like *H. beremendensis* and *P. furnessi* (Fostowicz-Frelik, 2007), the navicular body of MVL is circular. However, unlike *H. beremendensis*, the plantar process of MVL lacks a planto-medial fissure. On the plantar side of MVL, the plantar process is less angular and straighter laterally and medially. The distal contact with the three cuneiform bones in MVL is comparable to that of *H. beremendensis*. However, the facies articularis cuneiformis lateralis is slightly narrower in MVL. The articulation surface for the cuboid in MVL is also like that of *H. beremendensis.* Lastly, in contrast to *H. beremendensis*, the articulation surface for the calcaneus is rhomboid shaped.

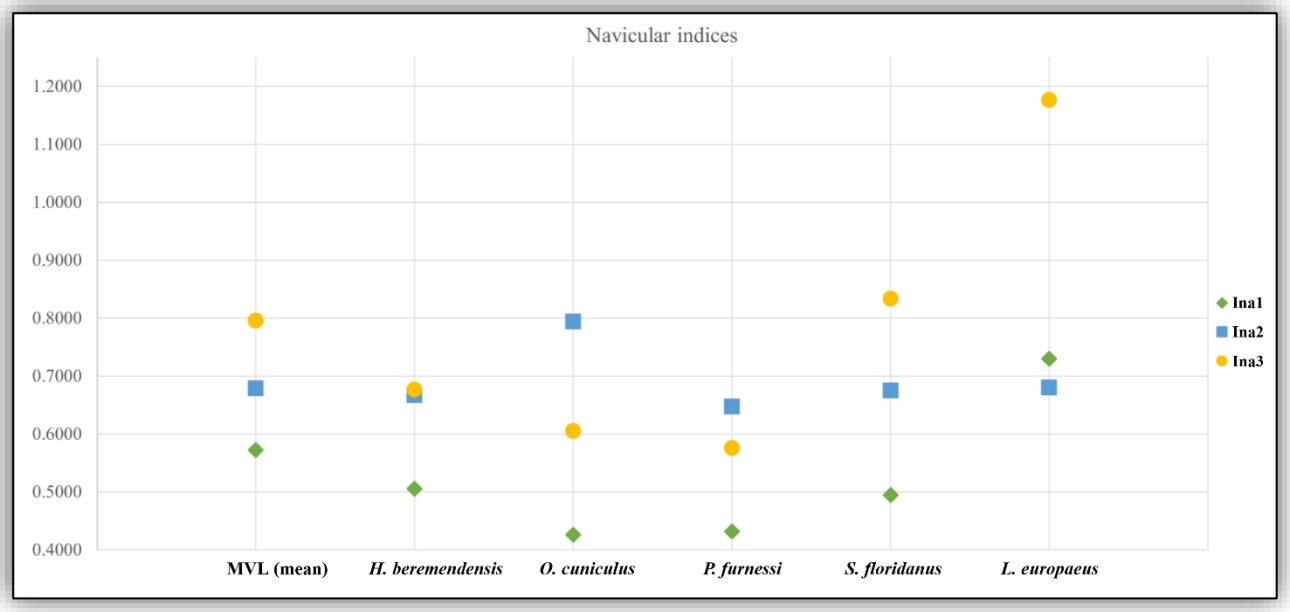

Figure 22. Indices of the navicular: **Ina1** (Lnab/Lnat), **Ina2** (Wna/Tna), and **Ina3** (Lnab/Wna). Indices were calculated based on Fostowicz - Frelik (2007) (with references therein) for *H. beremendensis*, *O. cuniculus*, *P. furnessi*, *S. floridanus*, and *L. europaeus*.

Table 28. List of indices for the navicular. Indices were calculated based on Fostowicz - Frelik (2007) (with references therein).

Taxa	**Ina1 – Lnab/Lnat**	**Ina2 – Wna/Tna**	**Ina3 – Lnab/Wna**
MVL mean	0.5725 (N=14)	0.6789 (N=14)	0.7954 (N=14)
H. beremendensis	0.5055 (N=41)	0.6667 (N=41)	0.6765 (N=41)
O. cuniculus	0.4261 (N=3)	0.7941 (N=3)	0.6049 (N=3)
P. furnessi	0.4318 (N=2)	0.6471 (N=2)	0.5758 (N=2)
S. floridanus	0.4945 (N=1)	0.6750 (N=1)	0.8333 (N=1)
L. europaeus	0.7299 (N=10)	0.6800 (N=10)	1.1765 (N=10)

Cuboid

The cuboid in leporids resembles a rhombohedron (Fostowicz-Frelik, 2007). In MVL, the length of the bone in relation to its width (Icu1; Fig. 23; Table 29) is comparable to that of *S. floridanus*, but it is slightly longer than in *H. beremendensis*, *L. europaeus*, and even more than in *O. cuniculus*. In addition, the width of the bone relative to its thickness (Icu2; Fig. 23; Table 29) is overall similar among the comparing taxa. Yet, MVL values are closer to those of *L. europaeus* and *O. cuniculus*, whereas *H. beremendensis*, *P. furnessi*, and *S. floridanus* have higher rates.

The cuboid bone of MVL shares with *H. beremendensis*, on the proximal surface, the large convex surface for the calcaneus (facies articularis calcanea) that is pronounced and triangular shaped, with a flat medial margin and a curved dorsal one; unlikely in *L. europaeus*, *S. floridanus*, and *O. cuniculus*, the same surface is not so strongly sloped and not so dorsally extended. In general, in *L. europaeus*, this surface is nearly square, whereas in rabbits, it is oval and lightly curved (Fostowicz-Frelik, 2007). MVL more closely resembles the condition described for rabbits. Especially in dorsal view, the articular surface for the calcaneus in *H. beremendensis* has a very distinct triangular shape, whereas in MVL, the edges are smoother, and the bending is less pronounced. Like in *H. beremendensis*, the contact surface for the navicular bone (facies articularis naviculais) is triangular. In contrast to *H. beremendensis*, however, the depression above the plantar tuberosity is not as deep in MVL in medial view, and the portion of this articulation above the facies articularis cuneiformis lateralis is shorter and rather angular. The distal articulation surface of the fourth and fifth metatarsal bones in MVL is pear-shaped, like that of *H. beremendensis*. However, in MVL, these two surfaces are situated slightly closer together.

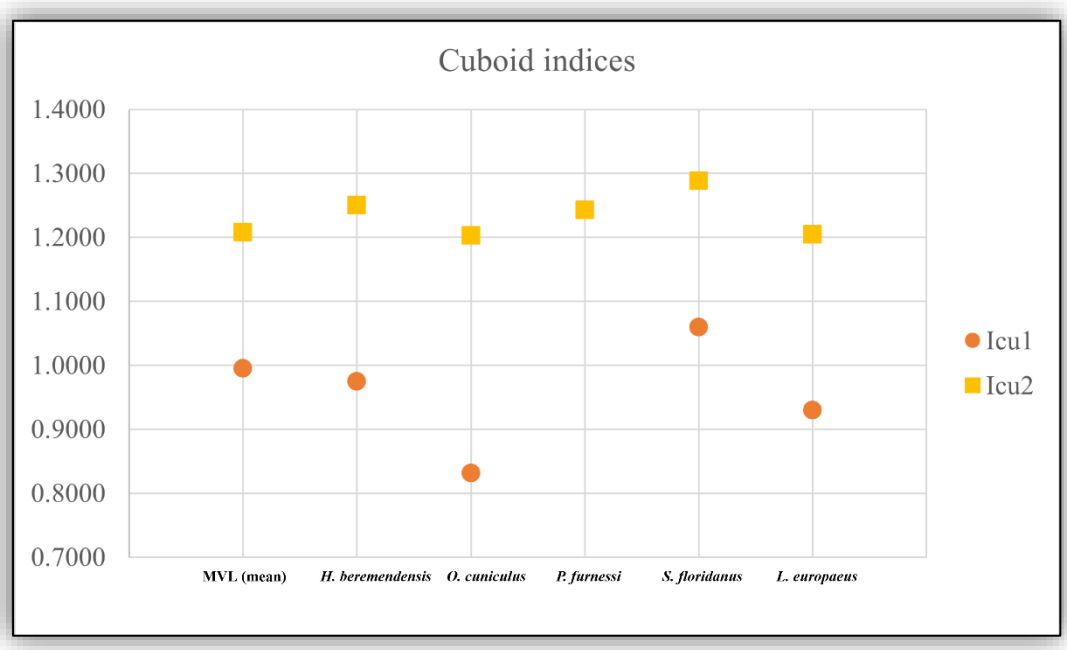

Figure 23. Indices of the cuboid bone: **Icu1** (Lcu/Wcu) and **Icu2** (Wcu/Tcu). Indices were calculated based on Fostowicz - Frelik (2007) (with references therein) for *H. beremendensis*, *O. cuniculus*, *P. furnessi*, *S. floridanus*, and *L. europaeus*.

Table 29. Indices for the cuboid bone. Indices were calculated based on Fostowicz - Frelik (2007) (with references therein).

Taxa	Icu1 – Lcu/Wcu	Icu2 – Wcu/Tcu
MVL mean	0.9952 (N=4)	1.2084 (N=4)
H. beremendensis	0.9750 (N=27)	1.2500 (N=28)
O. cuniculus	0.8315 (N=2)	1.2027 (N=2)
P. furnessi	-	1.2429 (N=1)
S. floridanus	1.0597 (N=1)	1.2885 (N=)1
L. europaeus	0.9300 (N=10)	1.2048 (N=10)

4.6 Body size estimation

The estimated values for body mass (BM) in the MVL sample are presented in Table 22 based on the different size proxies followed. The estimated BM for MVL varies from 1442.48 to 2972.30 gr with a mean of 2178.46 gr, based on the m1wtrig proxy. When estimated based on the toothrow length, the BM ranges from 1577.97 to1991.17 gr with a mean of 1832.94 gr. The GBOC parameter estimates a BM range between 1908.29 to 2499.38 gr with a mean of 2203.84 gr. The m1wtrig exhibits the widest range of estimated BM out of the three. However, it must be noted that the number of the specimens for the m1wtrig proxy was significantly higher (N=11) than for both TRL (N=4) and GBOC (N=2).

Regarding the postcranial bones, the femur metrics suggest a relatively consistent BM of around 2000 gr, with the mean BM from each of the three-femur metrics being fairly close to each other (Table 30). However, Dfed displays a much broader range of BM estimations.

In contrast to the femur, the humeral proxies present more varied BM estimations. The Lhu has a range of 1537.24 to 1853.47 gr (mean=1634.26 gr, N=2), which is slightly lower than that of the femur. This range is also within the lower estimates of the aforementioned proxies. It is noteworthy that, for the Dhup the estimated BM is significantly high and the highest of all the size proxies (Table 30); the opposite happens to Dhud, exhibiting the lowest estimated BM values (Table 30) The last size proxy for the humerus, Whud, show an estimated BM slightly higher than that of the teeth metrics, ranging from 2195.07 to 2678.7 gr (mean= 2414.37 gr, N=8).

The tibia offers an estimated BM ranging from 1993.98 to 2736.61 gr, higher than that of the dental and cranial proxies, and lower than that of the proxies of the humerus and the femur (Table 30).

For comparing the estimated BM with different taxa mostly dental proxies were applied. As already explained, there is no great availability of fossil lagomorph cranial and postcranial material. The m1wtrig is the only available metric to estimate the body mass of *T. dumitrescuae* from other sites based on the existing fossil evidence. The estimated body mass range obtained from the limited MEV material (Koufos and Koliadimou, 1993) is similar to that of MVL, ranging from 1873 to 2242 gr, with a mean of 2057.97 gr (N=2). Based on the reports of Čermak and Wagner (2013), *T. dumitrescuae* has an estimated BM of 2743 gr (N=1), which is comparable to the higher

values of the body mass range of MVL and close to the mean estimated BM for Ttipr for MVL. Again, it must be noted that this estimation is based on only one specimen. On the other hand, *T. meridionalis* has a quite wide estimated BM range of 416.87 to 2398.83 gr with a mean of 1609.99 gr (N=19) from the available measurements of Sen and Geraads (2023), which is much lighter than MVL. The Spanish *T. crusafonti* is even lighter than *T. meridionalis* and MVL, with an estimated body mass of 1400 gr based on the m1wtrig measurements of Koufos and Koliadimou (1993). In addition, *T. gambariani* has an estimated body mass of 1755.16 to 2569 gr, with a mean of 2164.9 gr based on the m1. *T. gambariani* seems to show a similar size range to MVL. *T. maritsae* displays the lowest estimated body mass of 618 gr, as expected by its size. It must be noted that, because of the plethora of material for *T. meridionalis* the estimated BM could be calculated also with the postcranial metrics which provide values up to 3213 gr based on Lfe.

According to the body mass reports from the Global Biodiversity Information Facility (GBIF), *O. cuniculus* can range from 1500 to 3000 gr. This fits perfectly with the estimated BM of MVL. *L. europaeus* is a lot heavier than the leporid of MVL, weighting from 3500 to 5000 gr. *S. floridanus* weight varies between 800 – 1500 gr, and thus is much lighter than MVL. Lastly, *P. furnessi* has a much wider range of body mass and can weigh between 2200 - 9000 gr, being larger on average than MVL.

Table 30. Body mass estimations (mean, min, and max) for the selected MVL material. The estimated BM is presented in grams.

Size proxy	mean	BM max	BM min
m1w trig	2178.46	2972.30	1442.48
CTL	1832.94	1991.17	1577.97
GBOC	2203.84	2499.38	1908.29
Lfe	1956.11	1962.12	1950.10
Wfepr	2082.31	2193.16	1853.60
Dfed	2001.41	2596.89	1459.81
Lhu	1634.26	1853.47	1537.24
Dhup	2956.96	3220.22	2664.17
Dhud	781.78	955.18	631.83
Whud	2414.37	2678.80	2195.07
Lti	1993.98	2123.25	1804.62
Ttipr	2736.61	3036.32	2487.45
Wtipr	2534.79	2876.08	2365.67
Wtidis	2428.02	2705.03	1842.43

5. Discussion

5.1. Taxonomical and anatomical remarks

The cranial anatomy of leporids, especially fossil ones had not been comprehensively documented. Cranial findings are uncommon in the fossil record, and when they do occur, they mostly comprise of fragments of the skull. One of the overall complete craniums is that of *A. hibbardi* from the Late Miocene of North America (White, 1991). The available cranial dimensions indicate that it is close to MVL, although observations were based on the illustrations by White (1991) and the available metric were limited. However, the fenestrations on the lateral side of the maxilla are not that prominent in *A. hibbardi* as in MVL. The orientation of the jugal is more anterior in *A. hibbardi* than in MVL. Lastly, the supraorbital process does not exhibit the delicate development observed in MVL and appear to be similar to that of *Lepus*. Another cranium that was selected for comparisons is *Hypolagus balearicus*. Although close in age to MVL, *H. balearicus* is an endemic species of the Balearic Islands (Quintana Cardona and Moncunill-Solé, 2014). The skull is in poor preservation and from the limited available metrics it is proportionally smaller than MVL. Within the genus of *Trischizolagus*, parts of the skull of *T. meridionalis* from the Plio-Pleistocene of Morocco were recently reported (Sen and Geraads, 2022). Although the material is not well preserved and limited, it is evident that MVL is generally larger than *T. meridionalis* and has a larger hard palate. Lastly, Averianov (1995) described some cranial remains of *T. dumitrescuae* from southern Moldova, which indicate that the foramen magnum is consistent with what is observed in MVL, yet the auditory bullae in MVL are larger to that assumed for Moldavian *T. dumitrescuae*.

Averianov and Tesakov (1997), examining the dental trends in the Mio-Pliocene *Trischizolagus* from Eastern Europe, concluded that *T. dumitrescuae* is most likely an ancestral form of *Lepus.* The Late Pliocene and Early Pleistocene (early - middle Villafranchian) was the time when a speciation event in *Trischizolagus* populations took place, leading to the origin of *Lepus* and *Oryctolagus* species (Averianov and Tesakov, 1997; Čermák and Wagner, 2013). Based on the recent comparative material available, it can be observed that the overall cranial development of MVL shares the robustness and large size of *Lepus*. However, the supraorbital process of the frontal, one of the most distinguishable aspects of *L. europaeus* are not present in MVL or appear to be somehow close. In addition, the development of the palatine in relation to the choanae in MVL is closer to that of *Oryctolagus* and the nasals are not as inflated, wide and straight as in *Lepus*. The main differential diagnosis of *O. cuniculus* from *L. europaeus* is limited to the size (*Lepus* bigger, *Oryctolagus* smaller) and locomotory adaptation's differences (Krapp, 2003). Those aspects will be discussed below. Given the limited cranial elements of *Trischizolagus* known so far, the MVL wealth cranial sample would be certainly crucial in a future in depth analysis to test the hypothesis of *Trischizolagus* – *Lepus/Oryctolagus* relationships (Averianov, 1995; Averianov and Tesakov, 1997). Furthermore, since the available comparative data of extant taxa was limited (only three specimens of each species), it may be probable that the significance of some cranial features could be biased. To overcome this, a future revision based on a larger number of extant specimens is necessary to provide more solid evidence. Additionally, skulls of the sympatric to *L. europaeus*, *L. timidus* Linnaeus, 1758 and the fossil *L. capanensis* Linnaeus, 1758 would be appropriate to be considered. Unfortunately, no comparative material for the latter two *Lepus* species were available to be included in this thesis.

Furthermore, there has been no remarks regarding different dental wear and mastication preferences in lagomorphs. Given the fact that in MVL, three of the crania exhibit different dental wear suggesting a preference for chewing one side of the maxilla, it is possible to speculate that they may be a predilection. Nevertheless, due to the absence of well-preserved lagomorph skulls with their teeth intact, no definitive conclusion can be drawn.

The taxonomy of leporids is primarily based on the pattern of the lower third premolar, which is considered to be one of the most diagnostic anatomical elements. The second upper premolar also plays an important classifying role but is not as significant as the p3. The modern *L. europaeus*, *S. floridanus*, and *O. cuniculus* show the leporine p3 pattern (López-Martínez, 2008). In certain species, there are cases where two intermediate p3 types are present:

- the "*Nekrolagus*" type of p3, which features an enamel lake situated between two isthmuses that connect the trigonid with the talonid, present in specimens of *Oryctolagus* and *Lepus*, and

- the "*Aluralagus*" type of p3, characterized by a wide single lingual isthmus, reported as a potential variation in *Sylvilagus*.

MVL specimens exhibit a more primitive p3 as opposed to the modern species, yet the "*Alilepus*" p3 pattern is considered to be a pre-stage to the "*Lepus*" p3 pattern (Averianov, 1995).

Historically, the complex and diagnostic p3 has provided the foundation for lagomorph evolutionary hypotheses, as well as for taxonomic discriminations of the leporid genera (Dice, 1929). Regarding the occlusal morphology of the p3, Dice (1929) divided the family Leporidae into three subfamilies based on the characteristics of this tooth. The first, Palaeolaginae, has the trigonid and talonid connected by a central narrow isthmus; the second, Archaeolagine, exhibits a trigonid and talonid connected by a large lingual isthmus; and the third, Leporinae, has the trigonid and talonid connected by a narrow lingual isthmus like other lower check teeth. This fundamental idea was accepted for several decades in the study of leporids (Averianov and Tesakov, 1997; López Martínez et al., 2007). Yet, relying solely on the occlusal morphology of p3 without considering other parameters often leads to formal conflicts in diagnosing and grouping taxa within subfamilies (López Martínez et al., 2007). Furthermore, phylogenetic analyses on cranial and dental features consider taxa of Palaeolaginae as a separate clade of Leporidae (Asher et al., 2005).

Nevertheless, the unique characteristics and variations in teeth among the Leporidae family make it possible to clearly differentiate the two main clades, Archaeolaginae and Leporidae, especially in fossil taxa. To gain a comprehensive understanding of leporid evolution and taxonomy, it is crucial to examine the changes in p3 throughout ontogeny. In addition, it is important to consider paleontological, geographical, and outgroup criteria (Averianov and Tesakov, 1997). However, it is worth noting that these criteria do not always align and may result in different evolutionary polarities (López Martínez et al., 2007; Čermák and Wagner, 2013). According to Čermák and Wagner (2013), using only the p3 may not be enough to accurately determine the species. Therefore, it is necessary to consider a combination of other features in the mandible and/or skull, if possible. However, the current understanding of the classification of fossil lagomorphs primarily relies on dental

material, focusing heavily on the p3. Detailed data on postcranial features and, in many cases, comprehensive knowledge of the cranium is not available for most fossil taxa.

Čermák and Wagner (2013) attribute *Trischizolagus* to the subfamily Leporinae based on the current understanding of phylogenetics and the evolutional history of the p3. According to Patnaik (2002), and López Martínez (2008), *Trischizolagus* is highly likely to be the most recent common ancestor of both *Oryctolagus* and *Lepus*. As Angelone et al. (2021) pointed out, the systematic classification of *T. dumitrescuae* poses significant challenges. The type species, *T. dumitrescuae*, originates from Măluşteni in Romania during the Early Pliocene. Averianov and Tesakov (1997) and Čermák and Wagner (2013) conducted studies that involved the examination of leporid remains from various localities across Europe, among them Bulgaria, Greece, Hungary, Italy, and Spain. They noted that the species exhibits a significant range in size that exceeds what would be considered appropriate for a species of Leporidae (Čermák and Wagner, 2013). In addition, in most cases, the number of specimens from each locality, especially the number of p3s, is not enough to fully comprehend the variation in individual morphology and to determine the most prevalent morphotype (Sen and Geraads, 2023). Nevertheless, the MVL material suggests a close correlation in both size and morphology not only for the p3 but for both the lower and upper molariforms, to that of the type species of *T. dumitrescuae* from Romania making it the most appropriate and suitable match to attribute to.

As previously described, the MVL material is monopolized by the "*Alilepus*" p3 pattern. In the early Ruscinian, the "*Alilepus*" p3 pattern was significantly more common than the "*Nekrolagus*" pattern in *T. dumitrescuae*, while the "*Hypolagus*" pattern was rare. There were no major changes observed in the composition of the "*Alilepus*" and "*Nekrolagus*" p3 patterns in the late Ruscinian period. However, during this time, a migration wave of archaeolagines, represented by *Hypolagus petenyii*, was observed in the leporid record of Central Europe (Čermak, 2009; Čermak and Wagner, 2013). Megalo Emvolon as a late Ruscinian fauna does not seem to be affected from this migration, given the fact of geographical proximity. Also, *H. petenyii* or any other species of this genus do not appear in the Greek fossil history (Vasileiadou and Sylvestrou, 2022) as we know so far. The core distribution of *T. dumitrescuae* is believed to be in the northwestern part of the peri-Paratethyan area, with most known finds correlated with the early Ruscinian. The more western occurrences, such as those from Muselievo, Măluşteni, and Beremend, are limited to the late Ruscinian (Čermak and Wagner, 2013).

Megalo Emvolon is assumed as the most diverse lagomorph locality for the Pliocene of Greece with three distinct leporid species. However, there is a debate about the validity of this leporid diversity. The presence of *T. dumitrescuae* in MEV is indisputable due to its distinct tetralobed trigonid form, well-developed hypoflexid and mesoflexid, 1 to 2 size ratio of the length of the trigonid to the talonid of the p3, and "*Alilepus*" pattern (Koufos and Koliadimou, 1993). The same applies for the MVL specimens, sharing the same features with both the previously discovered *T. dumitrescuae* from MEV, and those from Măluşteni and Beresti. Although the presence of *T. dumitrescuae* in Megalo Emvolon is therefore out of question, the presence of the other two lagomorph taxa is more problematic.

First of all, Steffens et al. (1979) reported from Megalo Emvolon-1 the finding of *Oryctolagus* cf. *laynensis*, but no further details or specifics are provided. This species has not been found in any other Greek locality and is only reported from the

Late Pliocene faunas of Spain and France (Vasileiadou and Sylvestrou, 2022 and references therein). Extensive later research in Megalo Emvolon doesn't record any evidence of this species in the locality. In the absence of concrete evidence, we therefore suggest that the species has to be excluded from the faunal list of the site.

Koufos and Koliadimou (1993) reported that, aside from *T. dumitrescuae*, there is also a small-sized *T.* cf. *maritsae* present in Megalo Emvolon-1. This species is only found in the Mediterranean region, and its taxonomic status is questionable due to limited fossil findings (Čermak and Wagner, 2013). *T. maritsae* is characterized by the predominance of the "*Hypolagus*" p3 pattern, similar to that of *Serengetilagus*. Moreover, this species is the smallest representative of the genus, and all known p3s apparently come from subadult individuals, adding another factor to their debatable classification. While the MEV specimens referred to *T.* cf. *maritsa* (MEV-1005) are clearly larger than those from Maritsa site in Rhodes Island, there is a clear morphometric difference between those attributed to *T. dumitrescuae* from the same site (MEV-1001, MEV-1002, MEV-1003) and MVL, indicating that there are indeed two different forms of *Trischizolagus*. Koufos and Koliadimou (1993) proposed two hypotheses: one is that there are two different morphs of *Trischizolagus* living together, namely a large-sized one with a well-developed mesoflexid in p3 and a small-sized one with a less developed or absent mesoflexid, named *T. dumitrescuae* and *T.* cf. *maritsae*, respectively. The second hypothesis is that the variation in size and mesoflexid development in p3 is of intraspecific value, and only one species existed, which should be named *T. dumitrescuae* (Koufos and Koliadimou, 1993). The size of the *T.* cf. *maritsae* material from MEV is significantly smaller than the size range of *T. dumitrescuae* (Table 22, Fig. 16) and the attribution of Koufos and Koliadimou (1993) remains applicable.

5.2. Palaeoecological remarks

The skull morphology of leporids is believed to be associated with their ecology, particularly their locomotion and vision, as suggested by DuBrul (1950) and Bramble (1989). The skull of leporids is highly distinct from that of other mammals, exhibiting a combination of features that set it apart. One of the most notable features is the wide dorsal arching of the skull, which is formed by the expansion and folding of the supraoccipital bone and a pronounced flexure near the basisphenoid/presphenoid suture (Wood-Bailey et al., 2022).

Two cranial traits that have attracted attention are the facial tilting and the fenestration of the lateral wall of the maxilla. These features are known to be associated with specific locomotory abilities. Generally, faster running species tend to have fenestration on both the dorsal and anteroventral surfaces of the maxillary corpus, as well as a more acute facial tilt angle (Wood-Bailey et al., 2022). Kraatz et al. (2015) identified facial tilting in leporids and observed that there is variation in different species. According to their hypothesis, the presence of certain cranial features is meant to enhance the orbit's frontation in order to improve vision for species with specialized, high-speed locomotion. It has been observed that the complexity and occurrence of these cranial adaptations vary depending on the way of locomotion. For instance, species that can run the fastest have significantly lighter skulls with greater degrees of fenestration in their crania, as well as more pronounced tilting in the facial region. This suggests that the increased facial tilt and fenestration of the lateral wall of the maxilla are functionally linked and work together to provide the necessary cranial support to

withstand the mechanical forces experienced during high-speed locomotion (Kraatz et al. 2015).

In the cranial material of MVL, the angle of facial tilt was determined by only two specimens ranging from 38º to 43º with a mean of 40.5º. According to Kraatz et al. (2015), an angle between 40 and 49º is determined as of moderate tilt and < 40º as more acute tilt. Interestingly the facial tilt of the leporid of MVL is at the middle of this range. In addition, as previously described the fenestration of the MVL skulls is very prominent and it is not only limited to the maxillary area. The maxillary fenestration in MVL is located in the dorsal as well as the anteroventral surface of the maxillary corpus, as that in *Lepus* which is the most advanced type observed in Lagomorpha (Kraatz et al., 2015). Based on the data at hand, the MVL leporid had a moderate to high tilted skull with a *Lepus*-like degree of maxillary fenestration. It can be therefore suggested that this skull structure would have aided in fast running, but it may not have been capable of achieving the same high speeds as modern *Lepus*.

Although generalized locomotors exhibit a less facial tilt, considered to be a primitive feature for lagomorphs (Dice, 1933; Asher et al., 2005), there is no clear determination of the cursorial or saltorial specification. Facial tilt does distinguish generalist locomotors clearly from more active taxa within leporids, but more specific aspects of the overall cranial morphology should be examined for further specification (Kraatz et al., 2015). This can also be noticed in MVL. It is interesting that although fully capable of achieving high speeds given the fact of the great maxillary fenestration, the facial tilt in MVL appears lower than expected following the same predictions. The maxillary fenestration of MVL seem to be well-developed and clearly not an in-between stage from the rabbit-like to the hare-like fenestration. The evolutionary correlation between the facial tilt and the development of the fenestration remains however unclear. Nevertheless, in the case of MVL, the degree of maxillary fenestration seems to precede that of the facial tilt.

Compared to the hindlimbs, there is a lack of quantitative data for the forelimbs to fully explore the locomotory function for MVL and the selected taxa for comparison. Averianov (1995) examined the partial skeleton of *T. dumitrescuae* found in Moldova. Based on this analysis, *T. dumitrescuae* was not adapted for fast running and had an ability for digging. The humerus of MVL shows a highly developed deltoid crest, similar to that found in *Lepus* and *T. dumitrescuae* from Moldova. This suggests that the deltoid muscle, responsible for abducting the bone, was quite strong. Although not as strong as in *Oryctolagus*, it is possible that MVL had good digging abilities. Gambaryan (1972) notes that the increased development of forelimb muscles in leporids only implies an improved ability to dig, as the forelimbs are not used for running or jumping. Unfortunately, no elaborate conclusion could be made for the scapula, radius, and ulna.

All leporids are adapted for running, but there are differences in their running abilities within the group. The way leporids move is called a “leaping gallop” because there's a phase when their whole body is in the air and no limb touches the ground (Maynard Smith and Savage, 1956). When studying how leporids have adapted for running, the most important features to consider are the morphology, proportions, and muscle attachments of their hind limb bones. This is because these features provide most of the propulsive force during the type of locomotion used by leporids (Gambaryan, 1974).

Gambaryan (1974) explains that the forelegs of leporids help with landing by absorbing the shock of hitting the ground and supporting the body, while momentum moves the body forward. In contrast, the hind limbs, particularly the hip and femur muscles, are the primary generators of horizontal movement (Alexander, 2003). If we look more closely at the "leaping gallop" type of locomotion, we can divide it into two subtypes. The first subtype is less adapted for running and is sometimes associated with fossorial adaptation. It's found in most fossil and modern genera, including rabbits and cottontails, and is often referred to as the "rabbit type" (Fostowicz-Frelik, 2007). The second subtype is highly adapted for running and long leaps and is restricted to the members of the genus *Lepus*, which includes hares and jackrabbits. Therefore, it's also known as the "hare type" (Gambaryan, 1974; Fostowicz-Frelik, 2007).

According to Sargis (2002) one of the most crucial hallmarks for cursoriality and the ability to perform powerful leaps in many of the terrestrial mammals is due to the relative increase of the width of the iliac wing. As Fostowicz-Frelik (2007) reports, *Lepus* has the relatively widest ilium, while the *Oryctolagus, Sylvilagus* and *Pentalagus* exhibit lower values. Unfortunately, this feature could not thoroughly be investigated in the studied material. As described before, it seems that the MVL exhibits an ilium that has a width in between those of *Lepus* and *Sylvilagus* or *Oryctolagus*. We can speculate that the action of glutei muscles was not that weak in MVL as in rabbits. It is possible that the leporid of MVL could perform leaps that were more powerful than that of *Oryctolagus* and *Sylvilagus* but were not as powerful as that of *Lepus*.

On the other hand, the length of the acetabulum in relation to the width of the body of the ilium (index Ico2), for MVL indicates a value very close to that of *O. cuniculus; S. floridanus* and *L. europaeus* display a similar Ico2 value that is however, lower than that of MVL. It is noteworthy that, the acetabulum length in relation to its height (index Ico1) is significantly lower in MVL than in all the comparative taxa. In contrast to the more circular aspect of the acetabulum in *Oryctolagus*, *Sylvilagus*, and *Lepus*, it is more elliptical to oval shaped in MVL. According to Sargis (2002), more circular acetabulum acts restrictively for the mobility of the hip joint, in contrast to the more elliptical acetabulum that allows more mobility at the hip joint, so greater ranges of lateral movements (Sargis, 2002). Although this characteristic is important for the arboreal climbers (Sargis, 2002) it is noteworthy that it is present in MVL. A future investigation is needed to define how this aspect could have affected the movement of the leporid of MVL.

Another factor worth discussing is the size and shape of the ischial tuberosity. As noted in Fostowicz-Frelik (2007), the ischial tuberosity in *L. europaeus* is robust and large, exhibiting an isometric character. In rabbits, this area is narrower and medio-laterally compressed. This difference suggests that the musculature connected to the ischial tuberosity in hares exhibits superior strength compared to other leporid taxa. This is due to the larger cross-sectional area of the hip muscles, leading to a relatively increased capacity for contraction (Fostowicz-Frelik, 2007). In that aspect, the leporid of MVL shows a rather hare morphotype with isometric ischial tuberosity. However, the lateral anterior point of the ischial tuberosity is more similar to that of the rabbits, suggesting that the pelvic muscles strength was not as strong as in *Lepus*.

Fostowicz-Frelik (2007) marks that the placement of the trochanter and the robustness of the femur bone in mammals plays a great role in saltoriality and cursoriality. From the Ife1 index we see that MVL as *H. beremendensis* have a slender built of the anterior part of the femur, similar to that also observed in *T. meridionalis*.

Oryctolagus, *Sylvilagus*, and *Lepus* display a similar level of slenderness each other, that is more robust than in MVL. The proximal trochanters in MVL are closely placed to each other, a character observed in *Lepus* and *Sylvilagus*. The intermediate development of this trait between *Oryctolagus* and *Lepus* suggests relatively high degree of cursoriality for MVL. Another feature that is of interest is the erectness of the trochanters. Medial bending of the greater trochanter increases the gluteus medius muscle's attachment area, boosting its hip joint extension force (Fostowicz-Frelik, 2015). MVL exhibits a relatively strong trochanter bending, similar to that of *Sylvilagus*, but not as strong as that of *Lepus*. Considering that most not-erect trochanters are observed in faster runners (Taylor, 1976; Fostowicz-Frelik, 2007), the leporid of MVL could run relatively fast, yet not be considered as a very fast runner.

The more abducted position of the thighs is considered to be a characteristic for burrowing behavior (Taylor, 1976; Fostowicz-Frelik, 2007). This seems to be connected to the level of intrusion of the femoral head to the dorsal part of the neck. According to Fostowicz-Frelik (2007), digging is linked to higher thigh abduction, helping the animal push the soil backwards, with the hindlegs supporting this activity more efficiently. The leporid of MVL exhibits a femolar head like that of *Lepus*. *Oryctolagus* has the longest and best-developed femoral neck, allowing transverse motion (Fostowicz-Frelik, 2007). Therefore, MVL may not have the ability to abduct the hip as much as *Oryctolagus*, suggesting weaker digging capabilities for MVL. This can also be supported, when viewing Ife5 index. In MVL, the cranio-caudal thickness of the distal extremity of the femur exceeds its width. Anemone and Covert (2000) report that deeper condyles are a strong indication of cursoriality, allowing the quadriceps femoris to push the knee more powerfully. Once again, the leporid of MVL is indicated as having relatively strong cursorial abilities.

The tibial tuberosity is in great significance within the tibiofibula. As reported by Fostowicz-Frelik (2007), a shorter tibial tuberosity, as that observed in *Lepus*, is an index that the leporid is highly cursorial. The relative length of the tibial tuberosity to the tibiofibular length (Iti3; Fig.19; Table 25) of MVL is closest to that of *S. floridanus* and *O. cuniculus*. However, *Sylvilagus* and *Oryctolagus* have slightly longer tibial tuberosities than that of MVL. Considering this feature, MVL may not be highly cursorial as *Lepus*, but had more developed cursorial abilities than the rabbits. In addition, MVL has a developed tibial distal end (Iti4; Fig. 19; Table 25). The distal end of the tibia deepens more prominently in MVL, slightly less in *Lepus*. On the other hand, *Oryctolagus* and *Pentalagus* exhibit tibiofibulae with distal ends that extend more medio-laterally and hence the Iti4 value is low (Fostowicz-Frelik, 2007).

According to Lyon (1904), Dawson (1958), and Averianov (1995), the ankle joint structure in leporids is generally consistent, although there may be variations in the size of the tarsal bones. The primary distinctions in foot shape are related to the elongation of the metatarsals and phalanges, that are not being examined in this thesis. The talus bone appears to be slender in cursorial genera (Fostowicz-Frelik, 2007). The index value (Ita1) for the overall built of the talus for MVL is closer to that of *O. cuniculus*, as seen in Figure 20, indicating a non-cursorial development. Interestingly, the Isa1 value for *T. dumitrescuae* from Moldova is closer to that of *L. europaeus* (Averianov, 1995). The length of the talus neck (Ita2) for MVL is closer to that of *S. floridanus*, while *L. europaeus* exhibits relatively a longer neck (Fig. 20; Table 26). As noted by Fostowicz-Frelik (2007), the astragalus head is positioned towards the posterior end relative to the calcaneus distal end, which promotes ankle joint stability

and limits foot mobility to flexion and extension only. Therefore, an elongated neck of the astragalus in leporids further enhances this feature (Fostowicz-Frelik, 2007). The elongation of the body of the calcaneus seems to be closely related to saltorial adaptations and is somewhat affected by the body mass (Fostowicz-Frelik, 2007). This is similar to the case of some small mammals where elongated calcaneus is associated with high jumping performance (Hildebrand, 1974; Anemone and Covert, 2000). MVL has a relatively high value of Ica3, close to that of *Sylvilagus* (Fig. 21; Table 27). Lastly, the navicular and cuboid bones are relatively elongated in cursorial species. Regarding the navicular, MVL shows an intermediate state of the length of the navicular body in relation to the length of the tuberosity (Ina1; Fig. 22; Table 28), exhibiting higher development than *S. floridanus* and less than *L. europaeus* (Fostowicz-Frelik, 2007). Gambaryan (1974) observed that the proportions of feet in animals are influenced by their habitat, with forest species like *L. timidus* having relatively longer feet compared to *L. europaeus*. This adaptation is believed to enhance the jumping ability of these animals, allowing them to perform powerful jumps of high steepness. Additionally, animals living in more closed and bushy habitats exhibit a greater angle of jump departure (Gambaryan, 1974).

In summary, by studying the forelimb and hindlimb morphology of the MVL leporid, we can identify specific adaptations and make an estimation about its locomotion style. The wider ischiac tuberocity, potentially robust ilium, and closer positioning of femoral trochanters near the proximal end of the femur indicate that the animal had well-developed flexor-extensor muscles suited for swift movement. This suggests that it had strong cursorial abilities along with the potential to jump high. The elongated body of the calcaneus in MVL is a morphological feature that strengthens the possibility of good jumping ability. In addition, the leporid of MVL had most likely the ability to dig, as both the fore- and hindlimb indicates to some extent.

Size of the body is a fundamental characteristic of the biology and ecology of the species, as it is closely related with several behavioral, ecological, life history, morphological, and physiological traits (Peters, 1983). It is known that the best proxy for body size is body mass (Gingerich et al., 1982). Therefore, the prediction of the BM of fossil species is very important for the knowledge of their biology as well as to quantify and understand their habitats and adaptations (Palombo, 2009a).

The BM within Lagomorpha varies significantly, from the smallest pikas, which weigh between 70 and 250 gr, to the largest, such as rabbits and hares, who can surpass the 5 kgr (Silva and Downing, 1995). Their moderate BM, falling between that of small and large herbivores, make then ideal prey for various predators, including small to medium-sized ones like foxes and birds of prey, as well as larger predators like wolves and bears (Valverde, 1964). However, BM differentials can be noted regarding the seasonal food availability, the breeding season, the winter conditions, the predation pressure, and the environmental factors (Wilson and Reeder, 1993).

As Moncunill-Solé et al. (2015) notes, not all models are equally successful. Although teeth are the most found fossils for lagomorphs, they are not the best BM estimators, as their models are weaker. Thus, BM estimations using dental proxies are not fully reliable (Moncunill-Solé et al., 2014). However, this is unfortunate considering the plethora of dental material in contrast to postcranial and cranial remains in the lagomorph fossil archive. On the other hand, though postcranial parameters are more reliable in BM estimations, in some cases the length models are better than the

epiphyseal ones (Moncunill-Solé et al., 2014). Moncunill-Solé et al. (2015) recommend the use of femoral and humeral length proxies for more reliable BM values.

Given these facts into consideration the estimated BM for MVL is around 1700 to 2000 gr, with the possibility to reach but not surpass 3000 gr; it is therefore comparable to the body mass of *O. cuniculus* and within the lower range size of *L. europaeus*. The humerus and femur length estimations of MVL are surprisingly in line with the estimations of teeth. However, the number of specimens measured for the humerus and femur length are less than that of the teeth results may be biased. As it is concluded by Moncunill-Solé et al (2014), the right proxies for the BM estimation should be in correlation to the locomotory tendence of the taxon being questioned and some size proxies may not provide reliable estimations and thus need to be disregarded. In that case, the Dhud proxy offers significantly low values for the estimations of the BM and therefore is not appropriate for reliable estimations.

Through an analysis of the MNI for each bone group, it was concluded that the MVL leporid is represented by at least fifteen (15) individuals in the site. This conclusion was drawn from the abundant count of calcaneus bones.

6. Conclusions

It is evident that, by its dental features and especially p3 morphology, the studied leporid material from Megalo Emvolon-4 (MVL) belongs into the genus *Trischizolagus* according to the following diagnostic features: 1) the rhombic outline of p3 with a broad lingual anteroconid and a well-developed anteroflexid; 2) the presence of simple and uncrenulated enamel; 3) the general pattern of the lower and upper check teeth; and 4) the overall size of the upper and lower check teeth (Averianov and Tesakov, 1997; López-Martínez et al., 2007; López-Martínez, 2008; Čermák and Wagner, 2013).

Furthermore, the existence of the "*Alilepus*" p3 pattern, with the tetralobe form of the trigonid, the well-developed mesoflexid and hypoflexid, the size ratio of the trigonid and talonid of the studied material indicates great similarities with *T. dumitrescuae*. In addition, the metrical comparisons with other *T. dumitrescuae* samples and especially those from Măluşteni, indicates that MVL material is very close in size and propotions to the Romanian specimens and should be attributed to *T. dumitrescuae*. Lastly, the new material of MVL is in morphological and metrical agreement to the dental remains of *T. dumitrescuae* previously described from Megalo Emvolon-1 (MEV) (Koliadimou and Koufos, 1994).

The MVL sample provides the first representation of what the cranium of *T. dumitrescuae*. The cranial comparison with extant taxa shows that MVL *T. dumitrescuae* combines both *Lepus* and *Oryctolagus* features. It shares with *Lepus* the large cranium and overall dimensions as well as the highly fenestrated skull in the maxillary region. It shares with *Oryctolagus*, the not so well-developed supraorbital processes and the not highly acute skull. This indicates that MVL exhibits a skull development in-between that of a hare and a rabbit.

The estimated BM of *T. dumitrescuae* in MVL is around 1.7 to 2 kilos, similar to that of a small-sized *L. europaeus* or average sized *O. cuniculus*. The morphological features of the fore- and hindlimbs, indicate that *T. dumitrescuae* in MVL was capable of fast running but not as fast as *L. europaeus* and may had some burrowing and digging adaptations. MLV *T. dumitrescuae* wide ischiac tuberocity, robust ilium, and close positioning of femoral trochanters near the proximal end of the femur indicate well-developed flexor-extensor muscles suited for swift movement. These assumptions can also be supported by the highly fenestrated skull of MVL *T. dumitrescuae* and the not so acute facial tilt of its cranium. Strong cursorial abilities and potential for high jumping, further supported by the elongated body of the calcaneus.

There has been no examination of the fossil assemblages at the MVL site from a palaeoecological perspective. According to Boev (2002), the Megalo Emvolon area was likely a mix of a forested savanna, light forest, and open lands with scattered bushes. However, no cervids are known from the locality. The absence of deer in this area is notable because they are founded in woodland habitats with scattered trees (Boev, 2002). Instead, all the known taxa from Megalo Emvolon are ground-dwelling species and not adapted for life in wooded areas. The peafowl (*Pavo bravardi*) discovered prefers habitats that are lightly forested and mainly open land with scattered bushes (Boev and Koufos, 2000; Boev, 2002). In addition, the primate found in the locality, *Dolichopithecus ruscinensis*, has morphological adaptations for life in the ground (Szalay & Delson, 1979). Hipparionine horses and bovids species found in

Megalo Emvolon typically inhabit more mixed/open and arid environments (Bernor et al., 2021). Moreover, spalacids are rodents with long lifespans that reside in arid grasslands and subsist entirely on subterranean tunnel networks (Bugarski-Stanojević et al., 2022). The mammalian fauna present at Megalo Emvolon suggests therefore that the region had a semi-arid climate (Eronen and Rook, 2004) supported by the giant snake (*Laophis crotaloides*) found there (Georgalis et al., 2014).

The suggested fast-running ecomorphological adaptations of the MVL leporid come in agreement with a mixed/open paleohabitat at Megalo Emvolon. As stated before, hares are frequently seen in open areas where they can utilize their speed to escape from predators, whereas rabbits tend to inhabit closed areas where they can hide from predators as they are not as swift as hares (Angerbjörn, 2003). However, further research should be made to recognize the potential of the MVL taxon for cursorial adaptation.

REFERENCES

Alexander, R.McN., 2003. Principles of Animal Locomotion. Princeton University Press, Princeton, pp. 371.

Anemone, R.L., Covert, H.H., 2000. New skeletal remains of *Omomys* (Primates, Omomyidae): functional morphology of the hindlimb and locomotor behavior of a Middle Eocene primate. Journal of Human Evolution 38, 607–633.

Angelone C., 2008. Contribution of complex discrete Fourier transform (CDFT) analysis to the systematics of the genus *Prolagus* (Ochotonidae, Lagomorpha, Mammalia). Neues Jahrbuch für Geologie und Paläontologie-Abhandlungen 249 (2), 129–138.

Angelone., C., Čermák. S., Moncunill-Solé, B., Rook, L., 2022. The body mass of *Paludotona* (Lagomorpha, Mammalia): first approach to the ecology of the last stem lagomorph (Tusco-Sardinia palaeobioprovince, Late Miocene). Bollettino della Società Paleontologica Italiana 61, 61–70.

Angelone, C., Moncunill-Solé, B., Kotsakis, T., 2019. Contribution of fossil Lagomorpha (Mammalia) to the refinement of the late Miocene-Quaternary palaeobiogeographical setting of Italy. Comptes Rendus Palevol 18, 1025–1040.

Angerbjörn, A., 2003. Hares and rabbits (Leporidae). In: Grzimek's Animal Life Encyclopedia. Second Edition. Volume 16 Mammals. Kleinman, D.G., Geist, V., McDade, M.C. (eds), Thomson Gale, 504–516.

Arambourg, C., Piveteau, J., 1929. Les vertebres du Pontien de Salonique. Annales de Paléontologie, 18, 1–139.

Asher, R. J., Meng, J., Wible, J.R., McKenna, M.C., Rougier, G.W., Dashzeveg, D., Novacek, M.J., 2005. Stem Lagomorpha and the Antiquity of Glires. Science, 307 (5712), 1091–1094.

Averianov, A.O., 1995. Osteology and adaptations of the Early Pliocene rabbit *Trischizolagus dumitrescuae* (Lagomorpha: Leporidae). Journal of Vertebrate Paleontology 1, 375–386.

Averianov, A.O., 1996. The Neogene rabbit *Hypolagus igromovi* Gureev, 1964 (Lagomorpha, Leporidae) from southern European Russia. Acta zoologica cracoviensia 39(1), 61–66.

Averianov, A.O., Tesakov, A.S., 1997. Evolutionary trends in Mio-Pliocene Leporinae, based on *Trischizolagus* (Mammalia, Lagomorpha). PalZ 71, 145–153.

Bachmayer, F., Mlynarski, M., Symeonidis, N., 1979. Fossile Schildkröten aus dem Pliozän von Megalo Emvolo (Karaburun) bei Saloniki (Griechenland). Annales Géologiques des Pays Helléniques 29, 267–276.

Boev, Z., 2002. Fossil record and disappearance of peafowl (*Pavo* Linnaeus) from the Balkan Peninsula and Europe (Aves: Phasianidae). Historia Naturalis Bulgarica, 14, 109–115.

Boev, Z., Koufos, G., 2000. Presence of *Pavo bravardi* (Gervais,1849) (Aves, Phasianidae) in the Ruscinian locality of Megalo Emvolon, Macedonia, Greece. Geologica Balcanica, 30, 69–74.

Boon-Kristkoiz, E., Kristkoiz, A.R., 1999. Order Lagomorpha. In: The Miocene Land Mammals of Europe, Rössner, G., Heissig, K. (eds), Verlag Dr. Friedrich Pfeil, 259–262.

Bugarski-Stanojević V., Stamenković G., Jojić V., Ćosić N., Ćirović D., Stojković O., Veličković J., Savić I., 2022. Cryptic Diversity of the European Blind Mole Rat *Nannospalax leucodon* Species Complex: Implications for Conservation. Animals (Basel) 12(9), 1097.

Burgin, C.J., Colella, J.P., Kahn, P.L., and Upham, N.S., 2018. How many species of mammals are there? Journal of Mammalian Evolution 99, 1–14.

Bramble, D.M., 1989. Cranial Specialization and Locomotor Habit in the Lagomorpha, American Zoologist 29, 303–317.

Čermák, S., 2009. The Plio-Pleistocene record of *Hypolagus* (Lagomorpha, Leporidae) from the Czech and Slovak Republics with comments on systematics and classification of the genus. Bulletin of Geosciences 84(3), 497–524.

Čermák, S., Angelone, C., Moncunill-Solé, B., 2021. *Prolagus* Pomel, 1853 (Lagomorpha, Mammalia) in the framework of the Pliocene faunal rearrangements in central Europe. Comptes Rendus Palevol 28, 597–617.

Čermák, S., Joniak, P., Rojay, B., 2019. A new early Pliocene locality Tepe Alagöz (Turkey) reveals a distinctive tooth phenotype of *Trischizolagus* (Lagomorpha, Leporidae) in Asia Minor. Palaeontologia Electronica, 1–21.

Čermák, S., Angelone, C., Sinitsa, M.V., 2015. New Late Miocene *Alilepus* (Lagomorpha, Mammalia) from Eastern Europe – a new light on the evolution of the earliest Old World Leporinae. Bulletin of Geosciences 90(2), 431–451.

Čermák, S., Angelone, C., 2013. Revision of the type material of the Pliocene species *Prolagus bilobus* Heller, 1936 (Mammalia, Lagomorpha), with comments on the taxonomic validity of *P. osmolskae* Fostowicz-Frelik, 2010. Bulletin of Geosciences 88(1), 45–50.

Čermák, S., Wagner, J., 2013. The Pliocene record of *Trischizolagus* and *Pliopentalagus* (Leporidae, Lagomorpha, Mammalia) in Central Europe, with comments on taxonomy and evolutionary history of Leporinae. Neues Jahrbuch für Geologie und Paläontologie 268, 97–111.

Chapman, J.A, Ceballos, G., 1990. Chapter 5: The Cottontails. In: Rabbits, Hares and Pikas. Chapman, J.A., Flux, E.C. (eds), Status Survey and Conservation Action Plan. IUCN, 95–110.

Chapman, J.A., Flux, J.E.C., 1990. Rabbits, hares and pikas. Status survey and conversation action plan. IUCN, 1–6.

Crespo, V., Vasile, Ș, Petculescu, A., Ratoi, B., Haiduc, B., 2023. The Early Pliocene small mammals (Eulipotyphla, Rodentia, Lagomorpha) from Bereşti and Măluşteni (eastern Romania): A fresh look at old collections. Earth and Environmental Science Transactions of The Royal Society of Edinburgh, 1–15.

Dawson, M.R., 1958. Later Tertiary Leporidae of North America. University of Kansas Paleontological Contributions, Vertebrata 6, 1–75.

de Bruijn, H., 1984. Remains of the mole-rat *Microspalax odessanus* Topachevski, from Karaburun (Greece, Macedonia) and the family Spalacidae. Proceedings Koninklijke Nederlandse Akademie van Wetenschappen B, 87, 41.

de Bruijn, H., Dawson, M.R., Mein, P., 1970. Upper Pliocene Rodentia, Lagomorpha and Insectivora (Mammalia) from the isle of Rhodes (Greece). Proceedings of the Koninklijke Nederlandse Akademie van Wetenschappen B 73, 535–584.

Dice, L.R., 1929. The phylogeny of the Leporidae, with description of a new genus. Journal of Mammalogy 10, 340–344.

Drakopoulou, C., Georgalis, G.L., Lazaridis, G., Kostopoulos, D.S., 2022. Am Early Pliocene Monitor Lizard (genus *Varanus*) from the Locality Megalo Emvolon (Northern Greece). 16th International Congress of the Geological Society of Greece, 17–19 October 2022, At: Patras, Greece Volume: Bulletin of the Geological Society of Greece, Special Publication 10.

DuBrul, E.L., 1950. Posture, locomotion and the skull in Lagomorpha. American Journal of Anatomy 87(2), 277–313.

Erbajeva, M.A., 2016. The Ochotonids of Eurasia: biochronology and taxonomic diversity. Biology Bulletin 43, 729–735.

Erbajeva, M.A., Mead, J.I., Alexeeva, N.V., Angelone, C., Swift, S.L., 2011. Taxonomic diversity of Late Cenozoic Asian and North American ochotonids. Palaeontologia Electronica 14, 9.

Eronen, J.T., Rook, L., 2004. The Mio-Pliocene European primate fossil record: Dynamics and habitat tracking. Journal of Human Evolution 47(5), 323–341.

Farag, F., Daghash, S., Khalifa, E., Hussein, M., Hagrass, S., 2012. Anatomical Studies on the Skull of the Domestic Rabbit (*Oryctolagus cuniculus*) With Special Reference to the Hyoid Apparatus. Journal of Veterinary Anatomy 5, 49–70.

Fladerer, F.A., Reiner, G., 1996. Evolutionary shifts in the first premolar pattern of *Hypolagus beremendensis* (Petényi, 1864) (Lagomorpha, Mammalia) in the Plio-Pleistocene of Central Europe. Acta Zoologica Cracoviensia 39, 147–160.

Flux, J.E.C., Aneermann, R., 1990. Chapter 4: The Hares and Jackrabbits. In: Rabbits, Hares and Pikas. Status Survey and Conservation Action Plan. Chapman, J.A., Flux, E.C. (eds), IUCN, 61–94.

Flynn, L.J., Winkler, A.J., Erbaeva, M., Alexeeva, N., Anders, U., Angelone, C., Cermák, S., Fladerer, F.A., Kraatz, B., Ruedas, L.A., Ruf, I., Tomida, Y., Veitschegger, K., Zhang, Z., 2014. The Leporid Datum: a Late Miocene biotic marker. Mammal Review 44, 164–176.

Gambaryan, P.P., 1972. The running of mammals. Adaptive features of locomotional organs. Nauka Publishing, Leningrad (in Russian). English edition: Gambaryan, P. P. 1974. How mammals run: anatomical adaptations. J. Wiley, New York; Israel program for scientific translations, Jerusalem, pp. 368.

Ge, D., Wen, Z., Xia, L., Zhang Z., Erbajeva, M., Huang, C., Yang, Q., 2013. Evolutionary history of lagomorphs in response to global environmental change. PLoS One 8, 1–15.

Georgalis, G.L., Kear, B.P., 2013. The fossil turtles of Greece: an overview of taxonomy and distribution. Geobios 46(4), 299–311.

Georgalis, L.G., Szyndlar Z., Kear, B.P., Delfino, M., 2016. New material of *Laophis crotaloides*, an enigmatic giant snake from Greece, with an overview of the largest fossil European vipers. Swiss Journal of Geosciences 109, 103–116.

Geraads, D., 1994. Rongeurs et Lagomorphes du Pleistocine moyen de la «Orotte des Rhinoceros», carriere Oulad Hamida I, a Casablanca, Maroc. Neues Jahrbuch für Geologie und Paläontologie 191(2), 147–172.

Gidley, J.W., 1912. The lagomorphs an independent order. Science 36 922, 258–256.

Gingerich, P.D., Smith, B.H., Rosenberg, K., 1982. Allometric scaling in the dentition of primates and prediction of body weight from tooth size in fossils. American Journal of Physical Anthropology 58(1), 81–100.

Graham, J.E., 2015. Chapter 41 - Lagomorpha (Pikas, Rabbits, and Hares). In: Fowler's Zoo and Wild Animal Medicine, Vol. 8. Miller, R.E., Fowler, M.E. (eds), Elsevier, 8375–8384.

Hammer, Ø., Harper, D.A.T., Ryan, P.D., 2001. PAST: Paleontological Statistics Software Package for Education and Data Analysis PAST. Palaeontologia Electronica 4, 1–9.

Hildebrand, M., 1974. Analysis of Vertebrate Structure. 710 pp. John Wiley and Sons, New York.

Hoffmann, R.S., Smith, A.T., 2005. Lagomorphs, In: Mammal Species of the World, 3rd Edition. Wilson, D.E., Reeder, D. M., (eds.), Johns Hopkins University Press, 185–211.

Janvier, P., and Montenat, C., 1971. Le plus ancien Uporide d'Europe occidentale, *Hispanolagus crusafontinov*. gen. nov. sp. du Miocene superieur de Mureia (Espagne). Bulletin Museum National d'Histoire Naturelle Paris 2(42), 780–788.

Kostopoulos, D.S., Sylvestrou, I., 2022. The Fossil Record of Suoids (Mammalia: Artiodactyla: Suoidae) in Greece. In: Fossil Vertebrates of Greece Vol. 2. Vlachos, E. (eds), Springer, Cham, 249–270.

Koufos, G.D., 2006. The Neogene mammal localities of Greece: faunas, chronology and biostratigraphy. Hellenic Journal of Geosciences 41, 183–214.

Koufos, G.D., 1997. The canids *Eucyon* and *Nyctereutes* from the Ruscinian of Macedonia, Greece. Palaeontologia i Evolucio, 30–48.

Koufos, G.D., Koliadimou, K., 1993. Two lagomorphs from the Pliocene of Macedonia (Greece). Bulletin of the Geological Society of Greece, 28, 117–129.

Koufos, G.D., Syrides, G., Koliadimou, K., 1991. A Pliocene primate from Macedonia. Journal of Human Evolution 21, 283–294.

Koufos, G.D., Vlachou, T., Gkeme, A., 2022. The Fossil Record of Equids (Mammalia: Perissodactyla: Equidae) in Greece. In: Fossil Vertebrates of Greece Vol. 2. Springer, Cham. Vlachos, E. (eds), 351–402.

Kraatz, B., Sherratt, E., Bumacod, N., Wedel, M.J., 2015. Ecological correlates to cranial morphology in Leporids (Mammalia, Lagomorpha) PeerJ 3, 1–20.

López Martínez, N., 1977. Nuevos lagomorfos (Mammalia) del Neogeno y Cuaternario Español. Trabajos sobre Neógeno-Cuaternario 8, 7–45.

López-Martínez N., 2001. Paleobiogeographical history of *Prolagus*, an European ochotonid (Lagomorpha). Lynx 32, 215–231.

López-Martinez, N., 2008. The Lagomorph Fossil Record and the Origin of the European Rabbit. In: Lagomorph Biology. Alves, P.C., Ferrand, N., Hackländer, K. (eds). Springer, 26–46.

López-Martínez, N., Likius, A., Mackaye, H.T., Vignaud, P., Brunet, M., 2007. A new Lagomorph from the Late Miocene of Chad (Central Africa). Un nuevo Lagomorfo del Mioceno superior de Chad (África central). Revista Española de Paleontología 22(1), 1–20.

Lu, X., 2003. Postnatal growth of skull linear measurements of Cape hare and *Lepus capensis* in northern China: An analysis in an adaptive context. Biological Journal of the Linnean Society 78, 343–353.

Lyon, M.W., 1904. Classification of the hares and their allies. Smithsonian Miscellaneous Collections 45, 321–447.

Maravelis, A.G., Bourli, N., Vlachos, E., Zelilidis, A., 2021. The Sedimentary Basins from the Miocene to the Present in Greece: Examples for the Most Studied Basins from North Greece. In: Fossil Vertebrates of Greece Vol. 2, Laurasiatherians, Artiodactyles, Perissodactyles, Carnivorans, and Island Endemics, 13–31.

Maravelis, A.G., Pantopoulos, G., Tserolas, P., Zelilidis, A., 2015. Accretionary prism forearc interactions as reflected in the sedimentary fill of southern Thrace Basin (Lemnos Island, NE Greece). International Journal of Earth Sciences 104, 1039–1060.

Maynard Smith, J., Savage, R.J.G., 1956. Some locomotory adaptations in mammals. Zoological Journal of the Linnean Society, 603–622.

Moncunill-Solé, B., Quintana, J., Jordana, X., Engelbrektsson, P., Köhler, M., 2015. The Weight of Fossil Leporids and Ochotonids: Body Mass Estimation Models for the Order Lagomorpha. Journal of Zoology 295, 4, 269–278.

Montuire, S., 2001. Lagomorpha (Rabbits, Hares and Pikas). eLS.

Naff, K.A., Craig, S., 2012. The domestic rabbit, *Oryctolagus cuniculus*: origins and history. In: The Laboratory Rabbit, Guinea Pig, Hamster, and Other Rodents. American College of Laboratory Animal Medicine, M. A. Suckow, K. A. Stevens, and R. P. Wilson (eds), Cambridge, MA: Academic Press, 157–163.

Owen, R., 1857. On the fossil vertebrae of a Serpent (*Laophis crotaloïdes*) discovered by Capt. Spratt, R.N., in a tertiary formation at Salonica. Quarterly Journal of the Geological Society of London 13, 196–199.

Palacios, F., López Martínez, N., 1980. Morfologia dentaria de las liebres europeas (Lagomorpha, Leporidae). Doñana Acta Vertebrata 7, 61–81.

Palombo, M.R., 2009. Biochronology, paleobiogeography and faunal turnover in western Mediterranean Cenozoic mammals. Integrative Zoology 4(4), 367–386.

Patnaik, R., 2002. Pliocene Leporidae (Lagomorpha, Mammalia) from the Upper Siwaliks of India: implications for phylogenetic relationships. Journal of Vertebrate Paleontology 22(2), 443–452.

Pelletier, M., Cochardb, D., Boudadi-Maligne, M., Crochet, J.Y., Bourguignon, L., 2015. Lower Pleistocene leporids (Lagomorpha, Mammalia) in Western Europe: New data from the Bois-de-Riquet (Lézignan-la-Cèbe, Hérault, France). Comptes Rendus Palevol 14, 371–385.

Peters, R.H., Wassenberg, K., 1983. The effect of body size on animal abundance. Oecologia 60, 89–96.

Piskoulis, P., Tsiourlini, I., Tsoukala, E., 2023. The Late and the Latest Pleistocene Chiroptera (Mammalia) from Loutra Almopias Cave a (Pella, Macedonia, Greece). Acta Chiropterologica. 25(1), 53–84

Popov, V.V., 2004. Pliocene small mammals (Mammalia, Lipotyphla, Chiroptera, Lagomorpha, Rodentia) from Muselievo (North Bulgaria). Geodiversitas 26, 403–491.

Qiu, Z., Storch, G., 2000. The early Pliocene micromammalian fauna of Bilike, Inner Mongolia, China (Mammalia: Lipotyphla, Chiroptera, Rodentia, Lagomorpha). Senckenbergiana lethaea 80, 173–229.

Quintana Cardona, J., Moncunill-Solé, B., 2014. *Hypolagus balearicus* Quintana, Bover, Alcover, Agustí & Bailon, 2010 (Mammalia: Leporidae): new data from the Neogene of Eivissa (Balearic Islands, Western Mediterranean). Geodiversitas 36(2), 283–310.

Radulesco, C., Samson, P., 1967. Contributions à la connaissance du complexe faunique de Malusteni-Beresti (Pléistocène inférieur), Roumanie I. Ord. Lagomorpha, Fam. Leporidae. Neues Jahrbuch für Geologie und Paläontologie, Monatshefte 1967(9), 544–563.

Rosin, A.V., Meriggi, A., Perez, S.S., 2010. Density and habitat requirements of introduced Eastern cotton tail Sylvilagus floridanus in northern Italy. Acta Theriologica 55, 139–151.

Rosin, A.V., Montagna, A., Meriggi, A., Serrano Perez. S., 2009. Density and habitat requirements of sympatric hares and cottontails in northern Italy. Hystrix 20, 101–110.14.

Sargis, E.J., 2002. Functional morphology of the hindlimb of tupaiids (Mammalia, Scandentia) and its phylogenetic implications. Journal of Morphology 254, 149–185.

Sen, S., 2020. Lagomorphs (Mammalia) from the early Pliocene of Dorkovo, Bulgaria. Fossil Imprint 76(1), 99–117.

Sen, S., and Geraads, D., 2023. Lagomorpha (Mammalia) from the Pliocene-Pleistocene locality of Ahl al Oughlam, Morocco. Palaeobiodiversity and Palaeoenvironments 103.

Smith, A.T., 2003. Lagomorpha (Pikas, rabbits, and hares). In: Grzimek's Animal Life Encyclopedia. Second Edition. Volume 16 Mammals. Kleinman, D.G., Geist, V., McDade, M.C. (eds), Thomson Gale, 479–489.

Smith, A.T., Weston, M.L., 1990. *Ochotona princeps*. Mammal Spec, 1–8.

Steffens, P., Bruijn, H. de, Meulenkamp, J.E., Benda, L., 1979. Field guide to the Neogene of northern Greece (Thessaloniki area and Strimon basin). Publications of the Department of Geology and Paleontology of the University of Athens series A 35, 1–14.

Sidiropoulou, V., 2017. Stratigraphic analysis of the sedimentation cycles of the Angelochori section of Thessaloniki. Bachelor thesis, Department of Geology, Aristotle University of Thessaloniki, pp. 66. (in Greek)

Silva, M., Downing, J.A., 1995. The Allometric Scaling of Density and Body Mass: A Nonlinear Relationship for Terrestrial Mammals. The American Naturalist 145(5), 704–727.

Sylvestrou, I., 2002. Stratigraphic, palaeontological and palaeogeographical study of the Neogene Quaternary deposits of Katerini basin, Northern Greece. PhD thesis, Department of Geology, Aristotle University of Thessaloniki, pp. 370.

Syrides, G., 1990. Lithostratigraphic, biostratigraphic and palaeogeographic study of the Neogene – Quaternary sedimentary deposits of Chalkidiki Peninsula, Macedonia, Greece. Ph.D. Thesis, Aristotle University of Thessaloniki, Thessaloniki, pp. 243. (in Greek).

Szalay F., and Delson, E., 1979. Evolutionary history of the Primates. New York: Academic Press.

Taylor, M.E., 1976. Functional anatomy of the hindlimb of some African Viverridae (Carnivora). Journal of Morphology 148, 227–254.

Tomida, Y., Jin, C., 2005. Reconsideration of the generic assignment of *Pliopentalagus nihewanensis* from the late Pliocene of Hebei China. Vertebrata Palasiatica 43, 297–303.

Valverde, J.A., 1964. Estructura de una comunidad de vertebrados terrestres. Monografías de la estación biológica de Doñana 1, 1–129.

Vasileiadou K., Koufos, G., Syrides, G., 2003. Silata, a new locality with micromammals from the Miocene / Pliocene boundary of the Chalkidiki peninsula, Macedonia, Greece. Deinsea 10(1), 549–562.

Vasileiadou, K., Sylvestrou, I., 2022. The Fossil Record of Hares, Rabbits, and Pikas (Mammalia: Lagomorpha) in Greece. In: Fossil Vertebrates of Greece Vol. 1. Vlachos, E. (eds), Springer, Cham, 611–637.

Vlachos, E., Kotsakis, T., Delfino, M., 2015. The chelonians from the Latest Miocene–Earliest Pliocene localities of Allatini and Pylea (East Thessaloniki, Macedonia, Greece). Comptes Rendus Palevol 14(3), 187–205.

von den Driesch, A., 1976. A Guide to the Measurement of Animal Bones from Archaeological Sites. Harvard University Press, pp. 136.

Voorhies, M.R., Timperley, C.L., 1997. A new *Pronotolagus* (Lagomorpha, Leporidae) and other Leporids from the Valentine Railway Quarries (Barstovian, Nebraska), and the Archaeolaginae-Leporine transition. Journal of Vertebrate Paleontology 17, 725–737.

Weston, M.L., 1982. A numerical revision of the genus *Ochotona* (Lagomorpha: Mammalia) and an examination of its phylogenetic relationships. Unpublished Ph.D. dissertation, University of British Columbia, Vancouver.

Wilson, D.E., Reeder, D.M., 2005. Mammals species of the world. A taxonomic and geographic reference. Baltimore: Johns Hopkins University Press.

White, J.A., 1991. North American Leporinae (Mammalia: Lagomorpha) from Late Miocene (Clarendonian) to latest Pliocene (Blancan). Journal of Vertebrate Paleontology 11, 67–89.

Wilson, D.E., and D.M,. Reeder, 1993. Mammal Species of the World, A Taxonomic and Geographic Reference. 2nd edition. Smithsonian Institution Press, Washington.

Wolniewicz, A.S., Fostowicz-Frelik, L., 2021. CT-Informed Skull Osteology of *Palaeolagus haydeni* (Mammalia: Lagomorpha) and its Bearing on the Reconstruction of the Early Lagomorph Body Plan. Frontiers in Ecology and Evolution 9, 1–24.

Wood-Bailey, A.P., Cox, P.G., Sharp, A.C., 2022. The evolution of unique cranial traits in leporid lagomorphs. PeerJ 10, 1–19.

Wu, W.Y., Flynn, L.J., 2017. The lagomorphs (Ochotonidae, Leporidae) of Yushe Basin. In: Late Cenozoic Yushe Basin, Shanxi Province, China: Geology and Fossil Mammals. Volume 2. Small Mammal Fossils of Yushe Basin. Flynn, L.J., Wu, W.Y. (eds), Vertebrate Paleobiology and Paleoanthropology, 31–57.

Zhang, C.F., Wang, Y., Deng, X.M., Biasatti, D., 2009. C4 expansion in the central inner Mongolia during the latest Miocene and early Pliocene. Earth and Planetary Science Letters 287, 311–319.

APPENDIX I

Table 31.List of the measurements obtained for *L. europaeus*, *O. cuniculus*, and *S. floridanus* from Naturalis Biodiversity Center. Measurements given in mm.

Size proxy		**CL**		**BL**		**DEL**		**GLN**		**GBN**		**FL**		**IFL**		**GBIF**		**PL**		**PB**		**CB**		**OZB**		**AZB**
***L. europaeus* ZMA 18.170**		8.3		7.5		4.5		3.75		1.51		3.3		2.2		0.8		0.35		1		0.8		4.15		4.3
***L.europaeus* 8985**		8.2		7.3		4.6		3.8		1.8		3.65		2.2		0.9		0.3		0.95		0.85		3.95		4.3
***L. europaeus* 13 .539**		8.4		7.4		4.7		4.1		2.3		3.5		2.3		0.9		0.35		1		0.9		4.1		4.3
***O. cuniculus* 13.335**		6.9		5.7		3.55		2.15		1.1		3		1.55		0.4		0.3		0.7		0.3		3.3		3.5
***O. cuniculus* 13.334**		6.7		6		3.7		3.4		1.2		3.2		1.8		0.5		0.4		0.7		0.3		3.3		3.5
***O. cuniclus* 13.333**		-		-		3.7		3.4		1.15		3.1		1.8		0.4		0.3		0.6		0.3		3.2		-
***S. floridanus* 13.252**		6.3		5.6		3.6		3.3		1.3		3		1.6		0.5		0.4		0.9		0.5		3.25		-
***S. floridanus* 13.254**		-		-		3.1		2.7		1.2		2.3		1.4		0.3		0.3		0.6		0.3		3		2.9
***S. floridanus* 13.253**		6.4		5.6		3.6		3.3		1.35		3.1		1.8		0.5		0.5		0.7		0.4		3.3		3.3

GBOC	1.5	1.4	1.45	1.2	1.25	-	1.1	-	1.3
GNB	3.1	3.15	3.15	2.5	2.6	2.6	2.3	2.2	2.3
BS	2.7	2.75	2.8	2.2	2.3	2.1	2.15	1.75	2
dl	1.8	1.8	2	1.3	1.3	1.4	1.2	1.15	1.3
al	1.55	1.6	1.6	1.1	1.2	1.25	1.3	1.1	1.2

Table 32. List of the comparative postcranial material of *T. meridionalis* (Sen and Geraads, 2023), *T. dumitrescuae* (Averianov, 1995), *H. beremendensis*, *O. cuniculus*, *P. furnessi*, *S. floridanus*, and *L. europaeus* (Fostowicz-Frelik, 2007). Measurements in mm.

Bone	**Size proxy**	***T. meridionalis* (Sen and Geraads, 2023)**	***T. dumitrescuae* (Averianov, 1995)**	***Hypolagus beremendensis* (Fostowicz-Frelik, 2007)**	***Oryctolagus cuniculus* (Fostowicz-Frelik, 2007)**	***Pentalagus furnessi* (Fostowicz-Frelik, 2007)**	***Sylvilagus floridanus* (Fostowicz-Frelik, 2007)**	***Lepus europaeus* (Fostowicz-Frelik, 2007)**
Scapula	Wscapr	12.13; 10.8-13.4 (N=7)	-	-	-	-	-	-
	Lnsca	-	6.2	-	-	-	-	-
	Lpasca	-	-	-	-	-	-	-
	Bglsca	-	-	-	-	-	-	-
Humerus	Lhu	71.4; 65.8-75.8 (N=5)	-	-	-	-	-	-
	Whupr	12.7; 11.1-13.6 (N=6)	14.25; 14.2-14.3 (N=2)	-	-	-	-	-
	width of shaft	4.83; 4.2-6.5 (N=24)	-	-	-	-	-	-
	Whud	9.75; 8.6-11.5 (N=31)	-	-	-	-	-	-
Radius	Lra	69.33; 66-74 (N=3)	-	-	-	-	-	-
	Wrapr	7.07; 6.8-7.4 (N=3)	-	-	-	-	-	-
	Drapr	5.75; 4.8-6.7	-	-	-	-	-	-

		(N=2)						
	Wrash	4.43; 3.6-5 (N=8)	-	-	-	-	-	-
	Wrad	6.58; 6.1-6.9 (N=6)	-	-	-	-	-	-
Ulna	Lul	77.9; 75-80.8 (N=2)	-	-	-	-	-	-
	Wulpr	6.16; 5.7-6.5 (N=19)	-	-	-	-	-	-
	Dulol	7.24; 6.2-8.2 (N=20)	-	-	-	-	-	-
	width of shaft	4.4; 4.1-4.6 (N=3)	-	-	-	-	-	-
	Lulol	-	10.1	-	-	-	-	-
	Wulraf	-	7.1	-	-	-	-	-
Coxal	Acetabulum diameter	8.28; 7.7-8.8 (N=5)	-	-	-	-	-	-
	Lisch	-	-	32.6 (N=4)	29.2 (N=1)	31.5 (N=1)	31.5 (N=1)	43 (N=2)
	Wilb	-	-	8.5 (N=65, SD=0.4)	7.6 (N=9, SD=0.6)	8.9 (N=4)	7.4 (N=5, SD=0.8)	11.8 (N=10, SD=0.5)
	Lac	-	-	9.7 (N=41, SD=0.5)	8.3 (N=9, SD=0.3)	10.7 (N=4)	7.8 (N=5, SD=0.8)	12.4 (N=10, SD=0.5)
	Hac	-	-	9.1 (N=41, SD=0.4)	7.9 (N=9, SD=0.3)	9.9 (N=4)	7.2 (N=5, SD=0.5)	11.9 (N=10, SD=0.4)
Femur	Lfe	88.34; 86.1-91.2 (N=8)	103.6; 103.3-103.8 (N=2)	94	82.6 (N=8, SD= 3.4)	89.5 (N=4)	81.8 (N=4)	132.4 (N=10, SD=2.2)
	Wfepr	17.47; 16.8-18.1 (N=3)	-	18.5 (N=5, SD=1.2)	18.9 (N=8, SD=0.6)	21.8 (N=4)	18.3 (N=5; SD=2.2)	30.4 (N=10, SD=1.5)
	Wfedis	14.44; 13.1-16 (N=11)	-	15.6 (N=60, SD= 0.8)	14 (N=8, SD= 0.5)	17.5 (N=4)	13.4 (N=5, SD=1.4)	20.4 (N=10, SD= 0.8)
	Wintf	-	-	4 (N=62, SD=0.5)	4 (N=7, SD=0.4)	5 (N=3)	3.8 (N=5, SD=0.7)	6.1 (N=10, SD=0.5)
	Wpag	-	-	5 (N=27, SD=0.7)	4.8 (N=7, SD= 0.4)	6.8 (N=4)	4.5 (N=5, SD=1.4)	7.3 (N=10, SD=0.7)
	Hdis	-	-	17.9 (N=13, SD= 0.7)	14.7 (N=7, SD=0.5)	17.2 (N=4)	13.6 (N=5, SD=1.4)	20.6 (N=10, SD=1.2)
	Whe	-	-	7.6 (N=33, SD=0.3)	6.6 (N=3)	8.6 (N=4)	6.3 (N=1)	10.3 (N=10, SD=0.4)
	Wfesh	-	-	7.7 (N=20, SD=0.6)	7 (N=8, SD=0.5)	8 (N=4)	7 (N=5, SD=0.7)	9.7 (N=10, SD=0.6)

	Tfesh	-	-	7.1 (N=20, SD=0.5)	6.7 (N=8, SD= 0.25)	7.6 (N=4)	6.5 (N=5, SD= 0.2)	8.9 (N=10, SD=0.5)
Tibiofibula	Lti	101.76; 98.2-106.7 (N=11)	-	111.4	90.4 (N=7, SD=3.8)	91.5 (N=3)	92.7 (N=4)	148.2 (N=10, SD=4.4)
	Wtipr	14.69; 13.5-16.2 N=14	-	15.5 (N=27, SD=1.3)	14.7 (N=8, SD=0.8)	17.9 (N=3)	14.4 (N=5, SD=1.6)	21 (N=10, SD=1.4)
	Wtish	6.02; 5.5-6.8 (N=20)	-	6.8 (N=13, SD=0.5)	5.9 (N=8, SD=0.3)	7.6 (N=3)	5.3 (N=5, SD=0.3)	7.6 (N=10, SD=0.2)
	Wtidis	11.8; 10.2-13.3 (N=21)	-	13.1 (N=70, SD=0.6)	12.4 (N=8, SD=0.6)	15.9 (N=3)	11.2 (N=4)	16.4 (N=10, SD=0.5)
	Ttidis	-	-	6.6 (N=70, SD=0.4)	5.3 (N=8, SD=0.8)	6.8 (N=3)	5.5 (N=4)	8.8 (N=10, SD=0.4)
	Dtipr	-	-	14.4 (N=28, SD=1)	13 (N=8, SD=0.5)	12.8 (N=3)	12.7 (N=5, SD=1.1)	19.7 (N=10, SD=0.8)
	Ttipr	-	-	16 (N=25, SD=1.2)	15.1 (N=8, SD=0.5)	14.2 (N=3)	14.5 (N=5, SD=1.3)	22.3 (N=10, SD=1)
	Htitu	-	-	19.1 (N=5, SD=1.4)	17.2 (N=8, SD=0.7)	25 (N=3)	18.2 (N=3)	24.8 (N=10, SD=1.5)
Astragalus	Las	12.5; 12-14 (N=17)	14.4	14.1 (N=80, SD=0.6)	11.9 (N=4)	13.7 (N=2)	10.8 (N=3)	17.3 (N=10, SD=0.5)
	Was	-	6.4	6.4 (N=80, SD=0.3)	6 (N=4)	8.1 (N=2)	5.3 (N=3)	8.1 (N=10, SD=0.4)
	Lasn	-	-	7 (N=80, SD= 0.4)	5.8 (N=4)	6.8 (N=2)	5.1 (N=3)	8.9 (N=10, SD=0.4)
Calcaneus	Lca	23.89; 22.3-27.2 (N=18)	28	26.4 (N=69, SD=1)	23 (N=4)	27 (N=3)	20.4 (N=2)	34.5 (N=10, SD=0.8)
	Wca	-	-	9.5 (N=63, SD=0.6)	8.1 (N=4)	11.8 (N=3)	7.2 (N=2)	11.7 (N=10, SD=0.8)
	Lcat	-	-	12.4 (N=69, SD=0.8)	11.2 (N=4)	13 (N=3)	8.8 (N=2)	17.4 (N=10, SD=1)
	Lcab	-	-	10.2 (N=69, SD=0.5)	8.5 (N=4)	9 (N=3)	8.2 (N=2)	12.6 (N=10, SD=0.5)
	Wcat	-	-	6.3 (N=66, N=0.3)	6.2 (N=4)	7.6 (N=3)	5.1 (N=2)	8.3 (N=10, SD=0.4)
Navicular	Lnab	-	-	4.6 (N=4, SD=0.3)	4.9 (N=3)	3.8 (N=2)	4.5 (N=1)	10 (N=10, SD=0.2)
	Lnat	-	-	9.1 (N=42, SD=0.6)	11.5 (N=3)	8.8 (N=2)	9.1 (N=1)	13.7 (N=10, SD=0.9)
	Wna	-	-	6.8 (N=41, SD=0.4)	8.1 (N=3)	6.6 (N=2)	5.4 (N=1)	8.5 (N=10, SD=0.5)

	Tna	-	-	10.2 (N=42, SD=0.6)	10.2 (N=3)	10.2 (N=2_	8 (N=1)	12.5 (N=10, SD=0.4)
Cuboid	Lcu	-	-	7.8 (N=27)	7.4 (N=2)	-	7.1 (N=1)	9.3 (N=10)
	Wcu	-	-	8 (N=28)	8.9 (N=2)	8.7 (N=1)	6.7 (N=1)	10 (N=10)
	Tcu	-	-	6.4 (N=29, SD=0.3)	7.4 (N=2)	7 (N=1)	5.2 (N=1)	8.3 (N=10, SD=0.2)

APPENDIX II

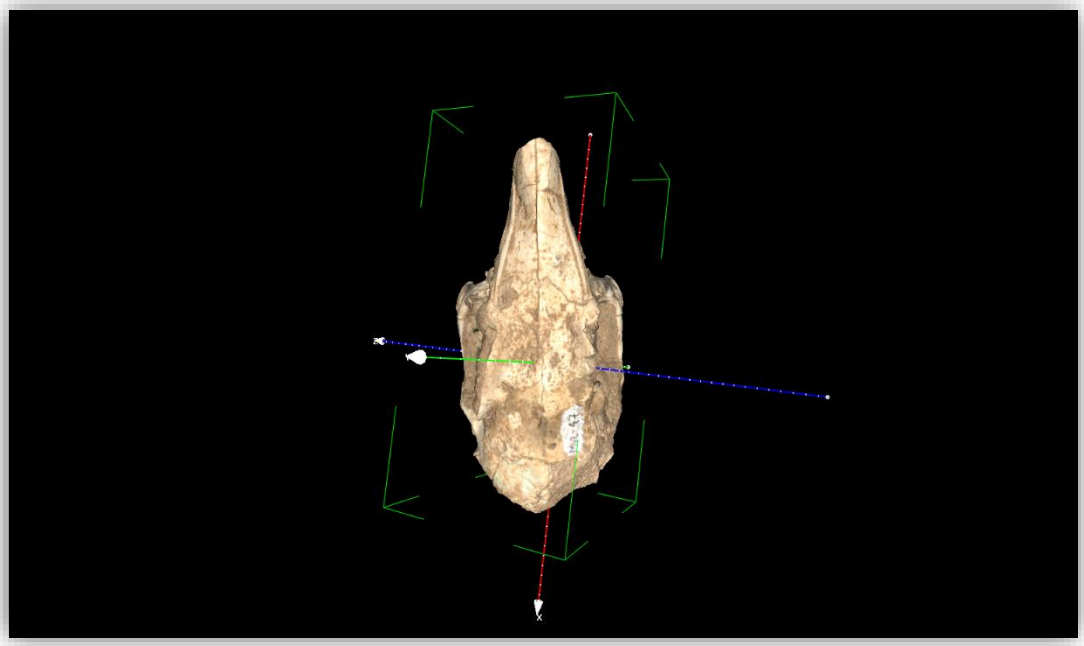

Figure 1. 3D scan of the dorsal side of MVL-47.

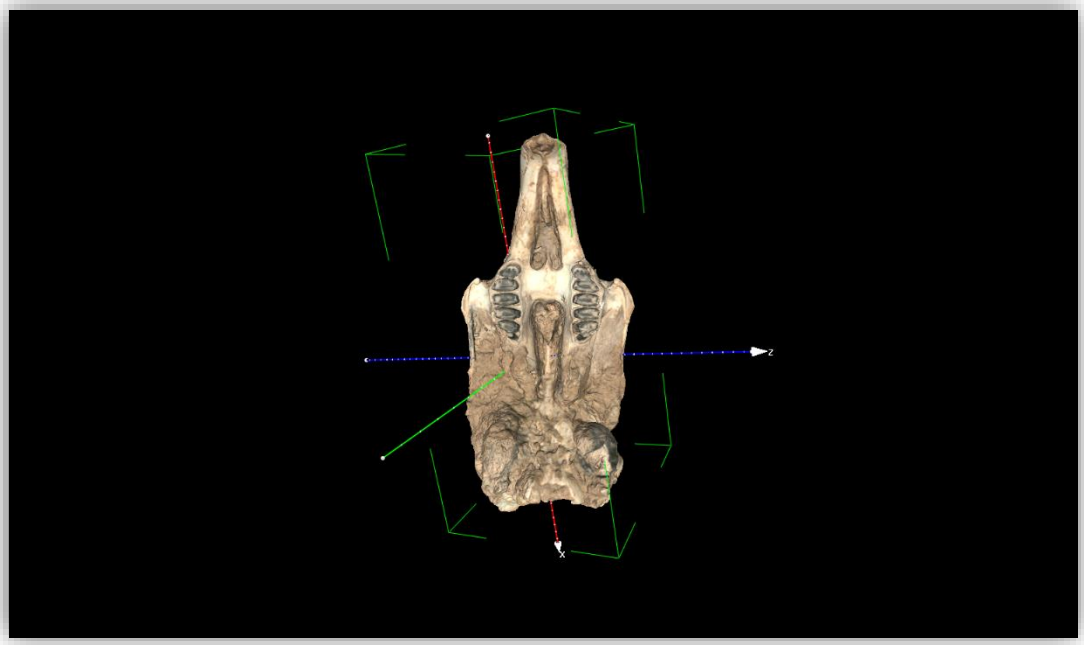

Figure 2. 3D scan of the ventral side of MVL-47.

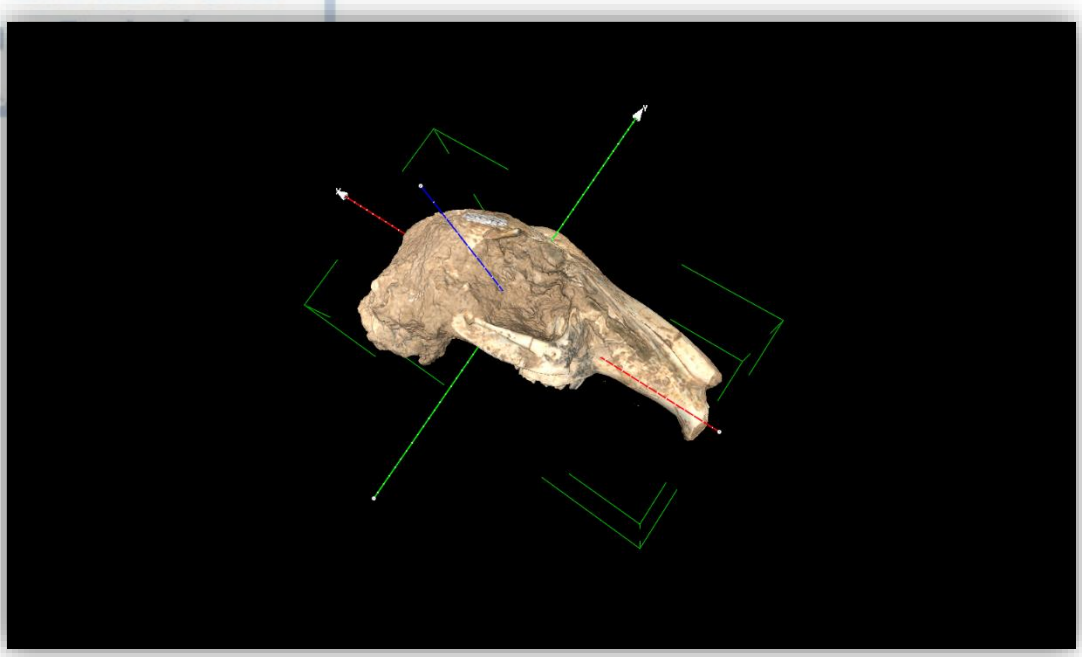

Figure 3. 3D scan of the right lateral side of MVL-47.

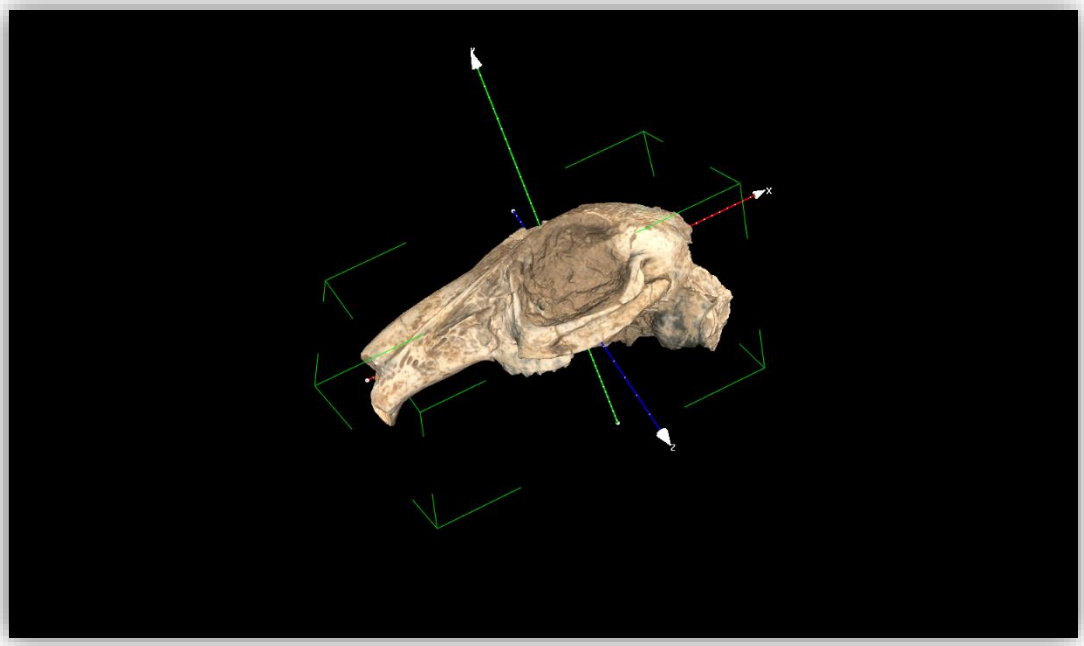

Figure 4. 3D scan of the left lateral side of MVL-47.

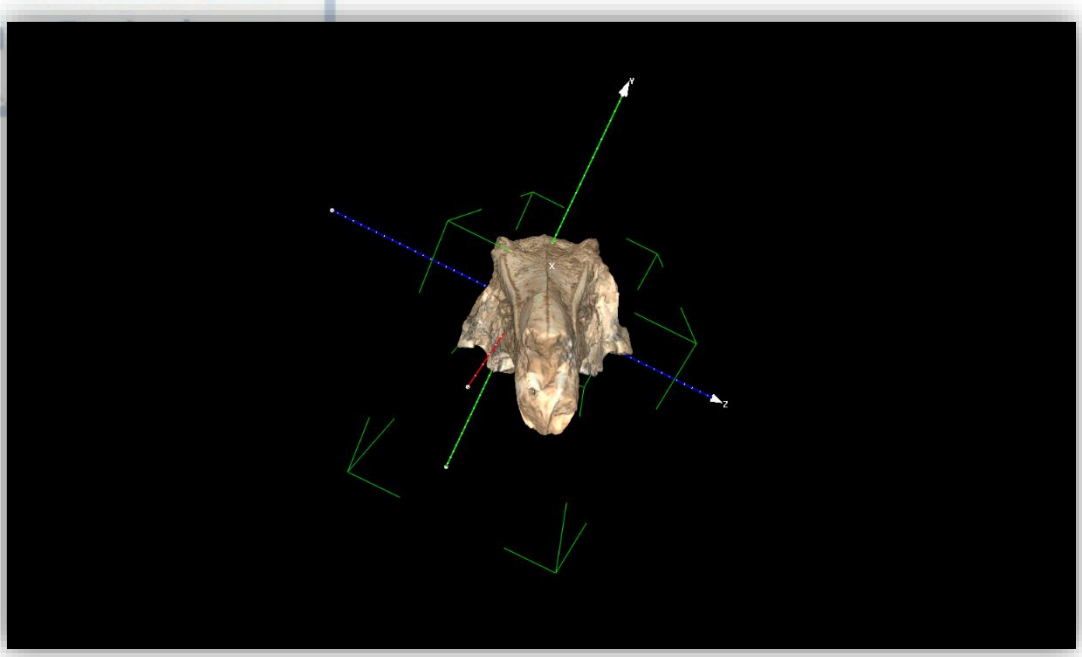

Figure 5. 3D scan of the anterior side of MVL-47.

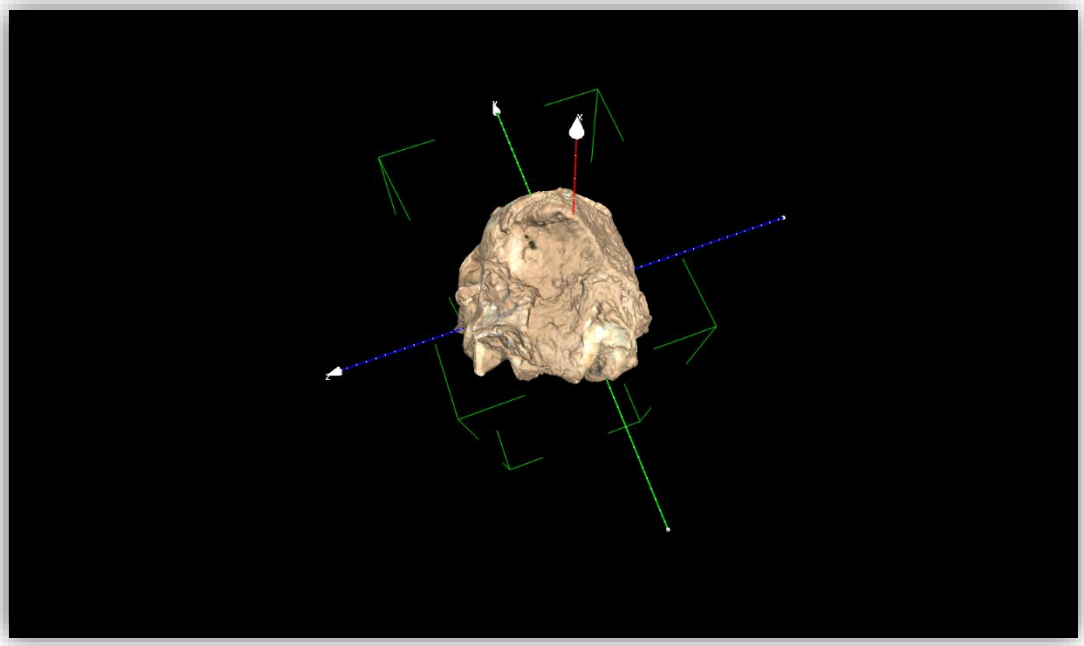

Figure 6. 3D scan of the posterior side of MVL-47.

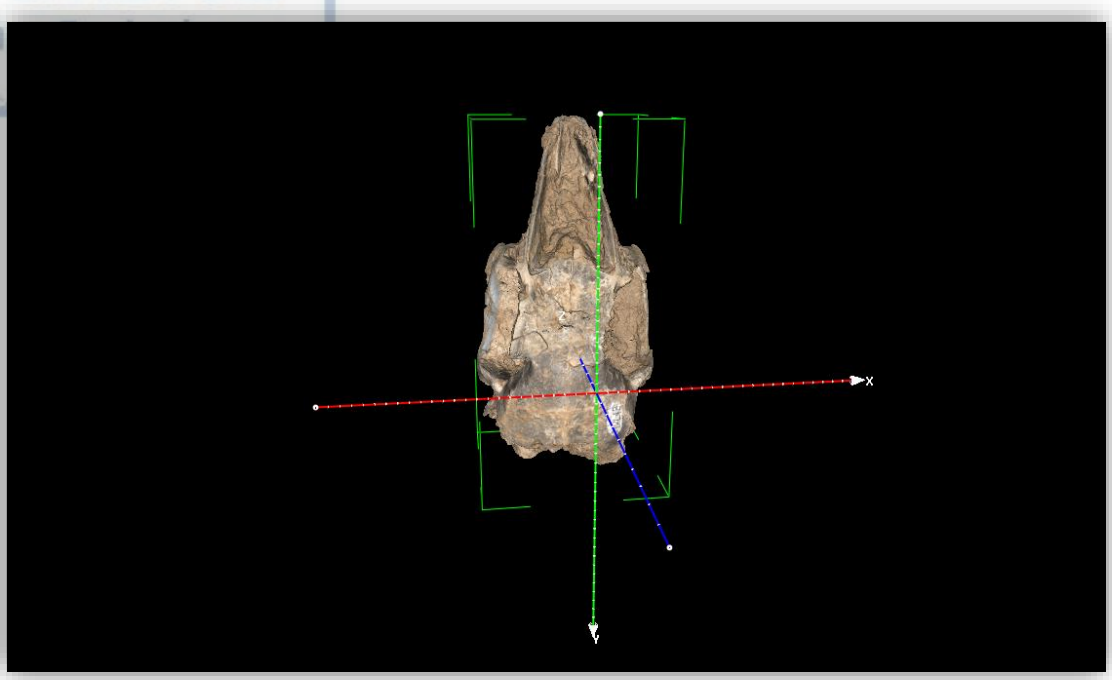

Figure 7. 3D scan of the dorsal side of MVL-48.

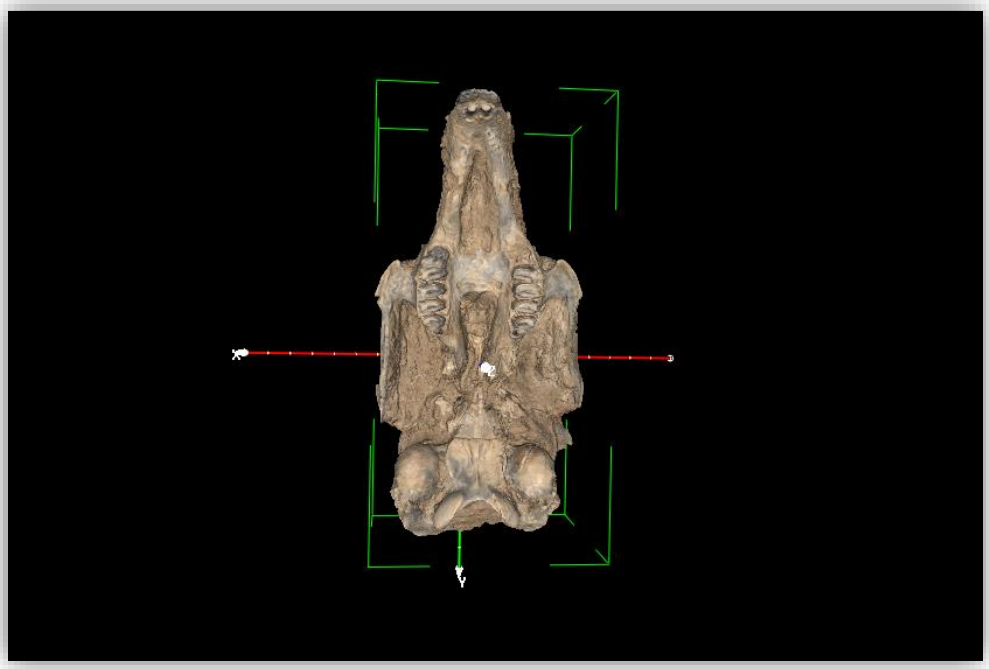

Figure 8. 3D scan of the ventral side of MVL-48.

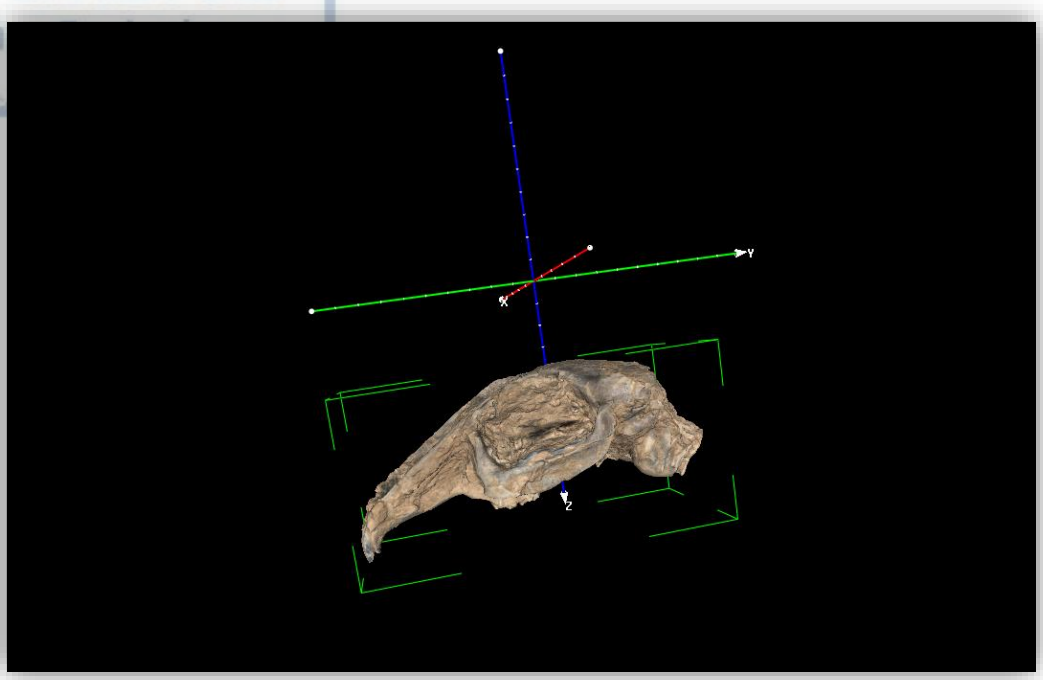

Figure 9. 3D scan of the left lateral side of MVL-48.

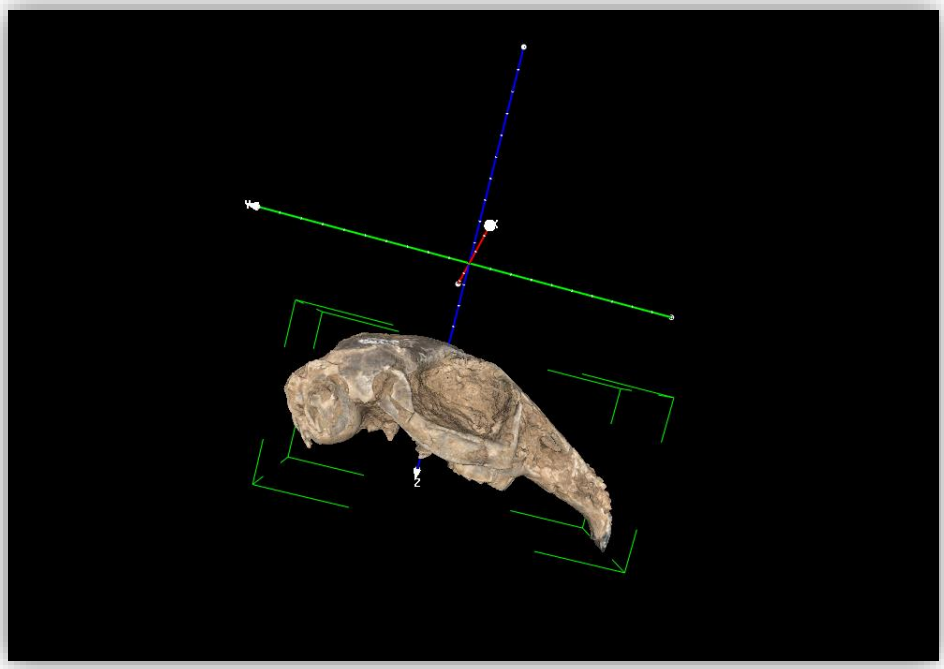

Figure 10. 3D scan of the right lateral side of MVL-48.

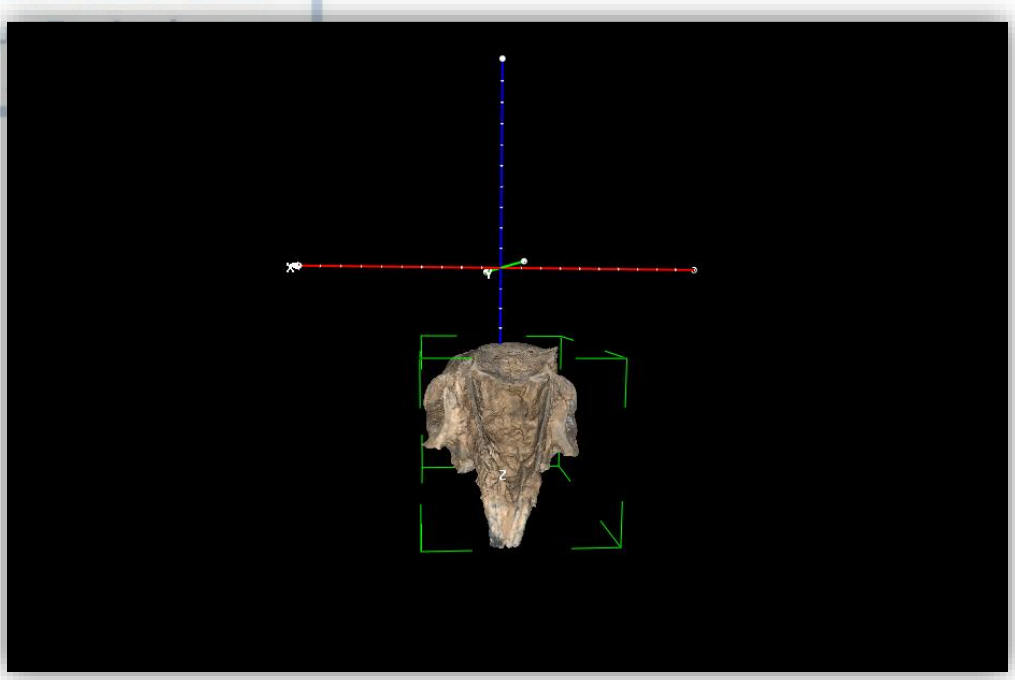

Figure 11. 3D scan of the anterior side of MVL-48.

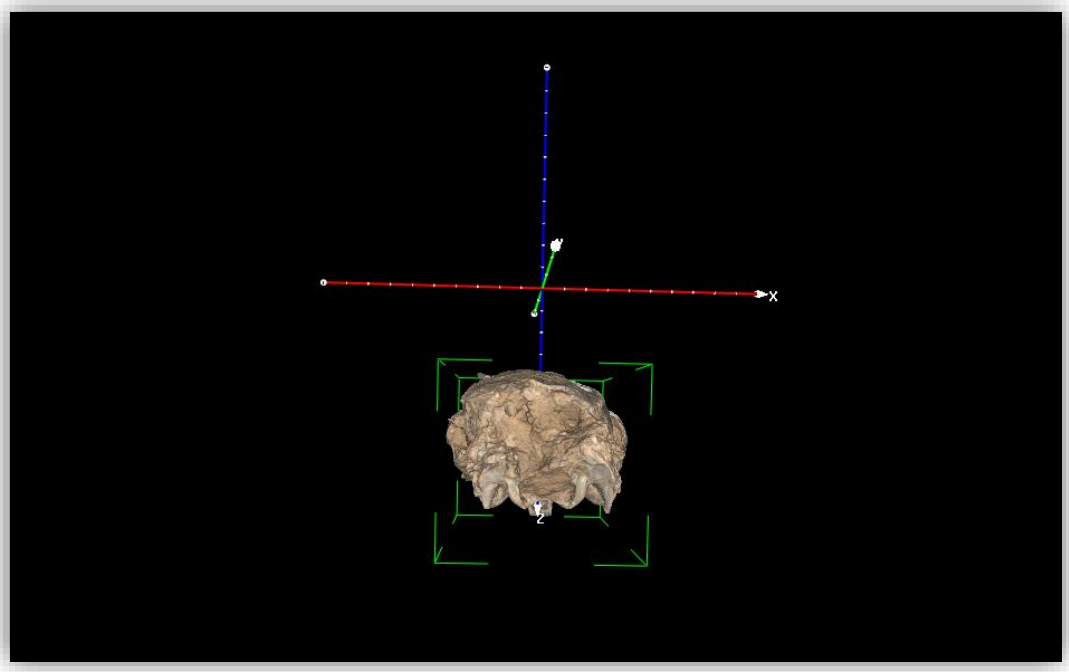

Figure 12. 3D scan of the posterior side of MVL-48.

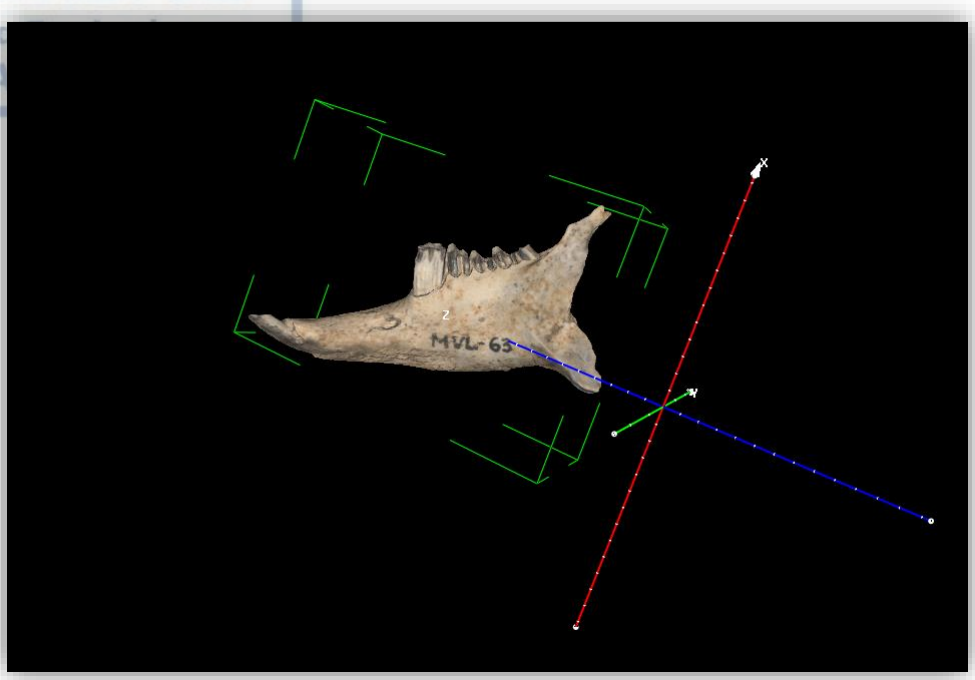

Figure 13. 3D scan of the lateral side of MVL-63.

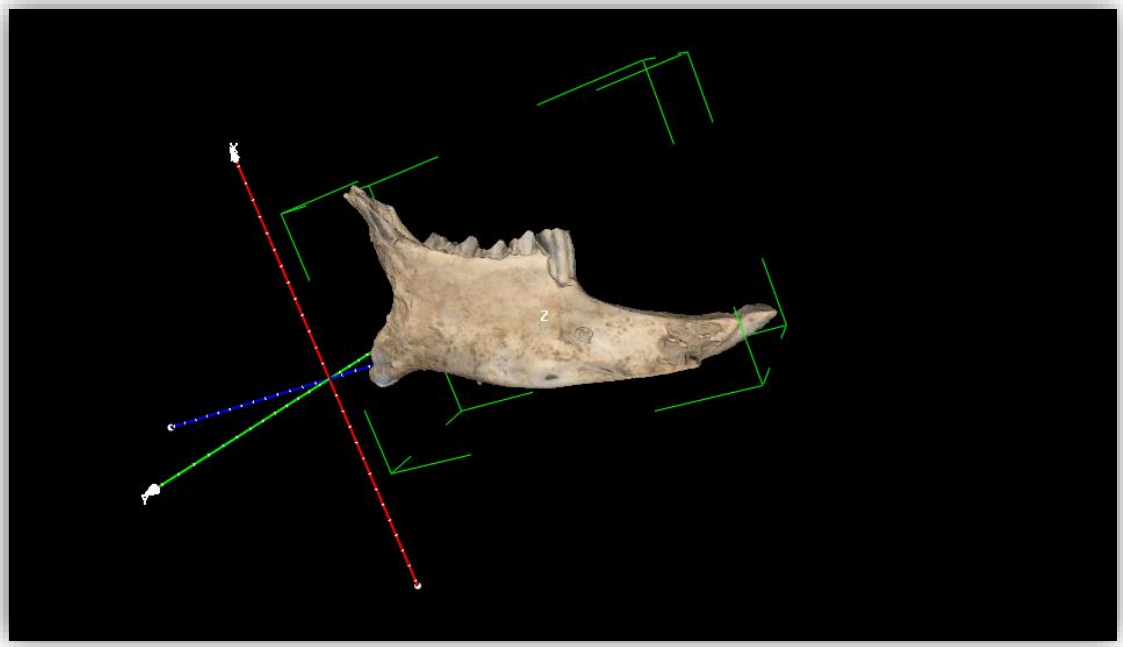

Figure 14. 3D scan of the medial side of MVL-63.

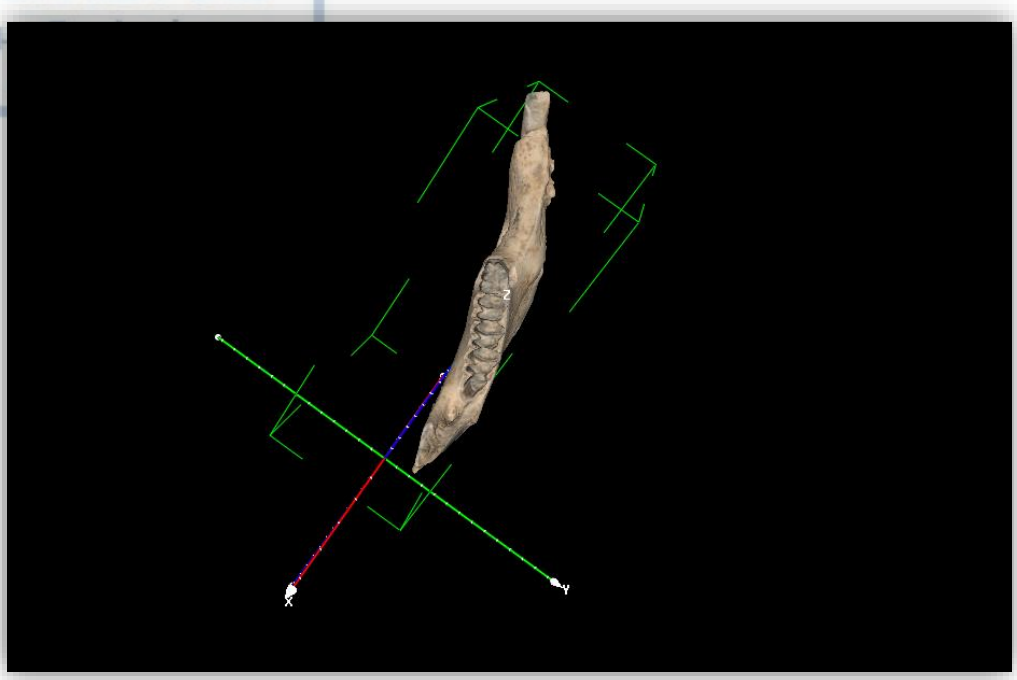

Figure 15. 3D scan of the occlusal side of MVL-63.

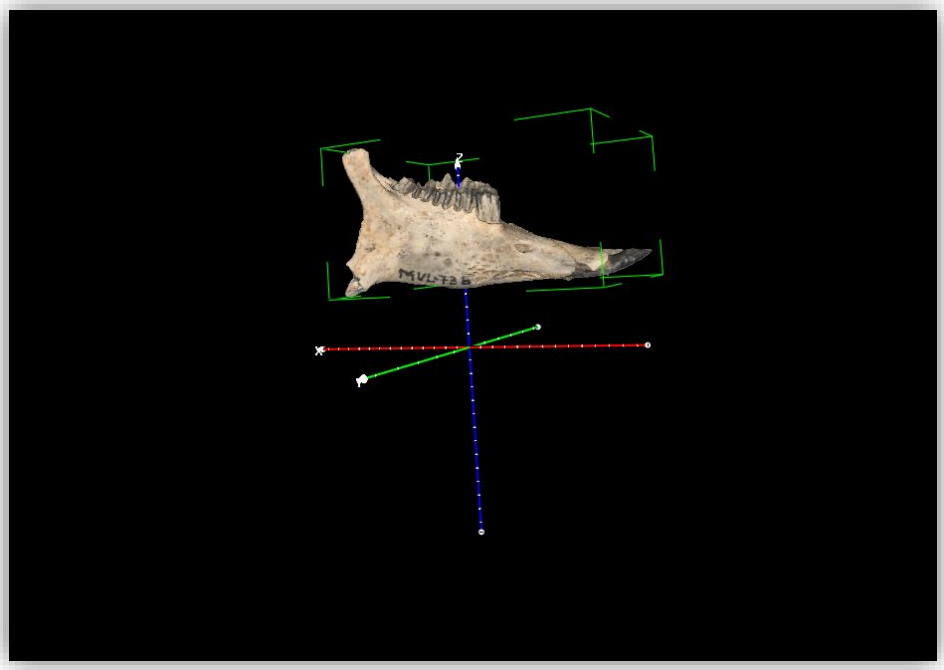

Figure 16. 3D scan of the lateral side of MVL-73b.

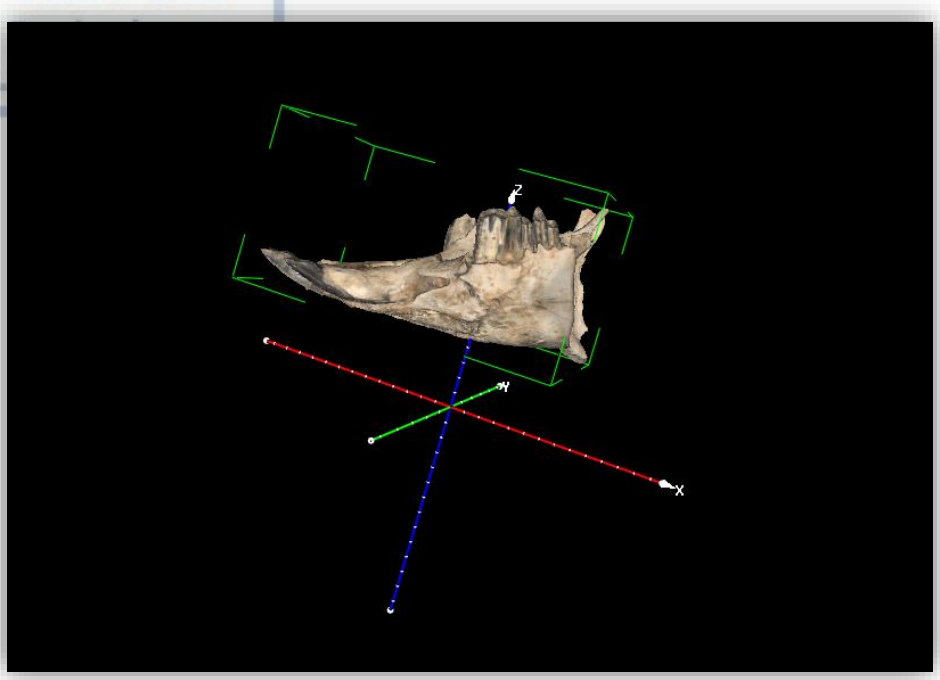

Figure 17. 3D scan of the medial side of MVL-73b.

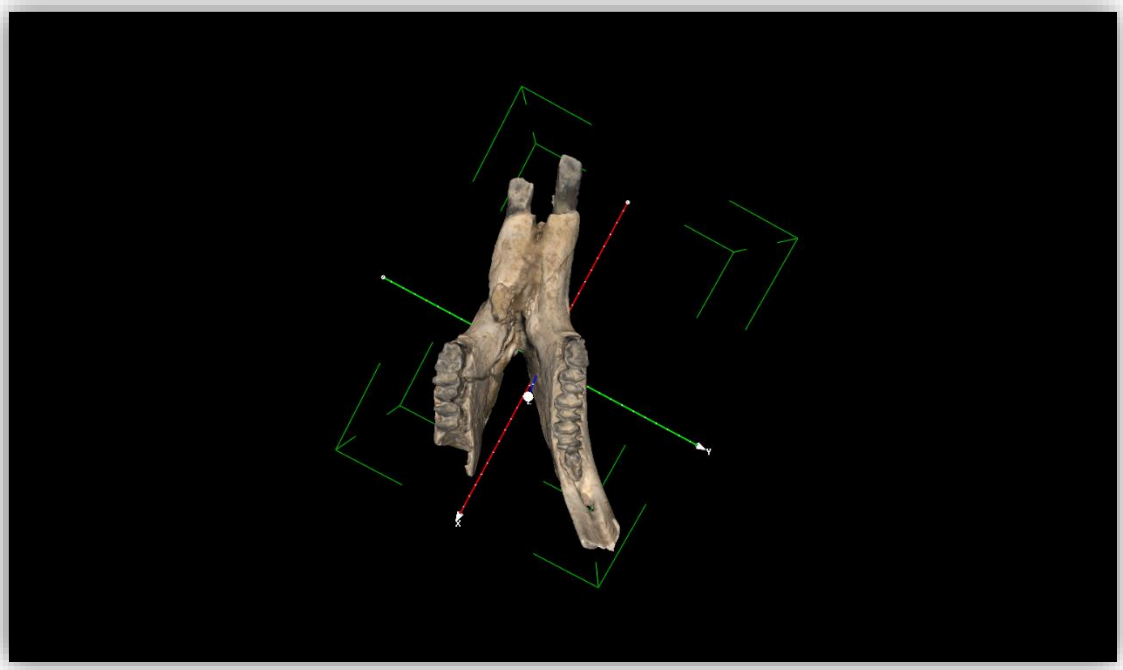

Figure 18. 3D scan of the occlusal side of MVL-73b.

Figure 19. 3D scan of the ventral side of MVL-73b.